

Supramolecular Assembly of Three-Dimensional Protein Networks

by

Fatima Omar Merza

A thesis

presented to the University of Waterloo

in fulfilment of the

thesis requirement for the degree of

Master of Science

in

Chemistry

Waterloo, Ontario, Canada, 2020

© Fatima Omar Merza 2020

Author's Declaration

I hereby declare that I am the sole author of this thesis. This is a true copy of the thesis, including any required final revisions, as accepted by my examiners.

I understand that my thesis may be made electronically available to the public.

Abstract

Intense interest is being focused on self-assembling biological networks and their practical applications, making them powerful tools for the next-generation of advanced bionanomaterials. This thesis project explores potential strategies to fabricate versatile protein networks in a supramolecular fashion. That will create a functionalized scaffold through the chemical attachment of a diverse range of molecules such as: enzymes, magnetic nanoparticles, and photolabile-based drugs.

The thesis hypothesis was that advanced bionanomaterial scaffolds could be fabricated from capsule proteins and linkers employing the high affinity biotin-avidin interaction. This bio-based platform leverages a cage-like proteinaceous molecule, which is ferritin. The protein ferritin is expressed in the tissues of many life forms and it features a rigid spherical structure with robust biochemical and thermophilic properties making it an attractive component for three-dimensional protein network design. Bioconjugation is an important tool in the fabrication of complex bionanomaterials.

The ferritin capsule protein was incorporated in the network by implementing bioconjugate techniques on its exterior surface, where the lysine residues were the main focus to undergo reactions in order to display free biotin molecules on the protein's surface. These biotins, along with the protein avidin, a protein having high affinity to biotin, self-associate via avidin-biotin complexation, and form the basis of a cross-linked network.

A wide range of PEGylated molecules were investigated to surface-modify ferritin to showcase the potential for functional diversity. Additionally, a multi-step bioconjugation strategy was developed to successfully tag ferritin with aldehyde-containing molecules, which can add

further novelty to the protein network. The designed and functionalized networks that are demonstrated in this research could potentially be capable of serving as a multi-enzyme protein complex, a smart photoreleased-drug bandage, and a porous filtration biomembrane.

Acknowledgements

I want to express my full appreciation to Professor John Honek for all his effort, support, and guidance throughout my master's program and for everything he has done to provide a professional research environment for all of us to learn and to grasp the scientific knowledge. To the most patient supervisor I ever had, thanks for helping me in becoming a better researcher. I would like to extend my special thanks to Maja Lopandic, a graduate student who I am lucky and thankful to work with. I learned a lot from her since day one. She was kind to always answer all my questions, and I would have not been able to make it without her encouragement and help in research and thesis writing.

My heartfelt thanks to Hawa Gyamfi, a former Ph.D. student for providing me the continuous guidance, life advice, and technical training. Thanks to all the former members in the Honek laboratory who always provided help and contributed to this project; Jameson Pfeffer, Jeffrey Wignarajah, David Kim, Taylor Urquhart, and Tom Daniel.

Greatest thanks to my family and friends in the United Arab Emirates for always being there to show support when I needed it during my hard times. Acknowledgment must be made to the AGFE foundation for education in the United Arab Emirates for funding my full tuition and for granting me the opportunity to pursue my M.Sc. degree in Canada.

Thanks to Dr. Richard Smith and Ms. Val Goodfellow from the mass spectrometry facility for providing the training, answering all my questions, and providing help in operating the MS instruments throughout the last two years. Finally, I would like to thank my committee members; Professor Thorsten Dieckmann and Professor Shawn Wettig for providing the time and effort to review my thesis.

Table of Contents

List of Figures	ix
List of Tables	xiv
List of Schemes	xv
Abbreviations	xvi
1 Chapter 1: Introduction to Bioconjugation and Protein Networks	1
1.1 The Ferritin Protein Superfamily	1
1.1.1 Ferritin Properties and Architecture.....	1
1.1.2 Description of Horse Spleen Ferritin and its Structural Features	5
1.1.3 Description of <i>Pyrococcus furiosus</i> Ferritin and its Structural Features	9
1.2 Bioconjugation Chemistry and Strategies	11
1.2.1 Lysine Modification.....	14
1.2.2 Cysteine Modification.....	15
1.2.3 Polyethylene Glycol Polymers.....	16
1.3 Protein Networks.....	18
1.3.1 Roles of Protein Networks in Nature	19
1.3.2 Biotechnological Applications.....	21
1.4 Research Hypothesis	25
2 Chapter 2: Protein Network Design and Fabrication.....	26
2.1 Background	26
2.1.1 Avidin-biotin Interaction	26
2.1.2 Cutinase Enzymes for PET Degradation	29
2.1.3 Photocleavable Biomaterials.....	30
2.2 Objectives.....	31
2.3 Materials.....	34
2.4 Methodology	35
2.4.1 Mass Spectrometry.....	35
2.4.2 Ultraviolet-Visible (UV-Vis) Absorbance Measurements.....	36
2.4.3 Biotinylation of HSF Protein Through Lysine Modification.....	37
2.4.4 Lysine Modification Using a Photocleavable Linker	39
2.4.5 Cysteine Modification of HSF Protein	39
2.4.6 Bioconjugation of Magnetic Beads.....	40

2.4.7	Protein Network Formation	42
2.4.8	SEM Characterization	43
2.4.9	Suspension of Biotinylated HiC Enzymes within the Ferritin-avidin Scaffold.....	44
2.4.10	Enzymatic Scaffold-PET Sample Preparation for Degradation Studies.....	45
2.4.11	The Assembly of a Photocleavable Protein Network	46
2.4.12	Photolysis of the Protein Network	46
2.5	Results and Discussion.....	47
2.5.1	Lysine Modification on HSF Protein.....	47
2.5.2	Cysteine modification on HSF protein	53
2.5.3	Biotinylated Magnetic Beads	55
2.5.4	B4F Quantitative Assay	56
2.5.5	Ferritin-avidin Network	58
2.5.6	SEM Characterization.....	64
2.5.7	The Effect of Enzyme-bound Ferritin-avidin Network on PET Degradation.....	66
2.5.8	Photolytic Behavior of PC biotin-PEG ₃ -NHS Carbonate Ester Containing Protein Network	74
3	Chapter 3: Development of a New Bioconjugation Strategy	78
3.1	Introduction	78
3.2	Objectives.....	83
3.3	Materials.....	84
3.4	Methodology	85
3.4.1	Reaction of N-ethylmaleimide with Tris-2-carboxyethylphosphene.....	85
3.4.2	³¹ P NMR.....	86
3.4.3	Optimization of Wittig Olefination Reaction Conditions	86
3.4.4	HSF Protein Surface Modification.....	87
3.4.5	Modified-HSF Sample Preparation for MS Analysis	88
3.4.6	Expression and Purification of PfFtn.....	90
3.4.7	Preparation of PfFtn-MAL Conjugate	92
3.4.8	Preparation of PfFtn-MAL-TCEP Conjugate	93
3.4.9	Reaction of mPEG-benzaldehyde with PfFtn-MAL-TCEP Conjugate	93
3.5	Results and Discussion.....	94
3.5.1	Characterization of the Reaction of N-ethylmaleimide with Trialkylphosphine....	94
3.5.2	³¹ P NMR Evaluation	94

3.5.3	Wittig Olefination Reaction of the TCEP-MAL Conjugate with Aldehyde Derivatives	96
3.5.4	MALDI Analysis of MAL-TCEP Adduct Formation on the HSF Surface	99
3.5.5	Characterization of HSF Protein	102
3.5.6	Characterization of the HSF-MAL-TCEP Adduct	104
3.5.7	Surface Modification of <i>Pyrococcus furiosus</i> Ferritin (PfFtn)	107
3.5.8	Purification of <i>Pyrococcus furiosus</i> Ferritin (PfFtn)	111
3.6	Conclusion	114
4	Chapter 4: Computational Studies on the Energetics of Bioconjugation Reactions	115
4.1	Overview	115
4.2	Methods	116
4.2.1	Thermochemical recipes	116
4.2.2	Density Functional Models	117
4.3	Results and Discussion	117
5	Chapter 5: Summary and Future Directions	130
5.1	Optimizations and Bioconjugation with Functional Aldehydes	132
5.2	Immobilizations on Polymer-supported TCEP Resins	133
5.3	Computational Studies	134

List of Figures

Figure 1.1. Regular ribbon structure of a bacterioferritin (PDB: 1BFR) monomer exhibiting the alpha-helical bundle. A-C and E helices are shown in distinct colors. Reproduced with permission under CC license from (Zhang & Orner, 2011).	2
Figure 1.2. Ribbon representation of human ferritin. The structure of ferritin resembles a 24-mer self-assembled symmetrical cage protein with 8 and 12 nm diameter dimensions, two types of chains (heavy and light) and two channels (C3 and C4) (PDB: 5N27). Reproduced with permission under CC license from (Jiang et al., 2020).....	3
Figure 1.3. Interior surface of ferritin has a net negative charge, indicated by the dominant red color of the acidic amino acid residues. B) Exterior surface of ferritin with a charge close to neutral. Reproduced with permission under CC license from (Zhao, 2010).	4
Figure 1.4. Structural model representation of one HSF subunit coloured in yellow, with 3 lysines coloured in red, exposed to the exterior surface. Structure was created using Chimera software employing protein structure PDB: 5ERK.	6
Figure 1.5. Structural model representation of <i>P. furiosus</i> highlighting one subunit in yellow. One subunit contains 10 lysine residues coloured in red, which are exposed to the exterior surface. Structure was created using Chimera software employing protein structure PDB: 2JD7.	10
Figure 1.6. DNA-peptide biomaterials. A) DNA-peptide bioconjugate. B) A self-assembled tetrahedral cage of DNA strands, manifesting peptide conjugation to the DNA scaffold. Reproduced with permission from (Stephanopoulos, 2019).	13
Figure 1.7. Fabrication and functionalization of hydrogel networks through maleimide bioconjugation. Reproduced with permission from (Cengiz et al., 2020).	13
Figure 1.8. Representation of protein side chains subjected to surface conjugation through reactive amino acid residues. Image generated by software program Chimera using PDB: 5ERK.	14
Figure 1.9. Chemical structure of poly(ethylene glycol) (PEG).	17
Figure 1.10. A representation of natural three-dimensional supramolecular protein networks. Polyhedral bacterial microcompartment (BMC) made of a few thousands BMC shell and vertex proteins. Reproduced with permission from (Yeates et al., 2013).....	19
Figure 1.11. An example of naturally occurring protein network. Self-assembled two-dimensional S-layer protein lattices. Reproduced with permission from (Baneyx & Matthaei, 2014).	20
Figure 1.12. X-ray structure of a toroidal protein, an example of naturally occurring protein network. Generated using Chimera software (PDB: 3P91).	21

Figure 1.13. Photocatalytic complex constructed by modifying the surface residues of a beta-helical nanotube using Re(I) and Ru(II) complexes exhibits higher reactivity of the CO ₂ to CO photocatalytic reduction with the multiply-modified construct. Reproduced with permission from (Yokoi et al., 2011).	23
Figure 1.14. A design of an ENC using ferritin and streptavidin. A) bFNP saturation with SA-HRP. B & C) Reaction of non-saturated bFNP with SA-HRP drives the formation of dimer, trimers, and tetramers. D) A diagram of the full construct of a sensitive ENC material. Reproduced with permission from (Men et al., 2015).....	24
Figure 1.15. An overview of the thesis project scheme that involves the fabrication of protein networks and the development of a new bioconjugation strategy.	25
Figure 2.1. Crystal structure of tetrameric avidin (PDB: 2AVI) with emphasis on the biotin binding site in one subunit. The structure was generated using Chimera employing the protein structure code PDB:1AVD.	26
Figure 2.2. Biotin molecule representing the six hydrogen bond interactions that take place at the binding site of avidin.....	28
Figure 2.3. A) Ribbon representation of HiC enzyme (PDB: 4OYY). The chemical structure of PET degradation products: B) BHET, C) MHET, and D) TPA.....	30
Figure 2.4. An illustration of a supramolecular protein scaffold assembled from biotinylated ferritin and avidin proteins.....	32
Figure 2.5. A broad design strategy. A wide range of capsule proteins, linker chains/proteins to be employed in the project.....	33
Figure 2.6. Biotinylation reagents. A) the chemical structure of Biotin-PEG(n)-NHS ester. B) the chemical structure of Biotin-PEG(n)-TFP ester. C) Trifunctional PEG “TFP-PEG ₄ -Lys (PEG ₄ -biotin) ₂ ”.....	38
Figure 2.7. Chemical structure of PC Biotin-PEG ₃ -NHS carbonate ester.	39
Figure 2.8. The chemical structure of the biotinylation reagent Biotin-PEG ₁₁ -MAL.....	40
Figure 2.9. Structure of biotin-4-fluorescein (B4F).	42
Figure 2.10. MALDI-TOF result of biotinylated ferritin subunits. A) a control spectrum shows a peak of one unmodified ferritin subunit. B) A modified ferritin subunit with biotin-PEG ₁₂ -TFP exhibits a control peak in addition to a second peak indicates one modification. C) Ferritin biotinylated with biotin-PEG ₂₄ -TFP. D) Ferritin biotinylated with biotin-bifurcated PEG ₄ -TFP.....	49
Figure 2.11. MALDI spectra of ferritin subunits cross-linked with biotin-PEG-NHS ester (MW=5000 Da). A) Ferritin control (not biotinylated). B) Biotinylation with 800-fold reagent at room temperature. C) Biotinylation with 800-fold reagent for 24 h at 4 °C.	52

Figure 2.12. Space-filled model of the horse spleen ferritin protein (PDB: 5ERK). The model shows one cysteine residue (yellow) in each subunit located in a buried position in the intermolecular grooves of the capsule protein. The images were generated using Chimera software.	54
Figure 2.13. B4F assay analysis bar chart indicating the successful displacement of B4F molecules by biotins on the magnetic beads confirming the biotinylation labelling with 87% yield.	57
Figure 2.14. Chemical assembly of biotin-PEG ₂₄ -ferritin capsules through an avidin mediator creates a flexible space of 49 nm.	58
Figure 2.15. Four biotinylated ferritin capsules with different PEG linker lengths are attached with an avidin through the biotin-binding sites. The figure utilized the structures of avidin (PDB: 1AVD), horse spleen ferritin (PDB: 5ERK) and the chemical structure of the various PEG linkers.	59
Figure 2.16. Protein networks. A) Control: unbiotinylated ferritin with avidin. B) Biotinylated ferritin with avidin. C) Biotinylated ferritin with streptavidin D) Biotinylated ferritin with neutravidin.	61
Figure 2.17. Ferritin-Avidin networks. A) A network assembled in 0.3 M NaCl. B) A network assembled in 1 M NaCl. C) A pre-assembled network with free D-biotin molecules added in a 4:1, biotin:avidin ratio.	63
Figure 2.18. A) Control of unbiotinylated ferritin and avidin on a glass slide. B) A thin film of a solid amorphous material made of biotinylated ferritin and avidin.	64
Figure 2.19. A) SEM image of biotinylated ferritin (PEG ₂₄ -TFP)-avidin material B) EDX analysis shows the chemical elements of the material.	65
Figure 2.20. Surface mapping of the hydrophobic patches responsible for non-specific interactions between: A) HiC enzyme (PDB: 4OYY) and B) avidin protein (PDB: 1AVD). Hydrophobic regions are shown in green. Images were generated using Schrödinger software. (Schrödinger Release 2020-2: BioLuminate, Schrödinger, LLC, New York, NY, 2020).	66
Figure 2.21. A, C) SEM micrographs of PET plastic exposed to 200 mM sodium phosphate buffer at pH 7.0. at 55 °C for 19 days. B, D) SEM micrographs of PET plastic exposed to 20 mg/ml HiC enzyme solution. Images A/B and C/D were taken with 1500 x and 20,000 x magnification, respectively.	68
Figure 2.22. A, C) SEM micrographs of PET plastic exposed to 200 mM sodium phosphate buffer at pH 7.0. at room temperature for 19 days. B, D) SEM micrographs of PET plastic exposed to 20 mg/ml HiC enzyme solution. Images A/B and C/D were taken with 1500 x and 20,000 x magnification, respectively.	69
Figure 2.23. SEM images of PET samples incubated at room temperature for 15 days. A, C) Image of untreated dry PET section taken with 1500 x and 20,000 x magnification. B, D) Untreated PET section exposed to 200 mM sodium phosphate buffer, pH 7.0 with 1500 x and 20,000 x magnification.	71

Figure 2.24. SEM images of PET after digestion by the enzyme-bound scaffold over the duration of 15 days at room temperature. The micrographs were taken with 1500 x, 20,000 x, and 118,146 x magnification. Images A, C, and E were taken using an SE detector, and images B, D, and F were taken using a BE detector.....	73
Figure 2.25. Results of MALDI-TOF for the photolytic protein network. A) Protein network with no exposure to UV light. B) 30 min UV light exposure. C) 45 minutes UV light exposure.	75
Figure 2.26. The mechanism of Norrish type II photocleavage at the carbamate moiety.....	76
Figure 2.27. Ferritin-avidin network exposed to UV light at 365 nm for 30 minutes.	77
Figure 2.28. The design of functionalized protein networks with photocleavable drug molecules for medical applications (e.g. Smart bandages).	77
Figure 3.1. Chemical structure of A) Tris-2-carboxyethyl phosphine (TCEP) reducing agent, and B) N-Ethylmaleimide.	78
Figure 3.2. Reaction of maleimide and TCEP in the presence of PEG-azides that resulted in retaining the protein conjugation. Reproduced with permission under CC license from (Kantner et al., 2017).	80
Figure 3.3. The chemical structure of the bioconjugation reagent MAL-dPEG ₄ -NHS ester.....	88
Figure 3.4. The amino acid sequence of His6-PfFtn construct.	92
Figure 3.5. The product of the TCEP and NEM reaction exhibiting a mass peak at 376.1172 m/z on ESI MS.....	94
Figure 3.6. The ³¹ P NMR spectrum of the NEM-TCEP product at chemical shift $\delta = 39.89-39.97$ ppm, and the TCEP-oxide byproduct at $\delta = 57.43-57.69$ ppm.	95
Figure 3.7. MS spectrum shows two distinct peaks of the aldehyde product at 246.11 m/z and the starting material at 376.11 m/z.....	97
Figure 3.8. ESI spectrum shows two distinct peaks of the aldehyde product at 378.19 m/z and the starting material of the aldehyde reagent at 269.13 m/z.	99
Figure 3.9. MALDI-TOF mass spectra of HSF conjugation. A) Spectrum of a mass peak at 20042 m/z, corresponding to the mass of a single native unmodified ferritin subunit with a side shoulder peak at 20399 m/z suggesting ferritin subunits were labelled with one PEG ₄ -MAL molecule. B) A mass peak of a single unmodified subunit at 20113 m/z with a shoulder peak at 20470 m/z that corresponds to one PEG ₄ -MAL modification.	100
Figure 3.10. A) TIC spectrum of HSF showing multiply charged protein ion peaks. B) The deconvoluted TIC spectrum represents an accurate mass that corresponds to one unmodified HSF subunit.....	103
Figure 3.11. A) TIC-ESI spectrum for the HSF-MAL-TCEP sample purified by gel Sephadex G-25. B) The deconvoluted ESI spectrum exhibiting the mass peak of the modified protein. C) MALDI mass spectrum of the same sample.	105

Figure 3.12. Deconvoluted ESI spectrum that exhibits a mass peak corresponding to a cleaved HSF fragment after an extended treatment with 0.1% FA. Beside the spectrum is the amino acid sequence of HSF. The black label is the sequence corresponding to the mass in the spectrum. The red labelled sequence indicates the cleaved fragment.	107
Figure 3.13. A) TIC-MS chromatogram of PfFtn. B) Deconvoluted ESI MS mass spectrum of one PfFtn subunit. C) Deconvoluted ESI MS spectrum shows two additional mass peaks correspond to one and two MAL modifications. D) Deconvoluted ESI MS spectrum of the PfFtn-MAL-TCEP product. .	109
Figure 3.14. The final product the surface functionalized ferritin. An (E)-isomer of a Wittig olefinated benzaldehyde, cross-linked on His-PfFtn capsule protein through a lysine targeted maleimide reagent.....	111
Figure 3.15. Deconvoluted ESI MS spectrum exhibits mass peaks corresponding to the final product formation with the mPEG ₄ -benzaldehyde attachment.	111
Figure 3.16. A) SDS-PAGE gel of PfFtn protein after purification with IMAC column. B) The elution profile for His-PfFtn purified using IMAC. C) SDS-PAGE gel of two PfFtn protein samples, before and after boiling.	113
Figure 4.1. The energies of activated esters (kJ/mol).	129
Figure 5.1. Schematic summary of the thesis project.	130
Figure 5.2. The maleimide conjugation approach for immobilization applications.	131
Figure 5.3. Two aldehyde reagents for bioconjugation with proteins. A) PEG12-benzaldehyde with dansyl group that exhibits a fluorescence activity. B) PEG12-benzaldehyde with biotin group that can attach robustly with avidin proteins.....	133

List of Tables

Table 1. Comparison of biotin-binding proteins.	29
Table 2. Experimental setup for protein networks.	43
Table 3. EDX elemental analysis profile of unbiotinylated control sample.	56
Table 4. EDX elemental analysis profile of biotinylated magnetic particle.	56
Table 5. Calculated energy values using the thermochemical recipes models	126
Table 6. Calculated energy values using the DFT models.....	128

List of Schemes

Scheme 2.1. The mechanism of carboxyl groups activation and biotinylation of magnetic beads.....	41
Scheme 3.1. Reaction of N-ethylmaleimide and TCEP agent to form a stable ylene adduct.	79
Scheme 3.2. Wittig reaction mechanism of an N-Ethyl maleimide-TCEP adduct with an aldehyde that produces E- and Z- alkenes, with the E-isomer being more thermodynamically favorable, and phosphine-oxide as a byproduct.....	81
Scheme 3.3. A novel bioconjugation strategy on ferritin proteins aims to attach a wide array of aldehyde molecules via Wittig olefination.	84
Scheme 3.4. Reaction mechanism of N-ethylmaleimide with tris-2-carboxyethylphosphine incubated for 1 hour at room temperature.	85
Scheme 3.5. Reaction scheme of NEM-TCEP adduct with p-anisaldehyde results in the alkene product with the E-isomer.	86
Scheme 3.6. Wittig reaction mechanism of NEM-TCEP and mPEG-benzaldehyde.	98
Scheme 4.1. Reactions of phenyl esters.	118
Scheme 4.2. Reactions of monosubstituted fluorophenyl esters.	118
Scheme 4.3. Reactions of difluorephenyl esters.	119
Scheme 4.4. Reactions of trifluorophenyl esters.	120
Scheme 4.5. Reactions of tetrafluorophenyl esters.	120
Scheme 4.6. Reactions of pentafluorophenyl esters.	121
Scheme 4.7. Reactions of acetyl chlorides.	121
Scheme 4.8. Reactions of sulfo-NHS esters.	122
Scheme 4.9. Reactions of p-nitrobenzyl esters.	122
Scheme 4.10. Reactions of methyl acetates.	122
Scheme 4.11. Reactions of thioesters.	123
Scheme 4.12. Reactions of N-hydroxysuccinimide esters.	123
Scheme 4.13. Schiff base formation.	123
Scheme 4.14. NEM-TCEP adduct formation.	123
Scheme 4.15. NEM-THPP formation.	124
Scheme 4.16. NEM-TCEP and THPP reactions in H ₂ O.	124
Scheme 4.17. Wittig reaction forming E- and Z-alkenes.	125
Scheme 5.1. The reaction of N-ethylmaleimide with TCEP produces an ylene, while its reaction with THPP results in reduction of the maleimide ring.....	135

Abbreviations

B4F	Biotin-4-Flourescein
BSA	Bovine serum albumin
Da	Daltons
DDH2O	Doubly distilled water
<i>E. coli</i>	<i>Escherichia coli</i>
EDC	1-Ethyl-3-(3-dimethylaminopropyl)carbodiimide
EDX	Energy dispersive X-ray spectroscopy
ESI	Electrospray ionization
FA	Formic acid
GdnHCl	Guanidine hydrochloride
His6-tag	Hexa-histidine affinity tag
HEPES	4-(2-Hydroxyethyl)-1-piperazineethanesulfonic acid
HiC	<i>Humicola insolens</i> cutinase
HSF	Horse spleen ferritin
IMAC	Immobilized metal affinity chromatography
IPTG	Isopropyl β -d-1-galactoside
K_d	Dissociation constant
KP	Potassium phosphate
MAL	Maleimide
MALDI	Matrix-assisted laser desorption/ionization
MS	Mass spectrometry

MES	2-Ethanesulfonic acid
MW	Molecular weight
MWCO	Molecular weight cut-off
μL	Microliters
NA	Neutravidin
NEM	N-Ethyl maleimide
NHS	<i>N</i> -Hydroxysuccinimide
PBS	Phosphate-buffered saline
PEG	Poly(ethylene glycol)
PET	Poly(ethylene terephthalate)
PfFtn	<i>Pyrococcus furiosus</i> ferritin
pI	Isoelectric point
SDS-PAGE	Sodium dodecyl sulfate polyacrylamide gel electrophoresis
SEM	Scanning electron microscopy
SA	Streptavidin
TCEP	Tris(2-carboxyethyl)phosphine
TFP	2,3,5,6-Tetrafluorophenol

1 Chapter 1: Introduction to Bioconjugation and Protein Networks

1.1 The Ferritin Protein Superfamily

1.1.1 Ferritin Properties and Architecture

The ferritin protein family is a class of multimer capsule proteins found ubiquitously in numerous organisms such as bacteria, archaea, and eukaryotes – with the exception of yeast (Zang et al., 2017) (Jutz et al., 2015) (Putri et al., 2015). The ferritin protein family typically has a highly preserved cage structure, although significant variations in the primary sequence, as much as 80%, are found among some ferritin subfamilies (Zang et al., 2017) (Theil, 2013). Ferritin's quaternary structure has twenty-four structurally-identical subunits. Each subunit reveals a bundle structure of four parallel alpha-helices (helices A-D), in addition to a short helix at the C-terminus coded by helix E (Figure 1.1) (Zhang & Orner, 2011). Each subunit has a molecular weight of approximately 19-21 kDa summing up to ~480 kDa when assembled as a 24-mer. The four parallel alpha-helices found in ferritin are structurally similar to the alpha-helices found in methane monooxygenase, ribonucleotide reductase and DNA binding protein from starved cells (Yévenes, 2017).

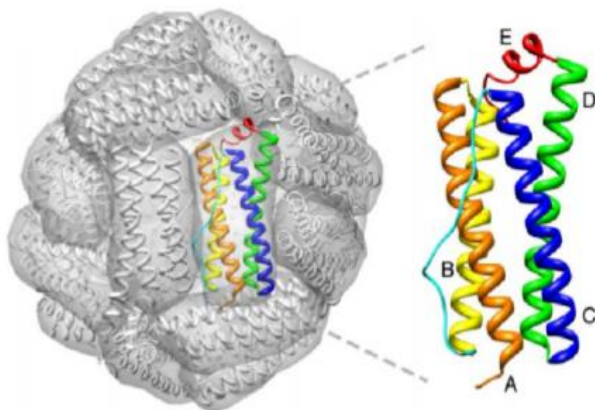


Figure 1.1. Regular ribbon structure of a bacterioferritin (PDB: 1BFR) monomer exhibiting the alpha-helical bundle. A-C and E helices are shown in distinct colors. Reproduced with permission under CC license from (Zhang & Orner, 2011).

The ferritin protein has an inner and outer diameter of 8 nm and 12 nm respectively (Figure 1.2). The C-terminal end of each monomeric HSF subunit folds towards the interior cavity of the capsule protein, while the N-terminal end extends to the outer surface of it. The N- and C-termini of ferritins are interesting sites for biochemical functionalization where molecular tags could be fused specifically onto them. Ferritin extracted and purified from mammalian tissues possess heavy (H) and light (L) chain subunits in the same quaternary structure, and their exact molecular weight and composition is diverse among different species and organs that they were isolated from, while the bacterial ferritins consist of only one type of subunit. The H-chain was found to facilitate the initial binding then oxidation of cellular iron. The L-chain subsequently contributes to the nucleation of ferrihydrite allowing it to migrate into the ferritin cage (Theil, 2013). Furthermore, the structural identity of the protein revealed eight C₃ channels with hydrophilic properties and six C₄ channels with hydrophobic properties (Jiang et al., 2020). An illustration of the ferritin structural details is shown in Figure 1.2.

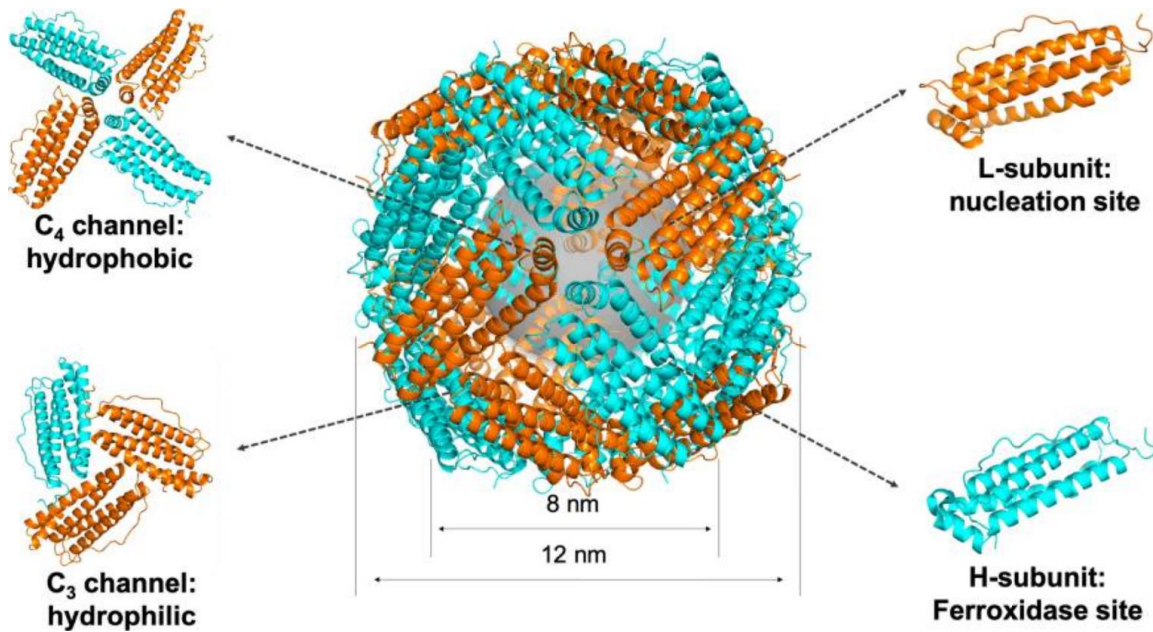


Figure 1.2. Ribbon representation of human ferritin. The structure of ferritin resembles a 24-mer self-assembled symmetrical cage protein with 8 and 12 nm diameter dimensions, two types of chains (heavy and light) and two channels (C₃ and C₄) (PDB: 5N27). Reproduced with permission under CC license from (Jiang et al., 2020).

Ferritin contributes to the reversible iron homeostasis in the cell and reduces oxidative stress (Orino et al., 2001). The excessive concentration of iron, Fe (II), in the cell leads to iron toxicity and results in the rise of reactive oxygen species (ROS) since iron catalyzes the Fenton reaction producing ROS that causes cell death (Kajarabille & Latunde-Dada, 2019). To avoid iron participation in this redox reaction, ferritin's primary function is to trap iron Fe (II) into the interior cavity of the protein's spherical cage to oxidize it to insoluble Fe (III) and store it in this non-toxic form until it is needed by the cell. The core stores iron as the inorganic ferrihydrite abbreviated by (FeOOH)_x and it could also contain phosphate. The interior centre of ferritin is a crucial part of the overall protein design since each capsule has the capacity to accommodate up to 4500 iron atoms inside the inner cavity (Harrison, 1986). The iron-free spherical protein shell version of ferritin is termed Apoferritin.

Ferritin is water-soluble and remarkably stable at extremes of pH and temperature conditions. The pH range where ferritin functions well while remaining in its quaternary structure is pH 3-10. A complete declustering of the 24-mer ferritin capsule assembly to monomers was recorded only at pH 2 and 11 (Zang et al., 2017). Moreover, this protein is thermostable, where some ferritins can endure high temperatures up to 85 °C (Schoonen & Van Hest, 2014).

Commonly, ferritins have a relatively acidic isoelectric point (pI) of 5.0-6.0, because their interior surfaces are rich with aspartate and glutamate which results in negative net charge of the interior cage (Zang et al., 2017). However, the exterior surface is not as acidic. Studies have shown that the net charge of the ferritin exterior shell is close to neutral or a little positive when at pH 7.0 (Zhao, 2010), (Figure 1.3). The acidic environment of the cavity makes it possible for positively charged nanoparticles, metal ions, or therapeutic organic molecules to diffuse through the nanopore channels of the ferritin shell via electrostatic interaction. This feature raises interesting, and also vital applications in the nanomaterials and medicinal chemistry disciplines.

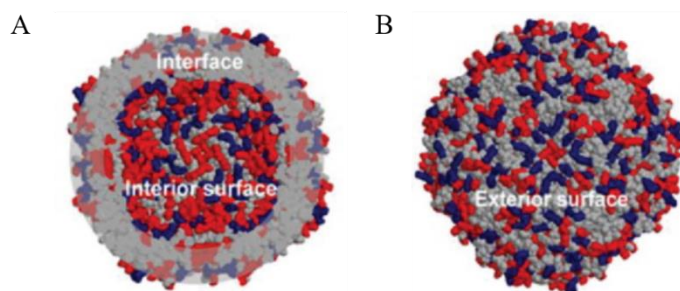


Figure 1.3. Interior surface of ferritin has a net negative charge, indicated by the dominant red color of the acidic amino acid residues. B) Exterior surface of ferritin with a charge close to neutral. Reproduced with permission under CC license from (Zhao, 2010).

The members of the ferritin superfamily acquire their name based on the organism from which the ferritin was isolated, such as human heart ferritin, horse spleen ferritin, bacterioferritin

(from *Escherichia coli*), *Pyrococcus furiosus* ferritin, and *Archaeoglobus fulgidus* ferritin. For years, the research in the Honek laboratory has focused on studying and exploring different subtypes of ferritin to construct potentially useful nanomaterials. In our research, horse spleen and *Pyrococcus furiosus* ferritins were the focus and will be discussed in further detail.

1.1.2 Description of Horse Spleen Ferritin and its Structural Features

The very first kind of the ferritin protein was discovered and isolated in 1937 from equine spleen by developing a unique purification method that employed cadmium sulphate salt precipitation (Laufberger, V. 1937). The crystal structure of horse spleen ferritin (HSF) was not solved until 1991, revealing two types of subunits with a high degree of homology, the H-chain and L-chain with a molecular weight of 21 and 19 kDa respectively, assembled to create a 24-meric capsule with octahedral symmetry (Lawson et al., 1991).

HSF is exceptionally stable under many different conditions. Therefore, it remained a good choice as a capsule protein for biochemical studies. HSF can preserve its quaternary structure, resisting denaturants such as urea and guanidinium chloride (GdnHCl) up to 6.0 M in the aqueous solution (Listowsky et al., 1972). More interestingly, the dissociation of HSF subunits was found to require 7.0 M of GdnHCl at pH 7.5, which is a sufficiently high concentration to denature a wide range of proteins (Listowsky et al., 1972).

The exterior surface of horse spleen ferritin provides a framework of various amino acid residues as reactive sites that can undergo cross-linking reactions in order to modify the surface of the protein. Lysine residues are commonly targeted for protein surface modification, in addition to cysteine residues. HSF is abundant with surface-exposed lysine residues. It was found that HSF

has a total of nine lysine residues in each subunit (PDB: 5ERK), three of which (K83, K97, K104) are exposed on the outer shell and available for modification (Figure 1.4).

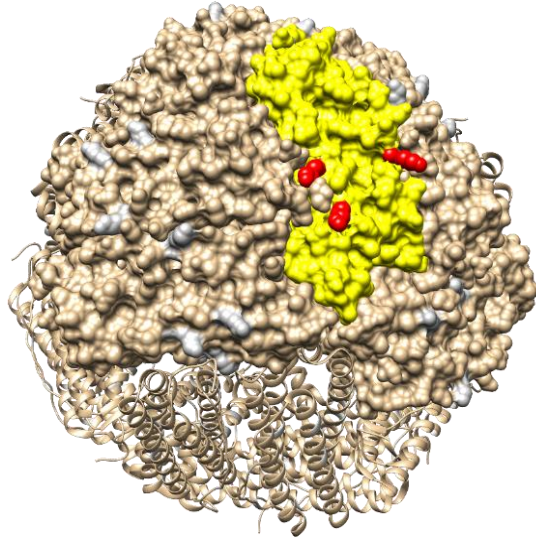


Figure 1.4. Structural model representation of one HSF subunit coloured in yellow, with 3 lysines coloured in red, exposed to the exterior surface. Structure was created using Chimera software employing protein structure PDB: 5ERK.

1.1.2.1 Carbohydrate Composition of Ferritin

It is well established that a variety of proteins undergo post-translational modifications to form a mature protein product following the biosynthesis by ribosomes. Glycosylation is a type of post-translational modification that is present in ferritin proteins isolated from different tissue sources. The carbohydrate content is essential in many protein-based biopharmaceutical drugs and intracellular proteins, where the sequence, number of glycans, and their correct attachment to the amino acids are crucial for targeting functionality, immunogenicity, folding, stability, and pharmacokinetics of the drug (Zhong & Wright, 2013).

Studies have reported that horse spleen ferritin is a glycoprotein, hence it possesses microheterogeneity in its structure (Arosio et al., 1978) (Urushizaki et al., 1971). For instance, ferritin can bind to the lectin, Concanavalin A, a mannose/glucose binding protein, which confirms that carbohydrates are present. Another clue that supports the heterogeneity of ferritin is an earlier isoelectric focusing study conducted on ferritin isolated from different horse organs. This work revealed several discrete and heterogenous isoelectric bands ranging from 4.1 to 5.1 (Arosio et al., 1978), that is close to a previous pI range of 4.22 to 4.6 obtained by Urushikazi and colleagues (Urushizaki et al., 1971). The change in the isoelectric point could be a manifestation of post-translational modification, and then to protein heterogeneity (Arosio et al., 1978).

Qualitative and quantitative analyses have targeted the carbohydrate residues on horse spleen ferritin to explore their exact composition and number. Research reported by Shinjyo et al. discovered 15 molecules of hexose, 10 of fucose, and 1 hexosamine on each ferritin molecule (Shinjyo et al., 1975). Several different methods were employed to determine the number of hexoses, fucoses, and hexosamines and included the phenol/H₂SO₄ method, the Gibbons method, and the Blix method, respectively (Shinjyo et al., 1975). To discover the identity of the hexoses that were present, techniques such as thin layer and gas chromatography were employed with comparison to known standards, and analysis of the data showed that both epimers, mannose, and galactose are present in a molar ratio of 2:1. The study observed a different number of determined hexoses per mole of molecules when the ferritin structure is disrupted. The intact horse spleen ferritin showed a quantity of 15 hexoses, which increased to 25 hexoses after denaturation. Shinjyo et al. suspects that the denaturation of the ferritin has enabled all the hexose residues to be released from the protein shell (Shinjyo et al., 1975). This leads to microheterogeneity of the capsule protein surface since fucose and hexosamine represent less than 1 carbohydrate residue per subunit. As to

the carbohydrate composition, ferritin has non-identical subunits, by which the distribution of carbohydrate residues varies in each subunit.

Other studies also detected the presence of carbohydrate attached to the protein, but with some variation. A research report by Munro & Linder indicated that the carbohydrate molecular composition in the same protein was comprised of: 16 hexoses (6 mannose and 10 galactose), 7 fucose, and 38 glucose residues comprising 2.4% of the total molecular weight of the spleen and liver apoferritin (Munro & Linder, 1978). Both ferritin and apoferritin were reported to have the same carbohydrate composition. It was suspected that these carbohydrate molecules are added only to ferritin subunits that are made by membrane-bound ribosomes and that is due to the presence of glycosylation enzymes near the endoplasmic reticulum membrane (Munro & Linder, 1978).

Glycosylation has been found to be associated with ferritin L-chains only. The carbohydrates lay at the exterior of the assembled protein, according to previous experimental work (Harrison, 1986). Each horse spleen ferritin subunit has a single N-linked glycosylation (Harrison, 1986), the type usually found in eukaryotic cells, which are commonly located at the sequence, Asn-Z-Ser/Thr where Z is any amino acid residue except proline (Zhong & Wright, 2013). Horse spleen ferritin's N-glycosylation sequence is consistent with that, by which the oligosaccharides were found to be at Asn(7)-Tyr(8)-Ser(9), (Harrison, 1986).

Raman spectroscopy was employed by a group of researchers to detect the presence of glycosylation on the horse spleen ferritin surface (Ashton et al., 2017). It is feasible to distinguish between the Raman spectra of glycosylated and non-glycosylated forms of the protein. Both quantitative and qualitative carbohydrate assessment of horse spleen ferritin proteins is achievable by Raman spectroscopy, where it was possible to have an accurate measurement for the

concentration of glycosylated ferritin using the generated spectroscopic data sets (Ashton et al., 2017).

1.1.3 Description of *Pyrococcus furiosus* Ferritin and its Structural Features

The thermally stable *Pyrococcus furiosus* ferritin (PfFtn) is a ferritin protein expressed by a hyperthermophile archaeon that is extremely stable even up to the high temperatures beyond the boiling point of water. Crystal structures of ferritin from archaea are limited. Only two ferritin protein structures from an archaeon source have been determined to date, the *Archaeoglobus fulgidus* ferritin (AfFtn) and the *Pyrococcus furiosus* ferritin (PfFtn). The PfFtn protein subunit exhibits the typical structural motif of a four alpha-helical (helices A-D) bundle (Honarmand Ebrahimi et al., 2013). PfFtn's quaternary structure is composed of 24 identical subunits, each with a molecular weight of 20 kDa, which is encountered similarly in known bacterial and eukaryotic ferritins. The PfFtn primary sequence is rich in lysine residues, with 15 lysines found in each subunit, and 10 of these lysines (K8, K75, K78, K85, K95, K99, K112, K135, K142, K145) are surface exposed for potential modification. A structural illustration of PfFtn employing PDB: 2JD7, is shown in (Figure 1.5). It should be noted that *Pyrococcus furiosus* ferritin lacks the short helix-E that is present in horse spleen ferritin and bacterioferritin (Andrews, 2010). The isoelectric focusing point of PfFtn has also been explored in prior studies. Apoferritin and iron-loaded PfFtn were both examined and had the same value of pI = 4.5 (Tatur et al., 2006), which is in the range of horse spleen ferritin's pI.

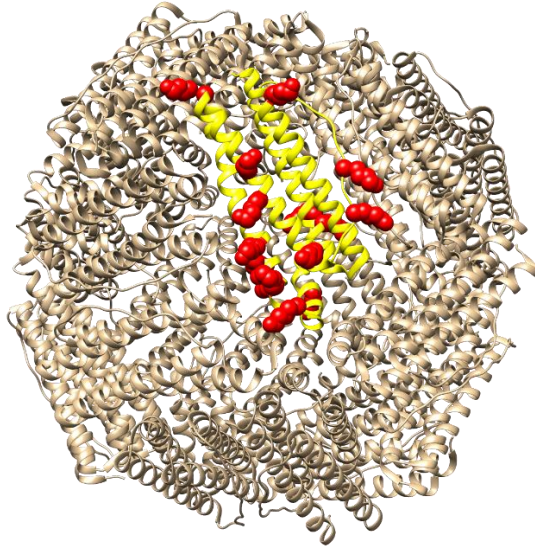


Figure 1.5. Structural model representation of *P. furiosus* highlighting one subunit in yellow. One subunit contains 10 lysine residues coloured in red, which are exposed to the exterior surface. Structure was created using Chimera software employing protein structure PDB: 2JD7.

Pyrococcus furiosus ferritin is an extremely thermostable archaeon protein that can withstand 24 hours in vitro incubation at 100 °C and autoclaving for some time at 120 °C and still maintaining its three-dimensional structure with no loss of the iron (Fe II) uptake activity (Tatur et al., 2006). PfFtn appeared to be the most stable ferritin that has been isolated so far. The thermostability of PfFtn in comparison to eight structurally similar ferritins was studied in order to investigate the factors involved in the resistance to thermal denaturation. The work done by Kannan & Vishveshwara revealed a cumulation of various factors such as hydrogen bonding, salt bridges, van der Waal interactions and the order of the primary amino acid sequence, more charged amino acid population, and fewer uncharged polar amino acids (Kannan & Vishveshwara, 2000). Other listed factors highlighted the presence of higher β -strand content, more hydrophobic β -branched amino acids (Eidsness et al., 1997). All of these factors together are believed to contribute to thermal stability of ferritin proteins, and many tend to appear in PfFtn. Furthermore, it appears that the preservation of the monomeric unit is very important to obtain protection from heat

denaturation, owing to the abundant number of intra-molecular/subunit hydrogen bonds between the atoms in the main chain and side chain (Tatur et al., 2007). Additionally, a former study by the same researcher tested the *P. furiosus* ferritin protein stability against several freeze-thaw cycles that are capable of damaging protein structure, which any biochemist is familiar with. Interestingly, the *P. furiosus* ferritin exhibited no drop in activity after three cycles (Tatur et al., 2006).

Scientists realized that the astonishing thermostability of PfFtn has an important value that is worth exploring and can effectively serve in biotechnological applications. A previous report investigated the utility of the thermally stable ferritin, PfFtn, as a biological template to synthesize inorganic nanoparticles while encapsulated inside the protein cage. The synthesis and encapsulation was achieved successfully at a temperature up to 120 °C while maintaining a capsule-like architecture of the PfFtn (Parker et al., 2008). Several studies have reported that the *P. furiosus* ferritin can be an excellent choice of template for controlled silver biomineralization (Kasyutich et al., 2010), for nano-sized palladium biocatalytic machines (Kanbak-Aksu et al., 2012), and for the efficient removal of arsenate and phosphate from drinking water (Sevcenco et al., 2015).

1.2 Bioconjugation Chemistry and Strategies

Chemical modifications of macromolecules afford powerful tools to study a broad range of complex biological systems and to develop many exciting applications in protein research, pharmaceutical science, and nanomaterial science. This makes bioconjugation chemistry an attractive and desirable scientific technique. Many strategies have been employed to link various chemical probes of interest to target native proteins in a site-selective manner. Chemical probes that can be attached to proteins, such as cross-linking reagents, affinity labels, and fluorescent

dyes, will result in protein-conjugate hybrids serving as powerful tools in proteomics related applications. Modern methodologies are being developed to exploit these versatile bioconjugation strategies for the support of human needs. As examples, fluorescent dye labelling for medical imaging (Zhu et al., 2017), prolonging therapeutic protein lifetime by polyethylene glycol surface labelling (Dozier & Distefano, 2015), or constructing protein-based biosensors (Dai et al., 2018), and more have been realized.

Visualization of live cellular processes such as protein expression levels, trafficking, and the change in protein folding states, are possible by utilizing the bioconjugation techniques intracellularly. These techniques include protein fusions, tyrosine ligation, biotinylation, fluorescein arsenical helix binder (FLAsH), and many others, which are used to observe proteins as the biological event is occurring (Moghaddam-Taaheri & Karlsson, 2018).

Furthermore, an interesting area in bioconjugation is the development of protein-oligonucleotide conjugates (POCs) and the application of these molecules has become widespread in recent years. The bioconjugation of proteins and DNA has demonstrated novelty in the area of bionanomaterials. Given the fact that the DNA is a programmable molecule, it allows the integration of multivalent peptides to be displayed in the biomaterial, in addition to the ability to control the nanoscale spacing between the multiple peptides within this scaffold. The peptide-targeted binding is directed by employing a heterobifunctional cross-linker to link peptides on one side, via the cysteine thiol group of one peptide, with the DNA molecule on the other side that has a complementary nucleotide functional group on the DNA targeting end (Stephanopoulos, 2019) (figure 1.6).

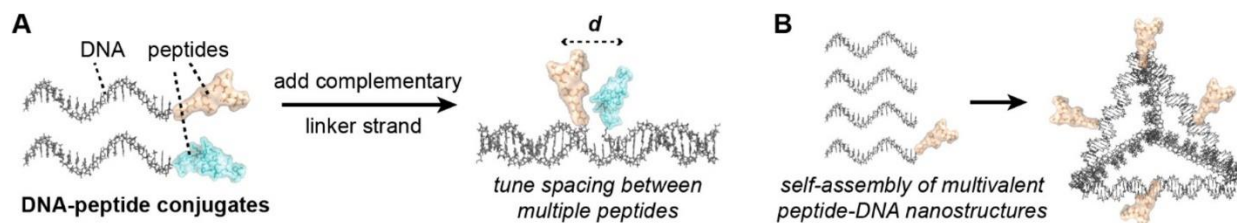


Figure 1.6. DNA-peptide biomaterials. A) DNA-peptide bioconjugate. B) A self-assembled tetrahedral cage of DNA strands, manifesting peptide conjugation to the DNA scaffold. Reproduced with permission from (Stephanopoulos, 2019).

Materials scientists are attentive to strategies being implemented in biochemistry. Research in numerous areas is being undertaken to produce materials with biomimicry properties by utilizing biological ligands, by which a popular application is in the area of advanced hydrogels. For example, a novel hydrogel material was fabricated using a polymer precursor that contains the maleimide group. The maleimide served as a dual-purpose functional group, where first it enabled the hydrogel fabrication through photochemical cross-linking under UV radiation to yield a micropatterned matrix material (Figure 1.7) (Cengiz et al., 2020). Then, the free maleimides in the hydrogel served as a bioconjugation tool to functionalize the hydrogel through thiol-Michael addition or Diels-Alder cycloadditions reactions (Figure 1.7) (Cengiz et al., 2020).

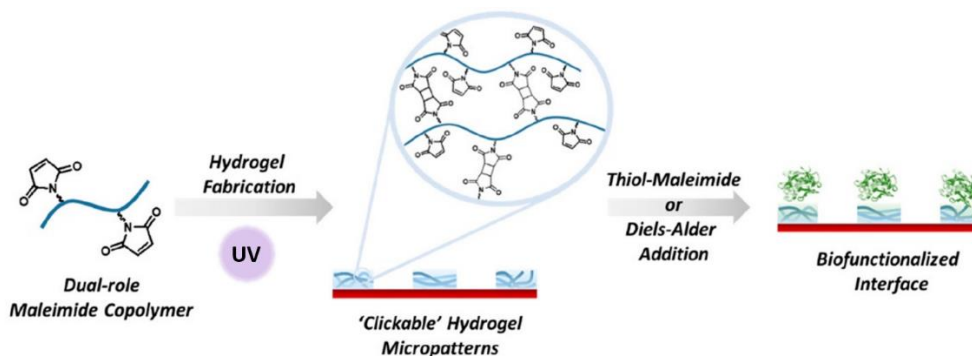


Figure 1.7. Fabrication and functionalization of hydrogel networks through maleimide bioconjugation. Reproduced with permission from (Cengiz et al., 2020).

There are many reactive amino acids in proteins that can be chemically modified such as, aspartate, arginine, cysteine, glutamate, histidine, lysine, tyrosine, and the N-terminus of a protein (Figure 1.8). Understanding the chemical characteristics of amino acids enables efficient chemo-selective incorporation of foreign molecules or synthetic probes onto target sites of a native protein scaffold affording a functional nanomaterial, through bioconjugation at these amino acid side chains. Exploiting this approach is of interest to the current research described in this thesis.

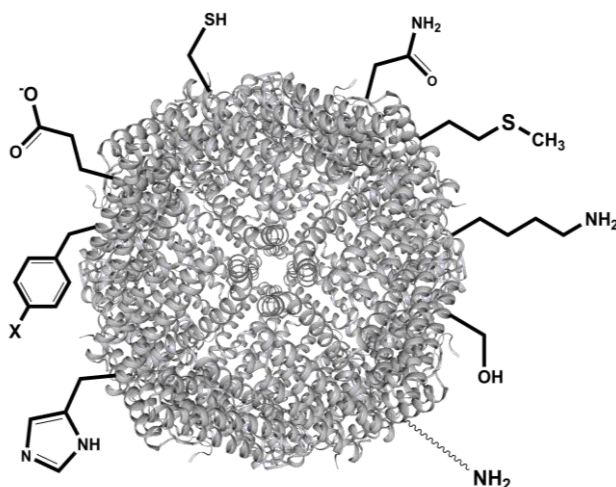


Figure 1.8. Representation of protein side chains subjected to surface conjugation through reactive amino acid residues. Image generated by software program Chimera using PDB: 5ERK.

1.2.1 Lysine Modification

The lysine side chain is one of the most frequently modified residues in bioconjugation reactions, due to their rich abundance in proteins constituting 5.9% of the sequence of human proteins (Matos et al., 2018). The reactive handle of lysine is the ϵ -amino group, which can be efficiently modified with the use of activated esters, isocyanates, isothiocyanates, sulfonyl chlorides, along with reductive aminations (Tamura & Hamachi, 2019). To obtain the optimum

conjugation yields, lysine modifications are carried out under basic conditions of $\text{pH} > 8$ to allow the amine group ($\text{pK}_a = 10$) to become deprotonated and thereby nucleophilic. The nucleophilic attack by lysine residues will drive the formation of a new bond on the protein (Koniev & Wagner, 2015).

Lysine modifications are random under standard conditions which utilize 100-fold or greater excess of reagent to the target protein. Heterogeneous products with different degrees of modifications are observed, and this strategy is implemented in various major applications. However, there exist strategies to produce homogeneously lysine-modified products (Nanna et al., 2017), and other site-selective methods aim for a single-modified amino group, but they usually demand an extensive primary sequence engineering or restricting the modification to the N-terminus of the native protein. A phenomenon has been proposed that in some systems, lysine residues exhibit a local pK_a variation, so with intentional control of the ambient pH , a lysine residue of interest is selected for conjugation. More interesting is a report that employed a computational-based study wherein a theoretical reagent (sulfonyl acrylate) could be predicted to yield a homogenous product with a single-lysine conjugation under standard conditions using a one-molar equivalence of reagent (Matos et al., 2018). This investigation revealed the exclusive chemoselectivity towards lysine amino acids and other nucleophilic residues, such as cysteine, if present, because of the stable intermediate formed by hydrogen bonding between the lysine amino group and the sulfonyl moiety of the reagent (Matos et al., 2018).

1.2.2 Cysteine Modification

The side chain of the amino acid cysteine is highly nucleophilic and is relatively low in abundance in proteins; existing with a genome-wide percentage of only 2.3% (Tamura & Hamachi, 2019). The nucleophilic thiol of cysteine can be modified via thiol alkylation (Michael addition)

using maleimide or α -halocarbonyl electrophiles. It is important to have well-reduced thiol groups by using reducing agents such as dithiothreitol (DTT) or tris-2-carboxyethyl phosphine (TCEP) prior to initiating the modification due to the propensity for air oxidation of cysteine to its disulfide form. It is also important to ensure that these agents are completely removed from the reaction mixture to avoid competition with reagents targeted primarily to modify cysteines (Kim et al., 2008).

Cysteine targeted modifications are excellent choices for chemoselective bioconjugation to afford selective cross-linking. At some conditions, such as the relatively high or low pH range, or the presence of a high concentration of thiol-containing nucleophiles around modified cysteine residues, the maleimide and the α -halocarbonyl-based reagents could be less efficient (Vinogradova et al., 2015). As a result, a number of approaches were developed in the literature utilizing transition metal-based reagents that have demonstrated efficiency in cysteine modifications and exhibited superior reaction kinetics, where less than five minutes reaction time in a pH range varies from 0.4 to 14 was reported to be successful (Messina et al., 2018). More importantly, as the aqueous environment is commonly chosen for bioconjugation reactions, a judicious choice of the organometallic ligand can afford water solubility (Vinogradova et al., 2015).

1.2.3 Polyethylene Glycol Polymers

Polyethylene glycol (PEG) is a water-soluble polymer chain consisting of repeating units of the basic hydrophilic ethylene glycol molecule (-CH₂-CH₂-O-). The structure is shown in (Figure 1.9). PEGs are highly mobile and flexible, and they have excellent water solubility (Ensing et al., 2019). This property is explained by the high density of oxygens, which are the hydrogen acceptor atoms. The use of PEG reagents of various free ending molecules has become a leading

and an acknowledged approach for the modification of proteins, peptides, or nucleic acid in the bioconjugation chemistry field due to the numerous biochemical advantages that PEG can confer. This method has been used for decades in bioconjugation reactions and is known as PEGylation.

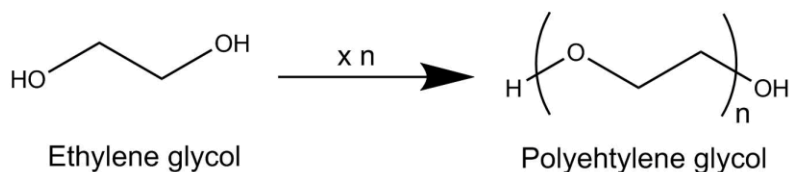


Figure 1.9. Chemical structure of poly(ethylene glycol) (PEG).

Polyethylene glycol molecules are also used extensively in nanomedicine. The PEG conjugated to proteins can reduce immunogenicity and create a molecular shield against proteases. In other words, it reduces the protein antigenicity, which refers to the recognition of a foreign invader by the immune system (Xiao et al., 2019). A hypothesis suggests that PEGylated proteins have more conformational stability, in comparison to the non-PEGylated counterpart. It has been suggested that the strength of protein salt-bridges is increased due to the presence of nearby conjugated polyethylene glycol (Xiao et al., 2019). More interestingly, different PEG reagents can serve as tethers of various short or long lengths to couple between molecules and surfaces to produce robust cross-linked materials and cellular sensors (Attwood et al., 2016).

A study performed by He and colleagues has demonstrated the novelty of PEGylated ferritins. Ferritin protein was encapsulated with nanoparticles (NPs) in the interior cavity and surface modified at the exterior cavity with PEG spacers of a defined molecular weight and length to create a bionanomaterial system of a two-dimensional composite that consists of ferritin-PEG molecules separated by controlled distances which were dependent on the length of the PEG attachment (He et al., 2013). This strategy was reported to be useful in the design of functional

devices requiring incorporated nanoparticles with the advantage of having controllable distances between NPs (He et al., 2013).

PEG modifiers are molecules of immense utility as thousands of literature articles have addressed them as typically being the better choice for numerous bioconjugation designs, according to a long scientific track record (Hermanson, 1996). The standard conjugation of PEG with proteins is achieved by incubating the target protein with a known molar ratio of the PEG derivatization reagent in a studied biochemical aqueous environment.

1.3 Protein Networks

Among the myriad of bio-building blocks found in nature, proteins possess a phenomenal range of structural and functional properties that have allowed them to participate as extremely effective molecular constituents to design a wide range of sophisticated biomaterial assemblies. Nature has first exploited proteins' architectural properties to construct bio-networks, by which countless examples are naturally manifested, for instance, the bacterial microcompartments (BMCs), toroidal oligomerizations, microtubule scaffolds, viral capsids, S-layer protein self-assembled lattices, and many more (Pieters et al., 2016). These assembled nanomachines perform critical roles in bacteria, viruses, and eukaryotic cells. Scientific advancements in understanding the highly-ordered assembly mechanisms that lead to structure formation have enabled the current creation of novel protein networks, that are utilized by humans for numerous bionanotechnological applications. Protein networks are capable of performing versatile functions such as biocatalysis, bioenergy, cargo delivery, vaccine development, and synthesis of hybrid materials (Howorka, 2011).

1.3.1 Roles of Protein Networks in Nature

Bacterial microcompartments are critical proteinaceous organelles produced by bacterial cells and essential for the bacterial cell's metabolism (Figure 1.10) (Yeates et al., 2013). Sequentially functional enzymes are evolutionarily encapsulated within the thin protein shell of a BMC. For example, the carboxysomes organelles, are BMCs found in cyanobacterium. They contain numerous ribulose-bisphosphate carboxylase (RuBisCO) enzymes that capture and process carbon dioxide, and carbonic anhydrase (CA) enzymes essential in catalyzing the reversible conversion of CO_2 and H_2O to bicarbonate anions that diffuse into the BMC. Both are important in carbon fixation processes and are used to produce energy-rich organic molecules, e.g. glucose (Long et al., 2018).

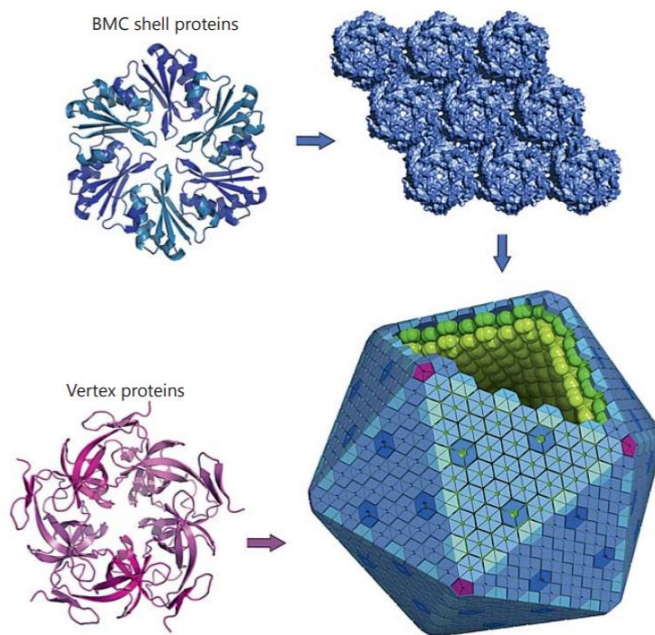


Figure 1.10. A representation of natural three-dimensional supramolecular protein networks. Polyhedral bacterial microcompartment (BMC) made of a few thousands BMC shell and vertex proteins. Reproduced with permission from (Yeates et al., 2013).

The S-layer (surface layer) scaffolds are found ubiquitously in life forms as a component of several Gram-positive and Gram-negative bacteria, and in all archaeal cell wall envelopes (Sára & Sleytr, 2000). These scaffolds have been characterized under the electron microscope as highly porous crystalline arrays of a mono-molecular thickness of typically 5-70 nm, and consist of proteins or glycoproteins (Gerbino et al., 2015). Their biological role is essential as a protective layer from the outer harmful environment including the change in peripheral pH levels (Alp et al., 2020), protection against mechanical threats, and thermal stabilization especially by the glycosylated protein constituents of the scaffold (Klingl, 2014). The importance of protein S-layers in bacteria has also been attributed to the removal of toxic metals and radionuclides from the polluted sediments and soils by biosorption and bioaccumulation mechanisms (Gerbino et al., 2015). An illustration of a self-assembled supramolecular S-layer produced by *Lysinibacillus sphaericus* bacterium is depicted in Figure 1.11 (Baneyx & Matthaei, 2014).

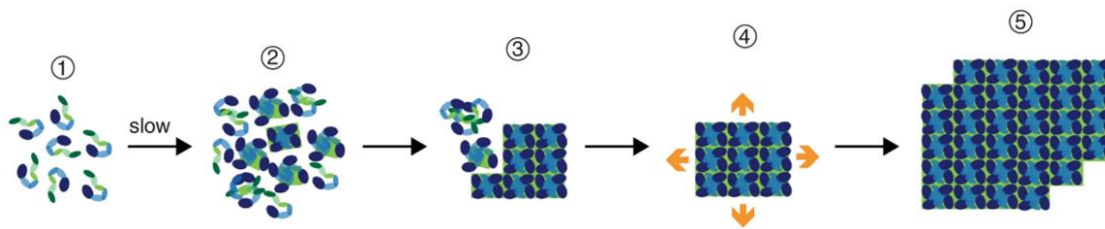


Figure 1.11. An example of naturally occurring protein network. Self-assembled two-dimensional S-layer protein lattices. Reproduced with permission from (Baneyx & Matthaei, 2014).

Toroidal oligomers are another interesting category of supramolecular self-assembled proteins associated with key roles in cellular processes such as DNA replication and RNA transcription of the human genome (Li et al., 2020). They resemble circularly assembled proteins wide enough to accommodate DNA strands (Figure 1.12). The ring-shaped protein structure of

toroidal proteins was found to function in increasing DNA synthesis processivity by binding to DNA polymerase during replication and at the same time encircling the double-stranded chain of DNA (Li et al., 2020). The amazing toroidal circular shape is also found in a class of antioxidant enzymes called peroxiredoxins. Arrays of cysteine-dependent quaternary-level proteins self-assemble to create peroxiredoxins that control cellular redox states by scavenging peroxides (Yewdall et al., 2018).

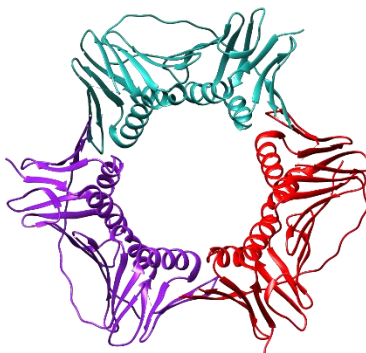


Figure 1.12. X-ray structure of a toroidal protein, an example of naturally occurring protein network. Generated using Chimera software (PDB: 3P91).

1.3.2 Biotechnological Applications

The detailed mechanisms by which self-assembly occurs for naturally existing scaffolds are yet not fully understood. Nevertheless, the process of self-assembly is driven by the thermodynamics of the constituents, and involve a combination of van der Waal forces, dipole-dipole interactions, the hydrophobic effect, hydrogen bonding, electrostatic interactions, and entropic forces. Given current knowledge on protein rational design, scientists are actively pursuing the design of protein networks for useful applications in bionanotechnology.

Considerable nanotechnological applications of recombinant S-layers were first reported in 1986 by Sleytr and Sára, by which the S-layer protein lattices were utilized to produce ultrafiltration porous membranes with tailored molecular sieving properties (Sleytr & Sára, 1986). Since then, bionanotechnological research has exponentially developed protein networks inspired by the bacterial S-layers topology. Immobilized biocatalysts, biotinylated ligand binding, and sensing materials for diagnostics, are all functional applications developed from those protein fusions (Sleytr et al., 2014). More interestingly, a multilayered protein bio-battery model was designed by the use of two types of the self-assembled ferritin protein, $\text{Fe}(\text{OH})_2$ iron-loaded and $\text{Co}(\text{OH})_3$ cobalt loaded ferritins (Watt et al., 2012). The biochemical properties of ferritin proteins, in addition to their structural properties, have demonstrated the feasibility of employing this building block in the fabrication of nanoscale energy storage systems (Watt et al., 2012). Furthermore, the advantages obtained by the complexity and structural diversity afforded by protein networks were also exploited to mimic cellular catalytic reactions within synthetic protein networks. Previous research has reported on the development of biocatalytic nanomaterials by site-specific conjugation of enzymes or other catalytic systems onto protein scaffolds (Yokoi et al., 2011). For example, it was reported that a multienzyme platform consisting of a triple stranded β -helical fusion protein, dually modified on the surface at lysine and cysteine residues with $\text{Re}(\text{I})$ and $\text{Ru}(\text{II})$ metal complexes respectively (Figure 1.13), resulted in the fabrication of a protein scaffold with a robust photoreductase activity that yielded higher CO_2 reduction efficiency, in comparison to the lower efficiency of a mixture of the individual protein-complexes (Yokoi et al., 2011).

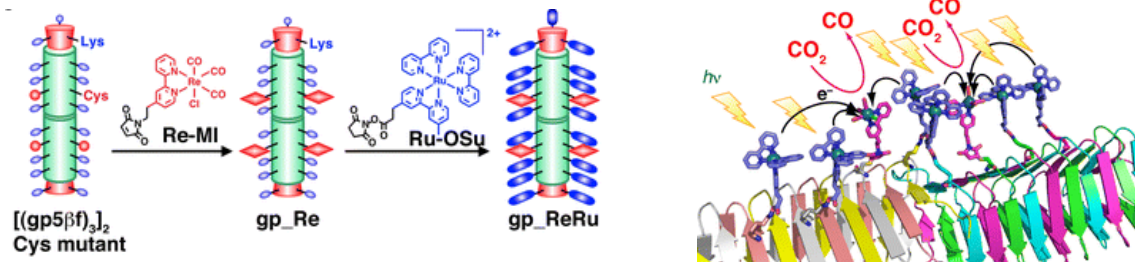


Figure 1.13. Photocatalytic complex constructed by modifying the surface residues of a beta-helical nanotube using Re(I) and Ru(II) complexes exhibits higher reactivity of the CO₂ to CO photocatalytic reduction with the multiply-modified construct. Reproduced with permission from (Yokoi et al., 2011).

Enzyme nanocomposites (ENC) are feasibly developed by self-assembling two functionalized nano-dimensional proteins, streptavidin coated with horseradish peroxidase (SA-HRP) and biotinylated human ferritin capsules (bFNPs), allowing the formation of a tunable sized protein network where the biotinylated ferritin plays as the backbone of the material (Figure 1.14) for application in ENC-based immunoassays (Men et al., 2015). The size of the overall construct is tuned by the control of the bFNPs:SA-HRP stoichiometric ratio, the lower the ratio, the larger the assembled construct. The functionality of the ENC was evaluated by using it as a substituent to the typical enzyme system employed in a conventional enzyme-linked immunosorbent assay (ELISA) assay. The chemical evaluation revealed an improved sensitivity of the immunoassay up to 10,000-fold when using the ENC-based method, a signal higher than that of a conventional assay due to the larger number of enzymes conjugated to the material (Men et al., 2015). One limitation of the streptavidin analogue mediated networks is that achieving uniformity of the network can fluctuate due to the tetra-biotin capacity of streptavidin.

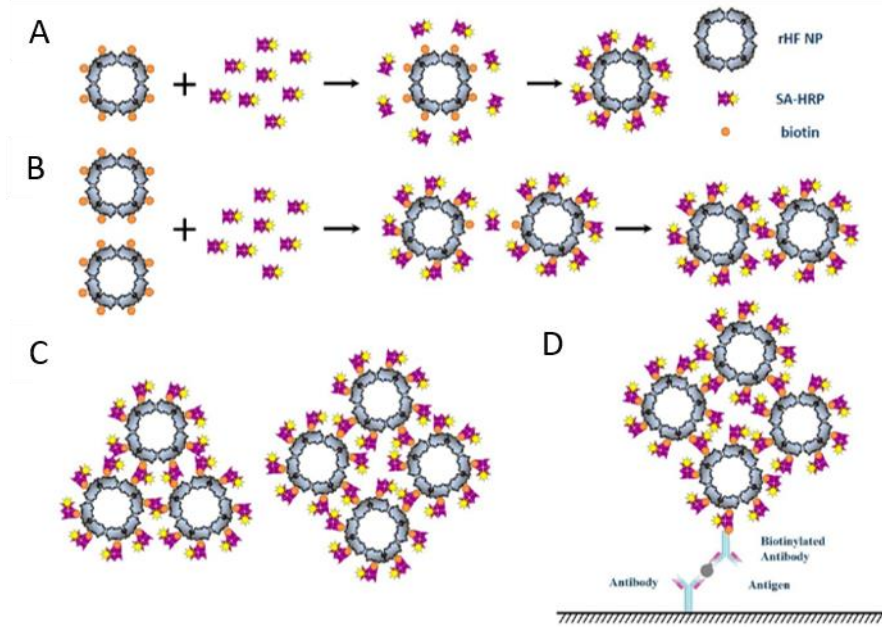


Figure 1.14. A design of an ENC using ferritin and streptavidin. A) bFNP saturation with SA-HRP. B & C) Reaction of non-saturated bFNP with SA-HRP drives the formation of dimer, trimers, and tetramers. D) A diagram of the full construct of a sensitive ENC material. Reproduced with permission from (Men et al., 2015).

1.4 Research Hypothesis

The controlled fabrication of molecular scaffolds to bind with drugs, catalysts, and enzymes, among other molecules, is an important area of current research, with applications in the areas of medical imaging, therapeutics, biosensors and immobilizations. The current research hypothesis is that nanodimensional capsule proteins can be interconnected using the biotin-avidin affinity interaction or through the maleimide functional group bioconjugation, to produce advanced molecular scaffolds that can be employed to bind and position photocleavable drugs, fluorophores, and enzymes onto and perhaps within the network. An illustration of the project full scheme is shown in Figure 1.15. These protein networks will be investigated employing a variety of techniques including mass spectrometry, electron microscopy, photochemistry, and enzyme kinetics.

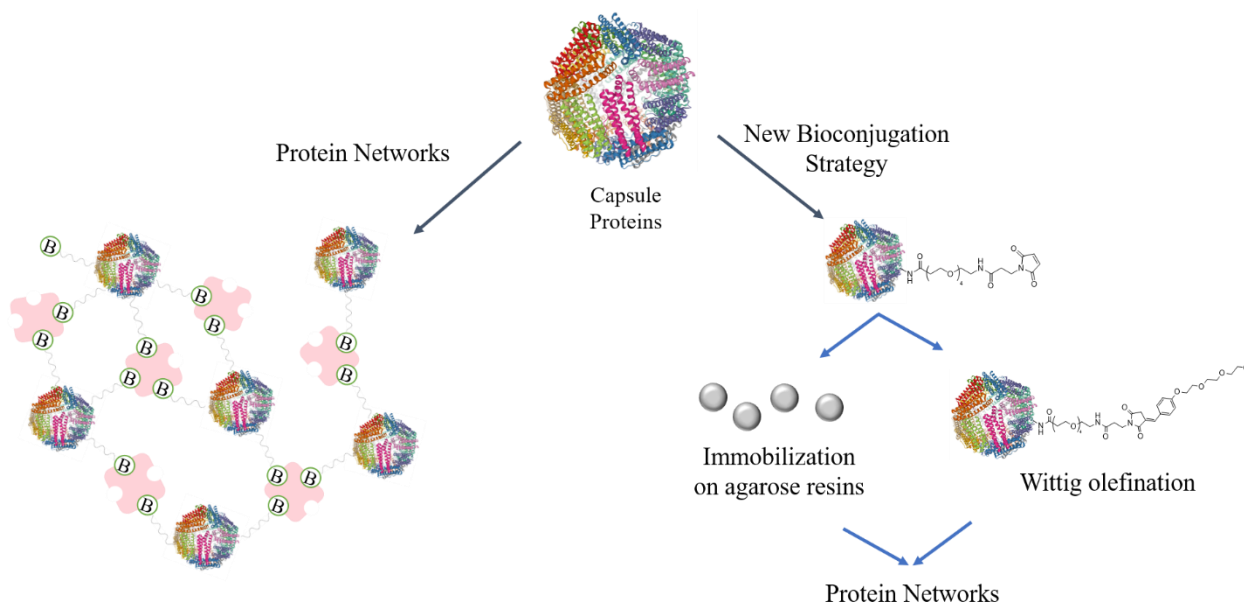


Figure 1.15. An overview of the thesis project scheme that involves the fabrication of protein networks and the development of a new bioconjugation strategy.

2 Chapter 2: Protein Network Design and Fabrication

2.1 Background

2.1.1 Avidin-biotin Interaction

Avidin is a homotetrameric biotin-binding glycoprotein expressed and deposited in the egg whites of several animals, and especially birds. The molecular weight of avidin is 67,000 Da and it was shown to have a basic pI of 10.5 (Jain & Cheng, 2017). The X-ray crystallographic structure of avidin revealed four identical monomers each of which consists of a 128 amino acid polypeptide chain comprising a sequence that is directly involved in the biotin-binding site as shown in Figure 2.1. Biotin, also known as vitamin H or vitamin B₇, is a water-soluble molecule (MW: 244.3 g/mol) and is involved in various metabolic processes in living cells. Biotin has been extensively associated with polyethylene glycol reagents as (R)_x-PEG_x-biotin for applications in biotechnology and molecular bioassays (Koniev & Wagner, 2015).

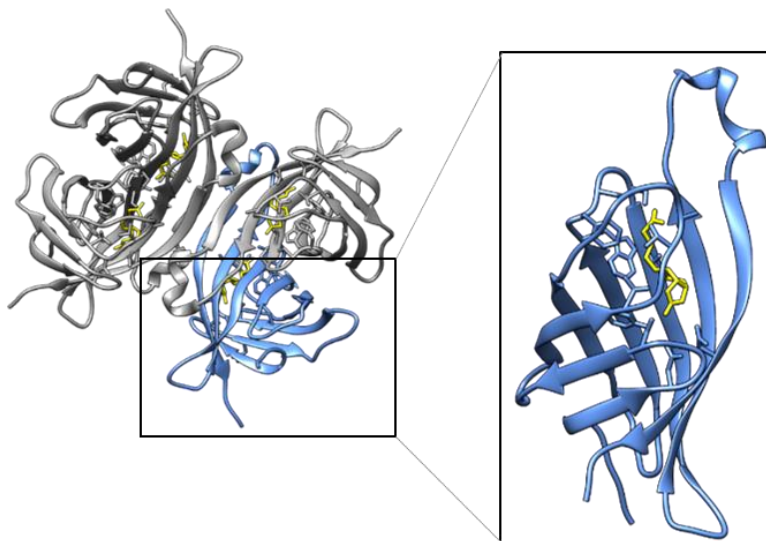


Figure 2.1. Crystal structure of tetrameric avidin (PDB: 2AVI) with emphasis on the biotin binding site in one subunit. The structure was generated using Chimera employing the protein structure code PDB:1AVD.

Numerous studies have demonstrated the significance of the “avidin-biotin” affinity interaction as a definitive breakthrough (González et al., 1999) (Jain & Cheng, 2017). It was determined to be the strongest non-covalent interaction in nature. Avidin’s binding pocket has an exceptional specificity and affinity to biotin molecules, as the dissociation constant (K_d) was determined to be 10^{-15} M (Jain & Cheng, 2017). The avidin-biotin complex is resistant to extremes of pH values, proteolytic enzymes, and declustering reagents (Hermanson, 1996) (Huberman et al., 2001) (Jain & Cheng, 2017). Moreover, the complex is resistant to a temperatures reaching 117 °C when avidin is fully saturated with biotin (González et al., 1999). The high-affinity interaction of biotin and avidin has been exploited in numerous applications in biotechnology such as diagnostics, affinity purification, biomolecular labelling, and successful contributions in tissue engineering research (Clapper et al., 2008). The strength of the avidin-biotin interaction appears in mimicking the strong antibody-antigen interaction; however, it is even stronger by $10^3 - 10^6$ times (Jain & Cheng, 2017). Biotins that are bound to the free binding sites of avidin are illustrated in yellow (Figure 2.1) residing non-covalently and tightly in the binding pocket of avidin subunits. Structural investigations of avidin monomers (PDB: 1AVD) revealed a classic β -barrel composed of eight anti-parallel right-handed twisted β -sheets (Figure 2.1) (Strzelczyk et al., 2013), where biotin is located at the wide end of the monomeric β -barrel.

Figure 2.2 is an illustration of the six hydrogen bond interactions that take place at the binding site of avidin. Three H-bonds form at the ureido oxygen atom with residues Asn12, Ser16, Tyr33, two H-bonds with the ureido nitrogen atom with residues Thr35 and Asn118, and one H-bond at the sulfur atom with (Thr77) (Huberman et al., 2001). The valeryl carboxyl moiety is also heavily involved in the H-bonding and contributes to the tight affinity (Livnah et al., 1993).

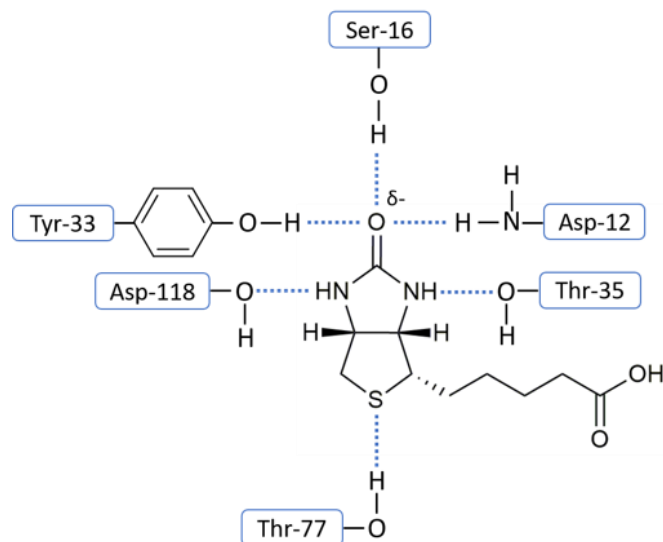


Figure 2.2. Biotin molecule representing the six hydrogen bond interactions that take place at the binding site of avidin.

As a glycosylated protein, avidin was found to possess a significant carbohydrate composition which consists of four to five mannose residues (MW: 180 g/mol) and three N-acetylglucosamine residues (MW: 221 g/mol) per subunit which constitutes up to 10% of the overall protein molecular mass, about 1,383-1,563 Da of carbohydrates in each subunit. The oligosaccharide content has no contribution to biotin binding to avidin (Hiller et al., 2015).

Equally important are two avidin derivatives that have very similar structures to avidin and were studied for their exceptional biotin-binding affinity. Streptavidin, a non-glycosylated protein isolated from bacterium *Streptomyces avidinii*, and the protein NeutrAvidin, which is an artificially produced deglycosylated form of avidin protein with a lowered isoelectric point (Livnah et al., 1993) (van Roy et al., 1993). A comparison of these three analogues is shown in Table 1.

Table 1. Comparison of biotin-binding proteins.

	Avidin (chicken)	Streptavidin (recombinant)	NeutrAvidin (avidin)
Molecular weight	67 kDa	53 kDa	60 kDa
Biotin-binding sites	4	4	4
Isoelectric point (pI)	10.5	5	6.3
Dissociation constant (K_d)	10^{-15} M	10^{-14} M	10^{-15} M
Cost per 10 mg	\$90.00 CAD ¹	\$712.00 CAD ¹	\$277.00 CAD ²

¹ Bioshop, Canada; ² ThermoFisher, Canada. Supply issues with Neutravidin were experienced

2.1.2 Cutinase Enzymes for PET Degradation

The protein cutinase is a hydrolase enzyme found in both bacteria and fungi species. Cutinase is secreted to catalyze the hydrolysis of ester bonds found in cutin, the main component of the cuticle that covers the surface of plants as a protective layer (Chen et al., 2013).

Several studies have begun to examine cutinases as industrial biocatalysts, particularly for their activity towards performing ester hydrolysis that serves the area of waste biodegradation (Chen et al., 2013). A recent study has determined that the enzyme cutinase, *Humicola insolens* cutinase (HiC) (Figure 2.3A), was able to display catalytic activity against poly(ethylene terephthalate) (PET) consumer plastic, a widely utilized thermoplastic polyester, causing a significant plastic degradation when examined under electron microscopy (Carniel et al., 2017). The active site of the HiC enzyme employs a serine catalytic triad, and is capable of the depolymerization of PET polymers into three compounds (Figure 2.3B, C & D), bis(hydroxyethyl)terephthalate (BHET), monohydroxyethyl terephthalate (MHET), and terephthalic acid (TPA) (Carniel et al., 2017).

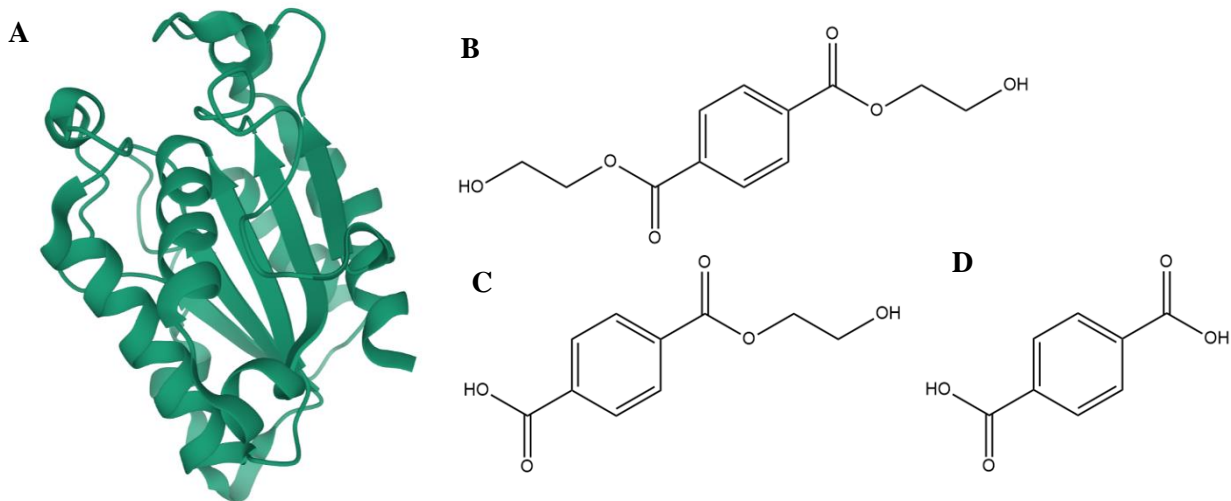


Figure 2.3. A) Ribbon representation of HiC enzyme (PDB: 4OYY). The chemical structure of PET degradation products: B) BHET, C) MHET, and D) TPA.

2.1.3 Photocleavable Biomaterials

Photocleavable agents are molecules serving as a bioconjugation reagent that links between two molecules and which can undergo decomposition of their molecular structures upon irradiation with light, generally ultra-violet light being employed for this purpose (Gomes & Gozzo, 2010). The functional groups of the photocleavable cross-linkers employed in the fabrication of photolytic materials can contain functional groups such as carbamate, carbonate, ester, or amide moieties. Particularly, photolabile cross-linking moieties follow any of the following classes; nitrobenzyls (NB), coumarins, disulfides, azo sulfonates, pyrene esters, metal-metal bonds, and vinyl ketones (Pasparakis et al., 2012), which possess variations in terms of their cleavage behavior. These materials are studied especially for their potential applications in the fields of tissue engineering, controlled drug delivery, therapeutics, biosensing, waste management, and food science (Levalley et al., 2020). A study of a photo-triggered drug release from a hydrogel material was researched by Härtner and colleagues. In their study, the model drug chlorambucil was covalently attached to

a photocleavable linker with a dicoumarin moiety via an ester bond into a methyl methacrylate polymer-based hydrogel. The findings presented a successful release of the drug from the hydrogel system upon UV irradiation (Härtner et al., 2007).

Concurrently, the heterobifunctional PEG-based 3D hydrogel materials with nitrobenzyl moieties are one of the most studied 3D networks in tissue engineering (Ji et al., 2017). These photodegradable hydrogel systems exhibit marked photolytic response under physiological pH, making them a perfect choice for the design of a biocompatible and tunable protein-based scaffold.

2.2 Objectives

In this part of the project, the objective is to show how to engineer a novel supramolecular protein scaffold using biotinylated multimeric ferritin capsule proteins, as a building block along with the protein avidin as a tetravalent mediator (Figure 2.4). The biotin-avidin non-covalent interaction is exploited in this context to facilitate the proximity of the capsule proteins to self-assemble the protein network. Use of the biotin-avidin affinity interaction is a strategic choice, as it resembles a highly specific interaction since it will occur independently of the protein's physical characteristics, e.g. hydrophobicity, or its chemical characteristics, e.g. surface charge, of the network constituents.

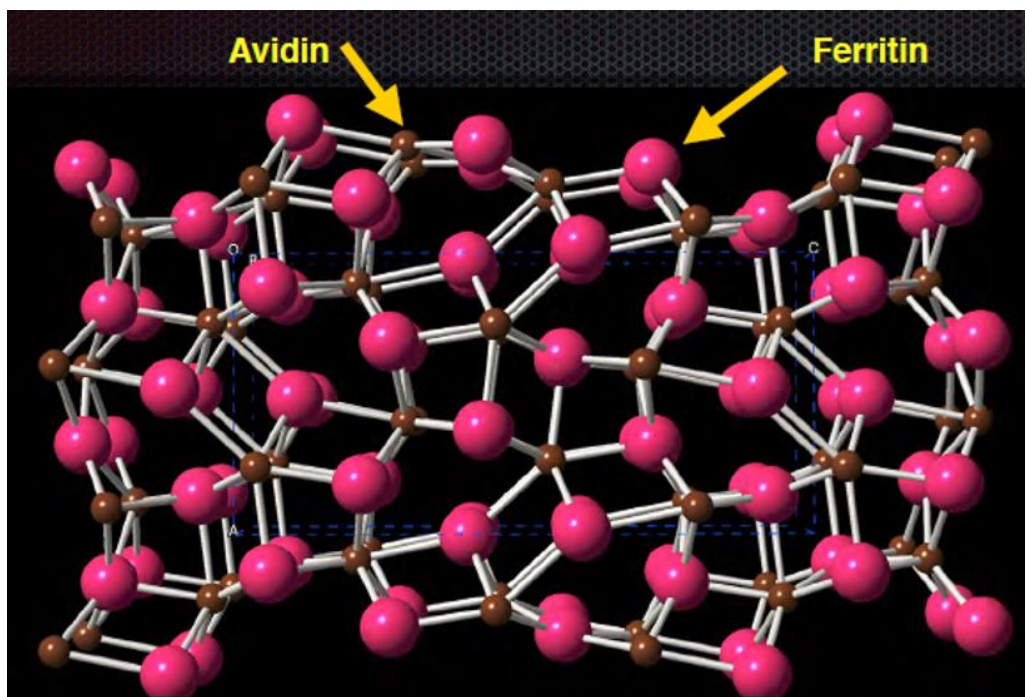


Figure 2.4. An illustration of a supramolecular protein scaffold assembled from biotinylated ferritin and avidin proteins.

The model capsule proteins will be chemically labelled with a diverse set of biotin-PEG reagents. The polyethylene glycol cross-linkers with biotin at one end will be installed on the outer surface of the protein horse spleen ferritin to act as a tether to link proteins into a scaffold-like material. This approach is pursued using a selection of PEG reagents with electrophilic leaving groups such as, NHS and TFP activated esters, which interact with the nucleophilic amino acid residues located on the protein surface to form a covalent amide bond. Additionally, PEG as a component to the cross-linking agents has been chosen for this project, instead of alkane-based cross-linkers, because it is water-soluble. The proteins of interest are soluble in aqueous buffer solutions, therefore PEG appeared to be the most reasonable and compatible choice.

The choice of avidin as the biotin-binding component was also considered from the point of view of commercial availability in sufficient quantities and expense, as well as the additional

presence of carbohydrate attachments. The presence of the carbohydrate component on avidin compared to its absence on other biotin-binding proteins, was considered as a potentially useful moiety since carbohydrate-binding proteins, termed lectins, might also bind to exposed carbohydrate residues on the protein network. This might allow for lectins labelled with a variety of molecules such as fluorophores, to bind to these protein networks, extending the sophistication of these biomaterials.

More importantly, we aim to show the versatility of the fabricated protein network in various applications. As illustrated (Figure 2.5), hundreds of potential conjugation choices and approaches could be pursued to provide novelty to this biomaterial. This chapter elaborates on the methodical design of a ferritin-avidin network reinforced with enzymatic, photocleavable, and magnetic functionalities.

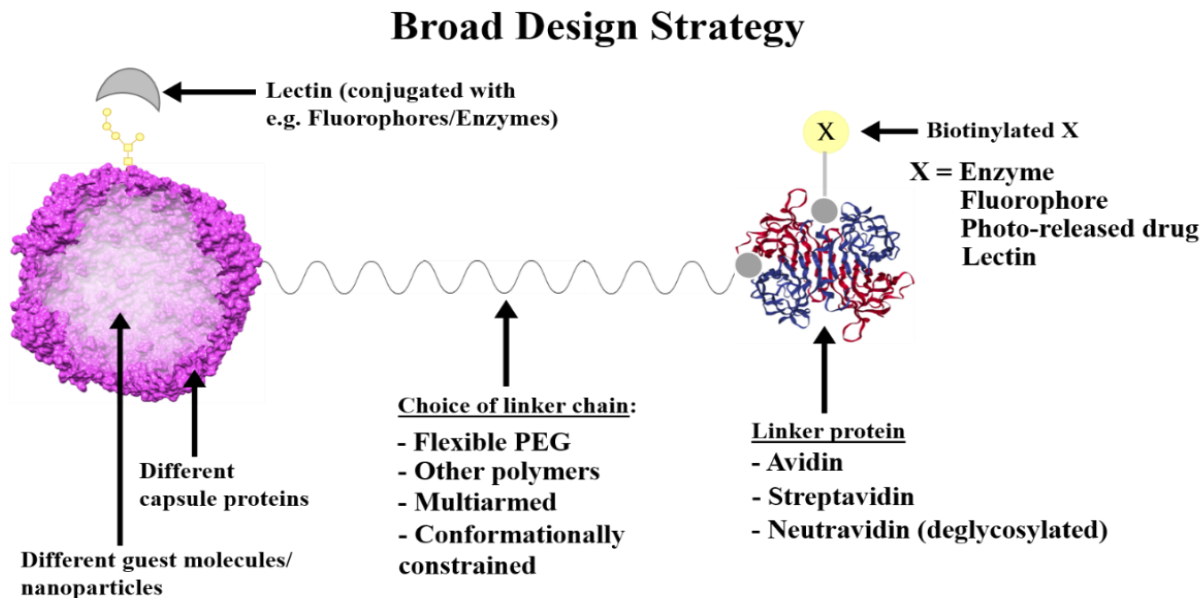


Figure 2.5. A broad design strategy. A wide range of capsule proteins, linker chains/proteins to be employed in the project.

2.3 Materials

The following compounds were obtained from the noted commercial sources: Horse spleen ferritin was obtained from Sigma-Aldrich (Oakville, Canada). biotin-dPEG[®]₁₂-TFP ester, biotin-dPEG[®]₂₄-TFP ester, biotin- TFP-PEG₄-Lys (PEG₄-biotin)₂, biotin-dPEG[®]₁₁-MAL, were obtained from Quanta BioDesign, Ltd. (Plain City, Ohio, USA). PC Biotin-PEG₃-NHS carbonate ester was purchased from BroadPharm (San Diego, CA, USA). PEG 2K and 5K were purchased from Creative PEG Works (Durham, NC, USA). Avidin was purchased from Bioshop Canada Inc. (Burlington, Ontario, Canada). Streptavidin was purchased from Cedarlane (Burlington, Ontario, Canada). Neutravidin was purchased from Thermo Fisher Scientific (Mississauga, Ontario, Canada). HiC was purchased from Alfa Aesar (Haverhill, Massachusetts, USA). Bovine serum albumin (BSA) was purchased from Bioshop Canada, Inc. Tween 20 was purchased from Sigma-Aldrich. Poly(ethylene terephthalate) film was purchased from Goodfellow, distributed by Delta Scientific. The poly(ethylene terephthalate) film purchased corresponded to the product number ES301445 and is a 0.25 mm-thick, 300x300 mm sheet of transparent, amorphous material. BeaverBeads Mag COOH were kindly supplied by GeneBiosystems, Inc. (Oakville, Ontario, Canada). EDC and NHS-biotin-dPEG[®]₃-NH₃⁺TFA⁻ were purchased from Quanta BioDesign, Ltd. (Plain City, Ohio, USA).

2.4 Methodology

2.4.1 Mass Spectrometry

2.4.1.1 ESI MS

The masses of the protein samples were determined using a soft ionization technique that employs a Thermo Scientific™ Q-Exactive Hybrid Quadrupole-Orbitrap (Waltham, MA, USA) mass spectrometer with an Electrospray Ionization Source (ESI). The protein samples to be analyzed were desalted by exchange with doubly distilled water (DDH₂O) using Amicon® Ultra Centrifugal Filters with a 10 kDa molecular weight cut-off (MWCO) for 4-5 centrifugation rounds at 6720 *g* (small benchtop lab centrifuge) to remove buffer salts, excess labelling reagent, or impurities and then were diluted to a final volume of 50 μL and a concentration of 1-10 pmol/μL using a mobile solvent mixture of 50:50 MeOH/H₂O:0.1% formic acid. The prepared sample was injected in the instrument at a flow rate of 10 μL/min in the positive mode (+ESI) through a metal capillary, where heat (300 °C) and high voltage (2.5-3.2 kV) are applied to assist the ionization process. Under the effect of the electric field, a droplet is formed at the exit of the capillary, which gradually sprayed into a mist of smaller charged droplets. Then the small droplets evaporate to generate gas-phase ion species. The ion species travel through the quadrupole mass filter that filters the uncharged neutral species, then the ion species fly to the orbitrap for mass to charge (*m/z*) ratio detection (Michalski et al., 2011). Mass to charge ion peaks were deconvoluted to resemble their corresponding molecular masses using BioPharma Finder™ Software from Thermo Fisher Scientific.

2.4.1.2 MALDI-TOF MS

Protein samples were analyzed using the matrix assisted laser desorption ionization-time of flight (MALDI-TOF) technique using a Bruker Autoflex Speed instrument for molecular mass detection. Samples to be analyzed were desalted prior to analysis using Amicon® Ultra Centrifugal Filters, following a purification protocol similar to the one used for ESI-MS samples. Protein samples were diluted with DDH₂O to a final concentration of 10 µM. Sample preparation was performed using the dried droplet method with a sample:matrix ratio of 1:1, by which a mixture of 1 µL of the purified protein sample with 1 µL of the sinapinic acid solution was made and pipetted onto a metal plate until it dried forming a crystalline droplet. The metal plate containing the sample was subsequently loaded into the MS instrument. The choice of using sinapinic acid was made as it was proven to be compatible with proteins in the 10-150 kDa mass range. Using sinapinic acid in this method is important as it is a matrix compound capable of protecting the sample from being destroyed by the UV-laser beam, while working as a laser energy-absorbent and proton source, making it essential to soft-ionize the protein sample, in addition to facilitating the vaporization of the sample (Clark et al., 2013). The mass spectrometer was calibrated with a protein standard consisting of: Alpha Lactalbumin (14,177 Da), Soybean Trypsin Inhibitor (19,977 Da), Trypsinogen (23,982 Da) and Carbonic Anhydrase (29,024 Da).

2.4.2 Ultraviolet-Visible (UV-Vis) Absorbance Measurements

The UV-Vis spectrophotometric absorbance measurements were carried out using the SpectraMax 5 microplate reader from (Molecular Devices, Sunnyvale, CA, USA) equipped with SoftMax® Pro Enterprise software. The solutions were placed in a Quartz Cuvette (1 cm pathlength, 1.5 mL volume).

2.4.3 Biotinylation of HSF Protein Through Lysine Modification

Horse spleen ferritin (55 mg/ml, 90.9 μ L) in 150 mM saline solution was purchased from Sigma-Aldrich. The concentration of the protein stock solution was confirmed by the Bradford and Lowry assays (Lu et al., 2010). The commercially available reagents biotin-PEG₄-NHS ester, biotin-PEG₁₂-TFP ester, biotin-PEG₂₄-TFP ester, and biotin-bifurcated PEG₄-TFP ester (Figure 2.6) were obtained from Quanta BioDesign, Ltd. to target the lysine residues on HSF. The reaction was performed in potassium phosphate (KP) buffer, 150 mM, at pH 7.4. This potassium phosphate buffer was prepared using 8 g of KH₂PO₄ and 16 g of K₂HPO₄ diluted in 100 mL DDH₂O, pH 7.4. The pH was adjusted using NaOH or HCl when necessary.

The HSF protein was dissolved in the 150 mM KP buffer with a final HSF concentration of 10 mg/ml as recommended by Hermanson (Hermanson, 1996). The biotinylation powder reagent was weighed using an analytical balance and immediately added to the reaction vial. The molar excess of the reagent to capsule was (capsule:reagent, 1:150-200 molar equiv.). The vial was vortexed carefully, then was incubated either for 1 hour at room temperature or overnight at 4 °C to allow the reaction to proceed. After the incubation time had elapsed, the mixture had undergone 4-5 rounds of washing with DDH₂O using a centrifugation-based size exclusion filter (Amicon[®] Ultra) with a (MWCO) of ~10,000 Da in an Eppendorf Minispin centrifuge at 6720 x g to subsequently remove the unconjugated biotin reagent, the buffer components, and the by-product tetrafluorophenol, resulting in only biotinylated ferritin ready for mass analysis. MALDI-

TOF in positive-ion linear mode was employed to determine the mass of the biotinylated monomeric HSF subunits and the degree of modification.

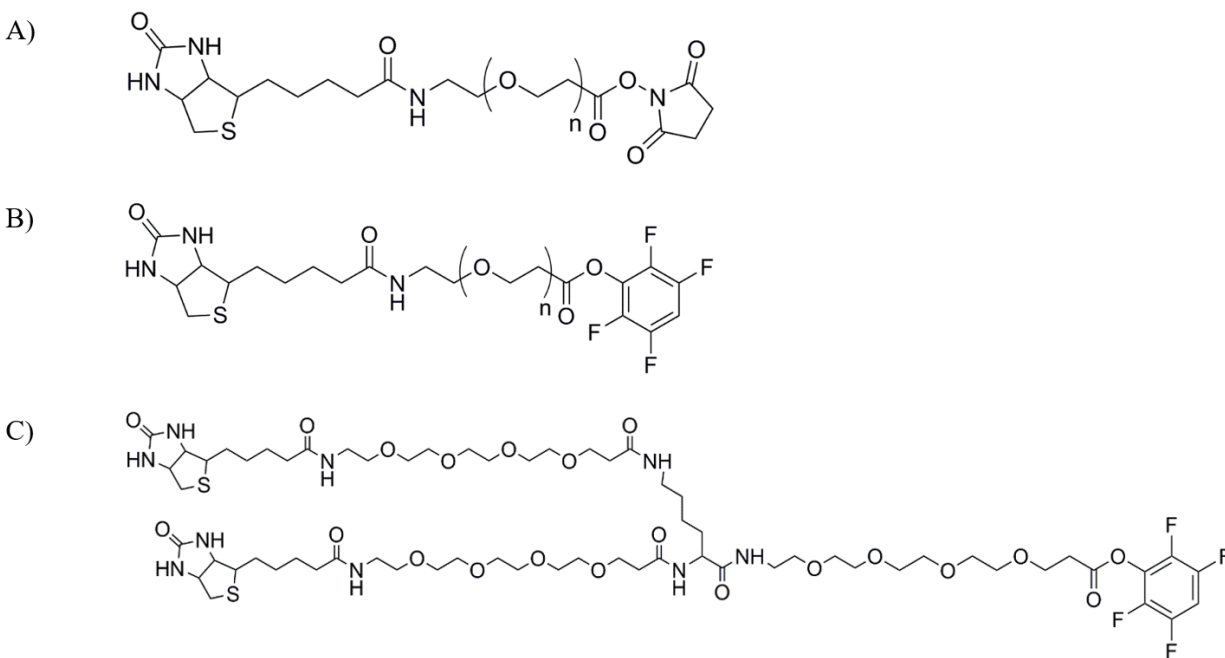


Figure 2.6. Biotinylation reagents. A) the chemical structure of Biotin-PEG(n)-NHS ester. B) the chemical structure of Biotin-PEG(n)-TFP ester. C) Trifunctional PEG “TFP-PEG₄-Lys (PEG₄-biotin)₂”.

Two additional reagents, biotin-PEG2K-NHS ester and biotin-PEG5K-NHS ester were purchased from Creative PEG Works (Durham, NC, USA), were also studied for conjugation with the HSF protein, following the same mentioned procedure. However, a wider range of molar excesses was utilized in these reactions. For the PEG5K spacer arm, 1:72, 1:100, 1:300, 1:360, 1:380, 1:800 molar excess of the commercial reagent was employed in the bioconjugation reaction. Furthermore, for the PEG2K, 1:200, and 1:3000 molar excess was used. Additionally, a time-point aliquot procedure was performed using the PEG 2K, where the reaction started with 1:150-fold excess and then an additional 150-fold excess was added after every 1 hour time-point for 5 hours, summing up to a total 750-fold at the end point. After each 1-hour cycle, an aliquot was pipetted

out, desalted using Amicon[®] Ultra filters, and taken to analysis using MALDI-TOF mass spectrometry.

The experiment which contained 1:3000-fold excess of PEG2K used 2 mg/ml of HSF protein, instead of 10 mg/ml. The reaction was conducted in a 100 mM KP buffer at pH 7.0 following a previously reported procedure (Shukla et al., 2013).

2.4.4 Lysine Modification Using a Photocleavable Linker

The HSF protein (55 mg/ml, 90.9 μ L) in saline solution was mixed at 23 $^{\circ}$ C with the 150 mM KP buffer solution and made up to 500 μ L with distilled water, making the final concentration of ferritin to be 10 mg/ml. This solution was then added to a 1.9 mg (218-molar equiv.) of the nitrobenzyl-based photolabile biotinylation reagent, PC biotin-PEG₃-NHS carbonate ester (Figure 2.7), in a centrifuge tube. The tube was incubated at room temperature for 1 hour, then desalted to remove buffer and unlinked reagent molecules using Amicon[®] Ultra filtration device for 5 rounds at 6720 x g.

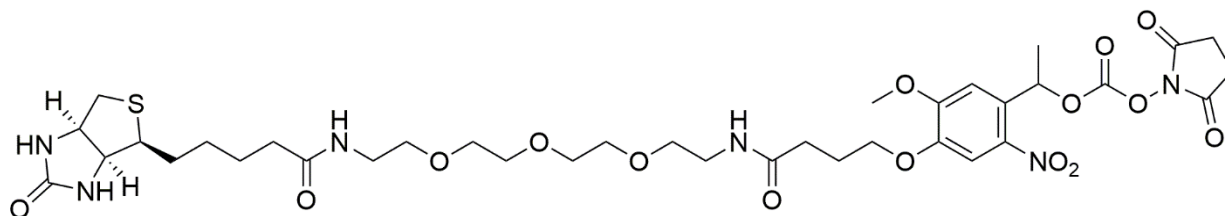


Figure 2.7. Chemical structure of PC Biotin-PEG₃-NHS carbonate ester.

2.4.5 Cysteine Modification of HSF Protein

Horse spleen ferritin (55 mg/ml) was conjugated with the commercial maleimide-based reagent Biotin-dPEG[®]₁₁-MAL (Figure 2.8) (2 mg resulting in a 210-fold molar excess) in 150 mM KP buffer solution at pH 7.4. A final 10 mg/ml concentration of HSF was employed. The reaction

was incubated at room temperature for 1 hour then purified using the Amicon[®] Ultra filtration device for 5 consecutive rounds against DDH₂O at 6720 x g to remove the unconjugated reagent and the buffer solution. The sample was analyzed with MALDI-TOF in positive-ion linear mode.

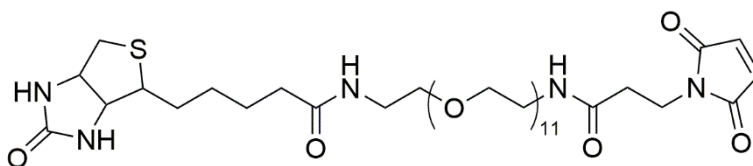


Figure 2.8. The chemical structure of the biotinylation reagent Biotin-PEG₁₁-MAL.

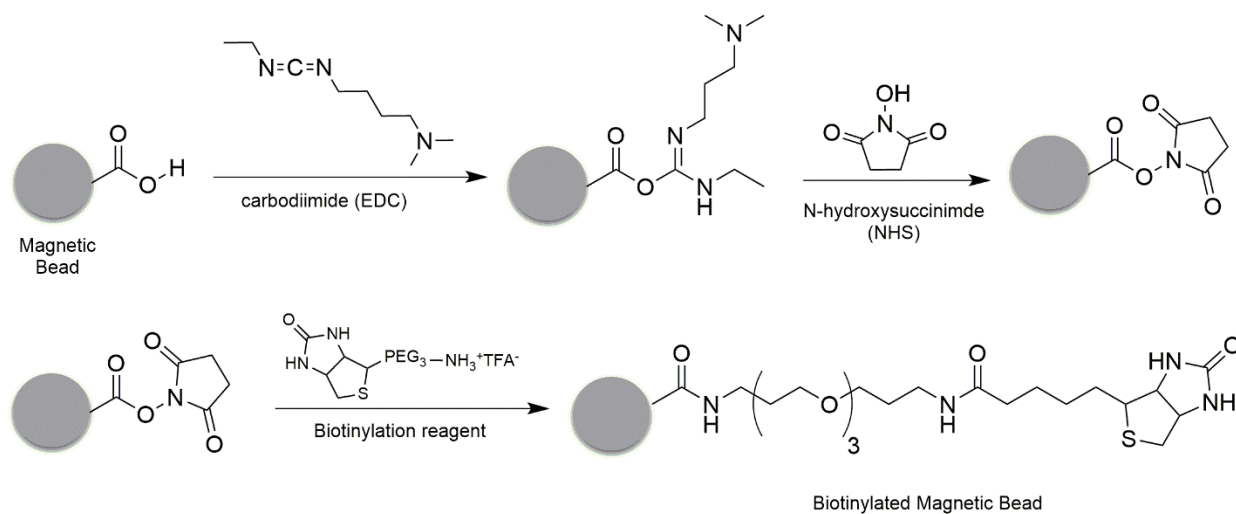
2.4.6 Bioconjugation of Magnetic Beads

2.4.6.1 Magnetic Beads Surface Carboxyl Activation

BeaverBeads Mag COOH (300 nm diameter) were kindly supplied by GeneBio Systems, Inc. The magnetic beads surface, which displayed carboxyl groups, had undergone carboxyl activation to achieve biotin reagent coupling. An aliquot (100 μ L, 10 mg/ml) was pipetted into a centrifuge tube, gently blended, then separated from the preservation solution (20% ethanol). A magnetic separator was used to facilitate the separation of the supernatant from the magnetic particles. A solution of 2-ethanesulfonic acid (MES) buffer (200 μ L, 100 mM, pH 5.0) was used to wash the magnetic beads twice, and 0.05% Tween 20 detergent was added to the buffer to improve the bead's dispersity. The wash supernatant was removed from the aliquot. Freshly made 10 mg/ml solutions of 1-ethyl-3-(3-dimethylaminopropyl)carbodiimide (EDC) and N-hydroxysuccinimide (NHS) were prepared with the 2-ethanesulfonic acid containing 0.05% Tween 20 (MEST) buffer. A 100 μ L of each, EDC then NHS solutions, were added to the magnetic beads to activate the surface carboxyl groups. Next, the magnetic beads were incubated for 30 minutes at room temperature.

2.4.6.2 Covalent Coupling of Magnetic Beads with Biotin

A 50 μL aliquot of the activated magnetic beads solution was used in this step. The solutions of EDC and NHS were discarded from the aliquot then the biotin coupling reagent, Biotin-PEG₃-NH₃⁺TFA⁻ (200 μL , 178 equiv.), in a phosphate-buffered saline (PBS) solution at pH 8.0 with 0.05% Tween 20 (PBST) was added to the beads. The reaction was incubated for 2 hours at room temperature. The 200 μL supernatant that contained the biotin reagent was separated from the beads by magnetic separation using a bar magnet held to the surface of the glass tube. A 200 μL solution of PBST buffer at pH 7.2 with 1% w/v glycine was added to the beads to react with any activated but uncoupled carboxyl groups. The solution was incubated for 1 hour at room temperature. The solution containing glycine was separated from the magnetic beads as described previously using a bar magnet. Then the beads were washed using PBS buffer for three times and preserved in 200 μL of PBS at 4 °C. The bioconjugation scheme is shown in (Scheme 2.1).



Scheme 2.1. The mechanism of carboxyl groups activation and biotinylation of magnetic beads.

2.4.6.3 Biotin-4-Fluorescein Quantification Assay

The assay was conducted in 1X PBS buffer (10 mM Na₂HPO₄, 1.8 mM KH₂PO₄, 137 mM NaCl, 2.7 mM KCl) at pH 7.4. A stock solution of biotin-4-fluorescein (B4F) (Figure 2.9) was prepared with a concentration of 16.8 μM with protection from light. The absorbance and concentration were measured using a UV-Vis spectrophotometer at 495 nm and an extinction coefficient of 68,000 M⁻¹ cm⁻¹. A calibration curve was created to convert the fluorescence data to molar values over the range of 0-730 nM of B4F in PBS buffer.

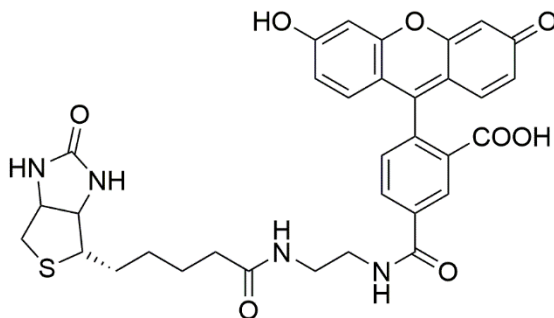


Figure 2.9. Structure of biotin-4-fluorescein (B4F).

The B4F solution was diluted with PBS buffer to 400 nM and pipetted into a quartz cuvette to measure the fluorescence at 490 nm excitation and 525 nm emission with a 515 nm cut-off. A solution of the biotin-binding protein, streptavidin, was prepared with a concentration of 100 nM and added to the B4F to quench the fluorescein intensity. Then, a sample containing 400 nM biotin on magnetic beads was added to the B4F/streptavidin solution in the cuvette to monitor the displacement of B4F by biotin on the beads.

2.4.7 Protein Network Formation

A set of experiments was conducted to study the protein network formation using three different biotin-binding scaffold mediating proteins (Table 2). The following biotin-binding

proteins; the avidin (Av), streptavidin (SA), and neutravidin (NA), were tested with the biotinylated ferritin capsule. The biotinylated ferritin used in these experiments was cross-linked with Biotin-PEG₂₄-TFP attachment. The concentrations used in these experiments were the following, [Av] = 29.25 mg/ml, [SA] = 23.75 mg/ml, [NA] = 29.25 mg/ml, [BF] = 10.37 mg/ml. The total volume of all the reaction mixtures in each experiment was set to 48.2 μ L. Moreover, two experiments were carried out to test the protein network formation in higher ionic strength solutions of 0.3 M and 1 M of sodium chloride (NaCl) salt. All the networks in Exp #1-5 (Table 2) were allowed to assemble in a glass vial while incubated at room temperature and the formation was monitored over a time duration up to 7 days.

Table 2. Experimental setup for protein networks.

Exp #	Av or Av* (μ L)	NaCl (μ L)	BF (μ L)	H ₂ O (μ L)	Total volume (μ L)
1	Av: 28.2	0	10	10	48.2
2	Av: 28.2	10 [0.3 M]	10	0	48.2
3	Av: 28.2	10 [1 M]	10	0	48.2
4	SA: 22.9	0	10	14.3	48.2
5	NA: 22.46	0	10	15.74	48.2

Av*: Avidin analogue (streptavidin or neutravidin)

2.4.8 SEM Characterization

Samples of biotinylated ferritin produced by reaction of ferritin with biotin-PEG₂₄-TFP, followed by interaction with avidin were prepared on pre-ultrasonicated silicon chips with methanol and isopropanol. The Zeiss Merlin[®] Scanning Electron Microscopy (SEM) instrument was employed in the characterization of the samples with a beam accelerating voltage of 10 kV.

2.4.9 Suspension of Biotinylated HiC Enzymes within the Ferritin-avidin Scaffold

Horse spleen ferritin protein (10 mg/ml) was cross-linked with TFP-PEG₂₄-biotin (190-fold molar excess) reagent in a 100 mM KP buffer at pH 7.4 and was incubated for 1 hour at room temperature to produce biotinylated ferritin, which afterward was confirmed with MALDI-MS. This product was combined with the protein avidin to create the supramolecular ferritin-avidin scaffold. Specifically, the assembly of the protein scaffold was conducted by incubating 50 mg/ml biotinylated ferritin solution with 50 mg/ml avidin solution in a 1:18 molar ratio, then allowing the mixture to self-assemble at room temperature for two hours. After two hours, the scaffold was washed with DDH₂O to eliminate the excess unbound avidin, then an additional round of washing was performed with 100 mM KP buffer, 150 mM NaCl, and 0.1 – 1% w/v bovine serum albumin (BSA) solution at pH 7.2. To ensure that all the unbound avidin was eliminated, the rinsed wash solution was measured using a UV-Vis spectrometer at 280 nm, where multiple washes were performed until the absorbance measures were detected at the background level indicating no UV absorbance to confirm the removal of the excess protein. The final scaffold was transferred to a new polypropylene centrifuge tube.

Later, the biotinylated HiC enzyme solution was introduced to the protein scaffold and incubated for 30 minutes at room temperature. Again, the mixture was washed with 100 mM sodium phosphate, 150 mM sodium chloride, 0.1% w/v BSA, and 0.05% v/v Tween 20 in order to rinse out any unbound biotinylated enzyme before starting an enzymatic assay to test the activity of the scaffold. While rinsing the unbound biotinylated enzyme from the scaffold solution in the polypropylene tubes, the assembled material was centrifuged between the washes at 6720 x g for 10 minutes to minimize the chances of material loss while pipetting during the wash steps. After washing, the final scaffold was transferred to a new polypropylene centrifuge tube. Ultimately, an

enzyme activity assay was conducted on the enzymatic ferritin-avidin scaffold with the p-NPB substrate, by which the substrate hydrolysis by the enzymatic scaffold was determined according to the UV absorbance measurements at 347 nm, described in detail in Jameson Pfeffer's M.Sc. thesis (Pfeffer, 2019), a former member of the Honek laboratory who provided the biotinylated HiC enzyme for these sets of experiments.

2.4.10 Enzymatic Scaffold-PET Sample Preparation for Degradation Studies

As a control sample, poly(ethylene terephthalate)-Glass Fiber (PET-GF) was cut into small sections of 1×1 cm and placed in 1.5 mL centrifuge tubes filled with 1.5 mL of 200 mM sodium phosphate buffer at pH 7.0. The buffer solution contained about 20 mg/ml of the HiC enzyme. The tube cap was tightly sealed using a piece of Parafilm to avoid solvent evaporation. The PET-enzymatic scaffold was incubated at room temperature or 55 °C to react over the next 15 days. After day 15, the PET sections were cleared with Tween 20 solution (0.1% v/v) then washed with DDH₂O.

In the enzymatic scaffold experiment, the effect of the bound enzyme was examined on PET. In this experiment, a small-sized petri dish was used as a container. A droplet of the scaffold in buffer solution was mounted on a PET section, then directly was placed in a petri dish. A 1 mL volume of buffer was pipetted as small droplets in the inner circumference of the dish to provide a humid surrounding environment for the scaffold, then the petri dish was covered. The storing conditions and the cleaning procedure implemented on this scaffold were the same as followed in the control experiment mentioned above.

Characterization of the PET sections designed above after 15 days incubation period was performed in the WATLAB using a scanning electron microscope (SEM) FEI Quanta FEG 250

with a 20 kV voltage setting. These experiments were accomplished collaboratively between Mr. Pfeffer and myself, where I provided the protein networks and performed the incubations and the results were discussed jointly.

2.4.11 The Assembly of a Photocleavable Protein Network

Biotinylated ferritin produced as a result of the reaction with the photocleavable linker, PC biotin-PEG₃-NHS carbonate ester, that yielded the conjugation of one biotin molecule attachment on each HSF subunit, was added directly (50 mg/ml) to freshly reconstituted avidin protein solution (50 mg/ml) using a molar ratio of 1:21 (ferritin:avidin) in a new glass vial. Additionally, a control experiment utilizing an unbiotinylated ferritin solution mixed with avidin was performed for comparison. The mixture was set at room temperature for further experimentation. These experiments were performed under my direction and in collaboration with a Chem494 exchange student, Thomas Daniel.

2.4.12 Photolysis of the Protein Network

Three samples (each 5 μ L) volumes were pipetted from the prepared protein network and placed into separate wells in a polystyrene microplate. A handheld UV radiation device with a wavelength at 365 nm, 6 W output was utilized to perform the network photolysis at three different time points. The three samples had the following labels; a control, 30 min, and 45 min, to assign the time duration of UV light exposure. Later, the sample masses were determined using MALDI-TOF MS after photolysis.

2.5 Results and Discussion

2.5.1 Lysine Modification on HSF Protein

The conjugation of PEG with proteins to achieve lysine modification through the formation of a covalent amide bond with the activated ester reagent, is termed an acylation reaction. The reaction is achieved by incubating the target protein with a known molar ratio of the PEG derivative reagent that contains the reactive ester moiety, in a studied biochemical aqueous environment. Several heterobifunctional cross-linking reagents were utilized for the modification of lysine residues on HSF. The biotinylation reactions of ferritin with the set of biotin-PEG_n-TFP reagents were originally prepared in a KP buffer at pH 7.4. The pKa of the ϵ -amino group of lysine residues is 10.5. Reaching a pH value of 10.5 or above in the conjugation reaction to fully deprotonate the ϵ -amino groups of lysine residues would risk the complete hydrolysis of the activated ester of the biotinylation reagent in the aqueous solution producing a non-reactive reagent. To slow the rate of the ester hydrolysis and at the same time produce a nucleophilic lysine residue, it is recommended that employing a suitable buffer in the range of pH 7-9 can maintain a pH that will establish partially deprotonated lysine ϵ -residues on a ferritin capsule that are nucleophilic enough to undergo the alkylation reaction (Hermanson, 1996). After preliminary purification of the biotinylated ferritin using an Amicon centrifugal filter, the samples were analyzed by MALDI-TOF MS. Modified protein samples were diluted to a final concentration of $\sim 10 \mu\text{M}$ and prepared for MALDI analysis using the dried droplet method, by which $1 \mu\text{L}$ of the purified protein sample was added to $1 \mu\text{L}$ of the sinapinic acid matrix and pipetted onto a plate until it dried and then was subsequently loaded into the instrument. The following paragraphs will describe the mass spectrometry result analysis of the protein conjugation.

MALDI-TOF MS was employed to analyze the HSF-conjugate masses, as this protein particularly, as for many glycosylated proteins, was challenging to analyze using the ESI technique due to the occurrence of ion suppression (Annesley, 2003). A close look at the literature reveals a lack in utilizing the ESI-MS approach to characterize horse spleen ferritin. Only a few reports in literature have demonstrated the use of MS on horse spleen ferritins, utilizing the MALDI-TOF MS technique (Lan & Zenobi, 2019) (Zeng et al., 2008).

The first spectrum, Figure 2.10A, is a control sample that shows a mass peak at 20005 m/z that corresponds to an unmodified monomeric HSF subunit. Spectrum B (Figure 2.10B) represents a ferritin subunit biotinylated by utilizing a 136-fold molar excess of biotin-PEG₁₂-TFP reagent. In spectrum B, two more significant mass peaks were detected and not found in the control. The second detected mass peak is at 20780 m/z, with an increment in the mass of approximately 806 m/z. This increase is consistent with the attachment of one biotin-PEG₁₂ (850 Da) molecule to each subunit. The third mass peak (Figure 2.10B) corresponds to two biotin-PEG₁₂ attachments per ferritin subunit, but in lower intensity compared to the second mass.

As regards to the HSF reaction with the biotin-PEG₂₄-TFP ester reagent, spectrum B belongs to a ferritin subunit conjugated by utilizing a (150-200) molar excess of the biotin-PEG₂₄-TFP reagent. A peak corresponding to 19999 Da was observed, in addition to a substantial peak at 21345 m/z (spectrum B). The peak at 21345 m/z is consistent with one biotin-PEG₂₄ molecule attached per subunit, by which the molecular weight of one biotin-PEG₂₄ attachment is 1378 Da. This chromatogram reveals a mixture of unmodified and mono-modified monomeric HSF subunits, in the reaction mixture. This result reveals an approximate overall average of 50%:50% labelling in each ferritin capsule.

With respect to Figure 2.10D, the mass spectrum exhibits a mass analysis of ferritin conjugated with the trifunctional PEG reagent, biotin-bifurcated PEG₄-TFP (TFP-PEG₄-Lys (PEG₄-biotin)₂). The spectrum represents a low-intensity peak of subunits conjugated with one biotin molecule.

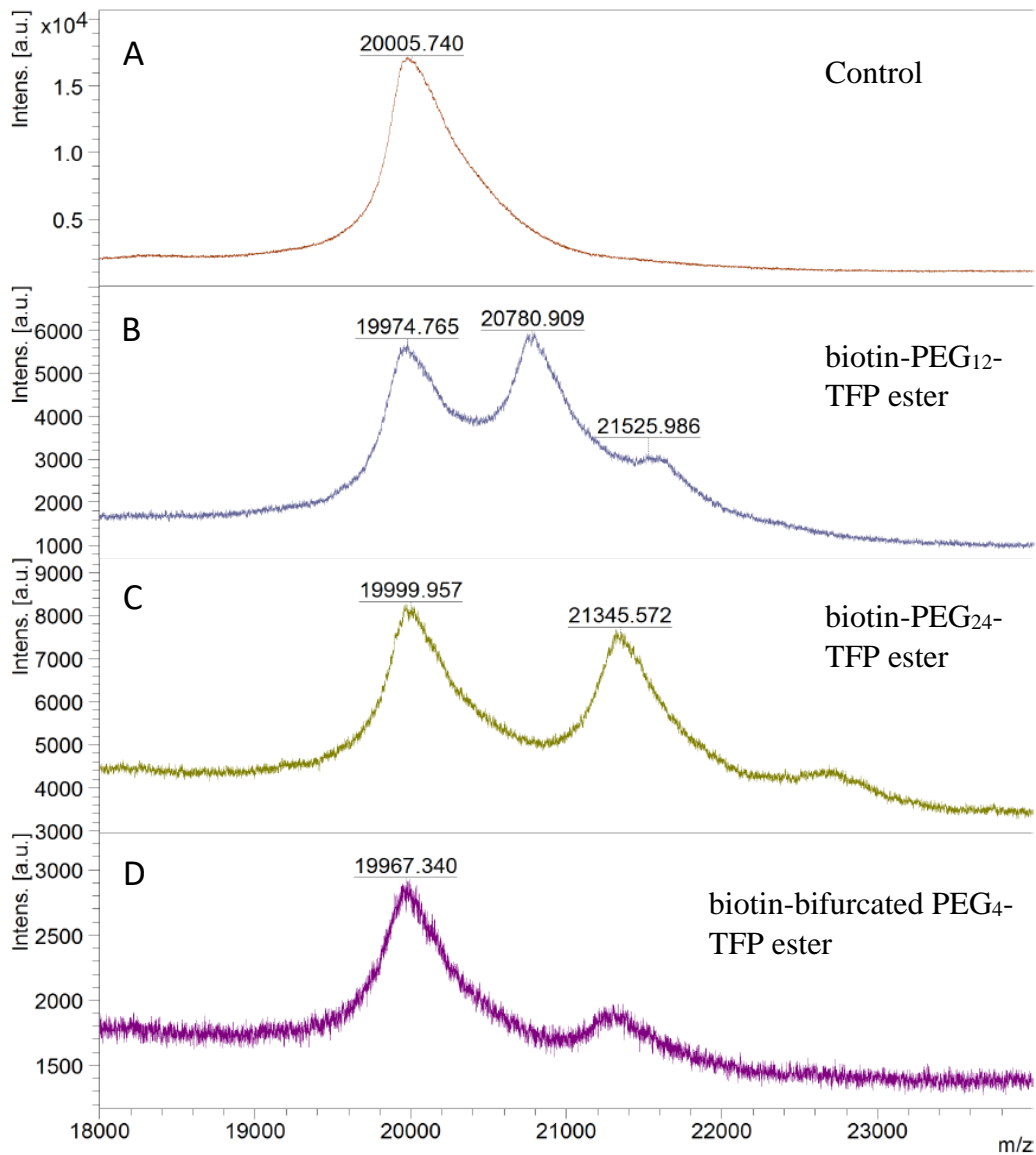


Figure 2.10. MALDI-TOF result of biotinylated ferritin subunits. A) a control spectrum shows a peak of one unmodified ferritin subunit. B) A modified ferritin subunit with biotin-PEG₁₂-TFP exhibits a control peak in addition to a second peak indicates one modification. C) Ferritin biotinylated with biotin-PEG₂₄-TFP. D) Ferritin biotinylated with biotin-bifurcated PEG₄-TFP.

The reagent with the PEG₄ linker has a fully extended maximum length of 1.92 nm, the PEG₁₂ linker has a maximum length of 4.75 nm and the PEG₂₄ linker has a maximum length of 9.9 nm (Quanta BioDesign). These nano-sized spacer arms play a key role in determining the spatial dimensions of the protein scaffold material, by which they extend the distance between the biotin molecule and the end of the conjugated amino acid (e.g. lysine) on the modified ferritin that will work as the building block.

Moving on to extend the protein network design, we chose to explore even longer spacer arms, so biotinylation reagents with longer PEG chains were studied. Biotin-PEG_n-NHS ester derivatives with molecular weights of 2000 Da and 5000 Da have approximately 45 and 113 ethylene glycol units in the chain, and a maximum arm length of 18.5 nm and 46.6 nm, respectively (Quanta BioDesign). A broad set of experiments utilizing different protein:reagent molar ratios were conducted in this project. Using PEG2K spacer arm, the set of 1:150, 1:200, and 1:3000, and using PEG5K spacer arm, the set of 1:72, 1:100, 1:300, 1:360, 1:380, 1:800 stoichiometric ratios were all attempted. In this work, the standard modification procedure was followed, in addition to several previously reported procedures that had adjusted minor conditions such as; incubation period and pH levels, were implemented as well. The resulting modifications were monitored using MALDI-TOF MS. All these procedures were found to be unsuccessful in the current research; wherein no modification was observed on the HSF protein subunits (data not shown). It is worth mentioning that during some of these experimental runs, an apparent protein precipitate was observed in the reaction vial.

However, one bioconjugation reaction among all the above-mentioned experiments was observed to show a clear, yet not significant modification. Those experiments employed the PEG5K reagent. The MS results for the bioconjugation utilizing the biotin-PEG5K-NHS ester

reagent with HSF protein are shown in Figure 2.11. Figure 2.11A is the spectrum of the control mass of unmodified ferritin. Two ferritin aliquots were each incubated with an 800-fold molar excess of the reagent for 1 hour at room temperature and for 24 hours at 4 °C, respectively. The mass spectrometry data from both samples (Figure 2.11B & C) exhibit low-intensity mass peaks at 25301 m/z and 25398 m/z indicating a low labelling yield, in contrast to the substantial yields of the reactions performed using shorter PEG linkers. Generally, the peak heights in mass spectrometry, unless a standard curve is made, should not indicate quantitative information because different compounds ionize differently in the MS, although very related structures may indeed ionize in a similar fashion and to a similar extent, like the ferritins we are analyzing here.

It is suspected that the length of the PEG spacer structure linking the chemical moiety to the protein target has an effect on the overall labelling yield. Perhaps the 2000 and 5000 Da molecules may have contributed a steric hindering effect that limited the NHS moiety's approach the reaction site.

NHS-ester reagents are the most commonly used reagents in bioconjugation reactions due to the well-established methods developed, and due to the broad commercial availability of various NHS-containing reagents (Hermanson, 1996). However, the NHS ester does hydrolyze rapidly in the aqueous solution during the bioconjugation reaction, which demands a very high excess of the reagent to obtain the desired degree of modification. On the other hand, TFP ester-based reagents exhibit longer half-lives in solution, which implies that TFP possesses a higher hydrolytic stability in comparison to the NHS ester (Lockett et al., 2008). Previous experiments carried out in the laboratory have shown that increased biotinylation levels can be obtained with TFP reagents, greater than those obtained by using NHS reagents, despite the use of a higher excess of NHS reagents.

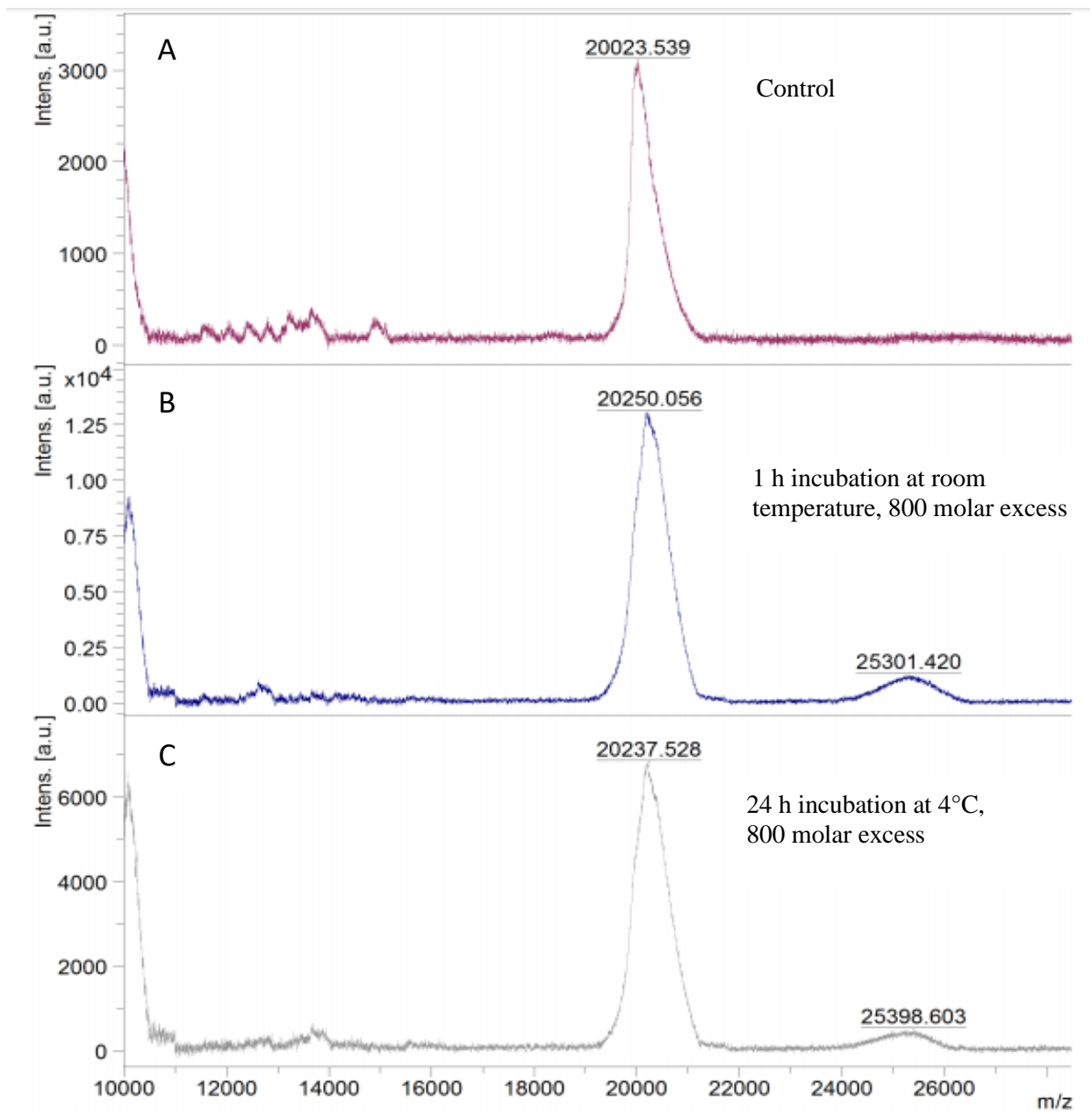


Figure 2.11. MALDI spectra of ferritin subunits cross-linked with biotin-PEG-NHS ester (MW=5000 Da). A) Ferritin control (not biotinylated). B) Biotinylation with 800-fold reagent at room temperature. C) Biotinylation with 800-fold reagent for 24 h at 4 °C.

2.5.2 Cysteine modification on HSF protein

Covalent cysteine-targeted modifications of proteins are common as well in the bioconjugate chemistry. In this section, thiol-cysteine modification experiments on HSF with a biotinylation reagent are discussed. The surface of the HSF capsule was bioconjugated with a biotin-PEG₁₁-MAL reagent, following the standard bioconjugation process using a 210-fold molar excess of the biotin reagent. Afterwards, the sample was buffer exchanged with DDH₂O using 10 kDa MWCO Amicon[®] Ultra centrifugal filters, then submitted to MS analysis. Analysis of the MALDI-TOF data showed no mass peak evidence of HSF cysteine bioconjugation with the biotin-PEG₁₁-MAL attachment (data not shown). Screening literature articles on possible cysteine surface modifications on ferritins revealed no recorded success for cysteine modification on a ferritin protein. According to the amino acid sequence of horse spleen ferritin (PDB: 5ERK), ferritin has one cysteine residue per subunit. It is common knowledge that successful chemical modifications occur on a surface exposed residue rather than internally buried amino acid residues. Therefore, in order to investigate the exact position of cysteine in the HSF quaternary structure and its level of exposure on the outer curvature of the capsule, the protein structure was modeled using UCSF Chimera software, employing the protein structure PDB: 5ERK (Goddard et al., 2005). Figure 2.12 presents the surface of HSF with three adjacent subunits highlighted. The model shows the cysteine residue in yellow clearly buried close to the intermolecular grooves of the capsule. The model supports the limited susceptibility for cysteine modification on HSF and the restricted tendency for the reagent to approach and modify the cysteine. This experiment is of importance for the project, as it will be discussed in more detail in Chapter 3.

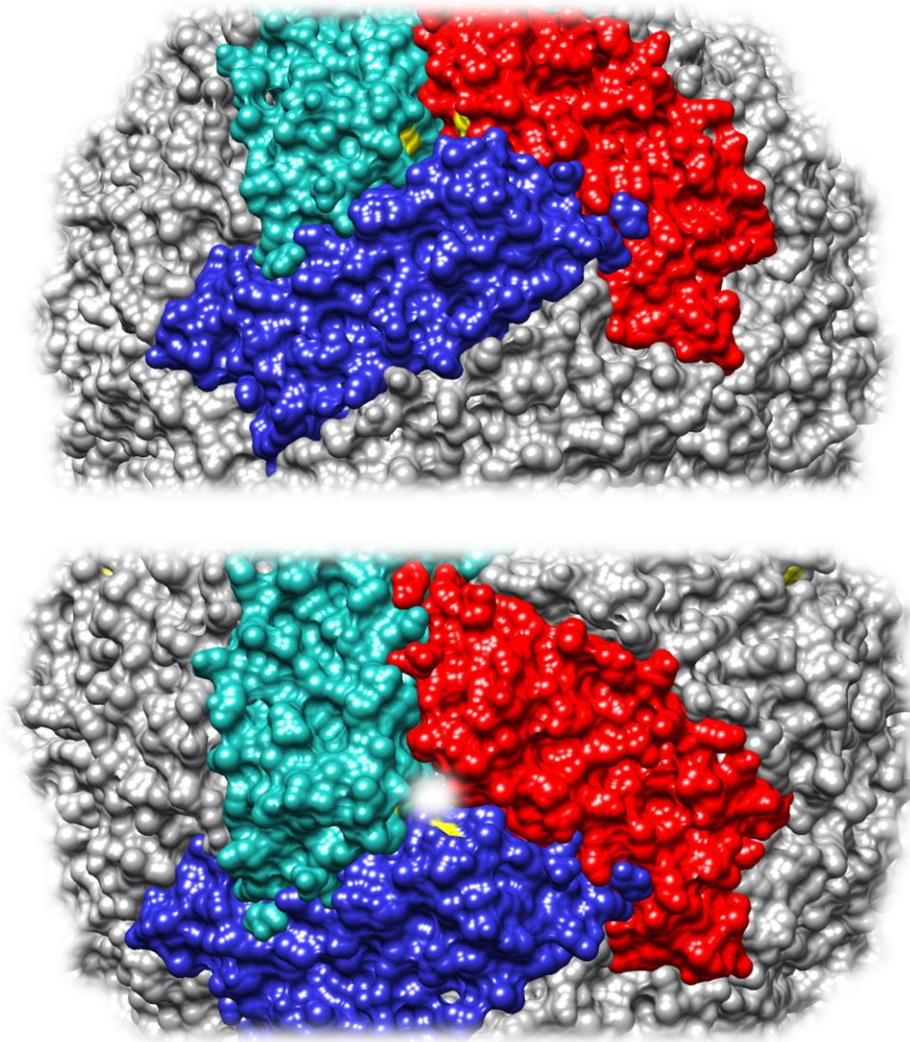


Figure 2.12. Space-filled model of the horse spleen ferritin protein (PDB: 5ERK). The model shows one cysteine residue (yellow) in each subunit located in a buried position in the intermolecular grooves of the capsule protein. The images were generated using Chimera software.

2.5.3 Biotinylated Magnetic Beads

2.5.3.1 Energy-Dispersive X-ray Spectroscopy

Studies on attaching magnetic beads to the protein networks were investigated in a preliminary manner in order to eventually be able to use magnetic fields to recover catalytic protein networks for reuse. The carboxyl groups on the magnetic bead's surface were activated and coupled with a biotin reagent. Since magnetic beads cannot be characterizable using any of the previously employed mass spectrometry techniques, a different analytical technique was pursued. Energy-Dispersive X-ray Spectroscopy (EDX) was used as a qualitative tool to characterize the chemical or elemental composition of the beads. Since these magnetic particles are made of an agarose polysaccharide shell and filled with iron (III) oxide in the core, it was expected that a signal for the elements C, H, N, and Fe would be detectable.

The result of EDX elemental analysis for a control sample of unbiotinylated magnetic beads is shown in Table 3. The elemental composition consisted of a considerable percentage of carbon (C), and oxygen (O), which makes up the agarose polysaccharide shell, and most importantly iron (Fe), which fills the core of the beads in the form of iron (III) oxide, Fe_3O_4 . Moreover, the silicon (Si) composition indicated in the table is referred to as the silicon chip that was used to carry the sample on the sample holder. Table 4 shows the elemental profile of the biotinylated magnetic beads sample. The analysis detected a signal for nitrogen (N) composition, which was not found in the control sample. Here it is referred to the imidazolinone ring in biotin molecules. Although sulfur is a major element of the tetrahydrothiophene ring of the biotin, the EDX detector did not reveal a significant atomic percentage of it, since the instrumentation setup did not have a high sensitivity for sulfur element detection.

Table 3. EDX elemental analysis profile of unbiotinylated control sample.

Element	Weight %	Atomic %
C K	13.96	26.58
N K	-0.48	-0.78
O K	7.66	10.95
Si K	76.71	62.46
S	-0.32	-0.23
Fe	2.46	1.01
Totals	100.00	

Table 4. EDX elemental analysis profile of biotinylated magnetic particle.

Element	Weight%	Atomic%
C K	19.23	33.60
N K	1.62	2.43
O K	12.29	16.12
Si K	61.29	45.79
S K	-0.12	-0.08
Fe K	5.68	2.13
Totals	100.00	

2.5.4 B4F Quantitative Assay

The degree of biotinylation on the surface of the magnetic beads was determined using the B4F assay. This assay used the biotin-containing fluorescein molecule, B4F, to monitor the biotin ligand exchange in the binding sites of streptavidin by tracking the decrease in the initial fluorescence signal upon adding streptavidin, and the increase in the fluorescence signal upon

adding a different biotin analogue that will displace B4F from the streptavidin, releasing them in solution.

The results of the assay showed a significant biotin labelling on the beads (Figure 2.13). The concentration of B4F in sample (3) deduced from the B4F amount in sample (2) yielded a concentration of 350.63 nM of B4F that was displaced by the biotins on the beads, which corresponds to the total quantity of biotins found on the surface of the magnetic beads (Figure 2.13). Multiplying this value by the dilution factor (800/2.13), a biotin concentration of 131.7 μM was attained in the original magnetic beads sample. The original sample of the magnetic beads contains 150 μM COOH surface carboxyl groups that could be biotinylated. Achieving biotin concentration of 131.7 μM on the beads surface, yields 87.8% surface labelling. The experiment was duplicated, sample (4), and 131.4 μM (87.6 %) yield was attained with 0.24% error.

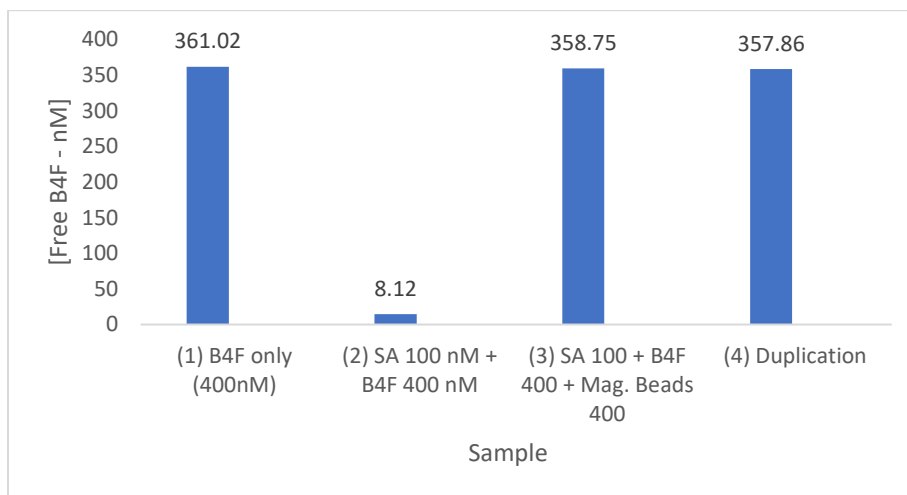


Figure 2.13. B4F assay analysis bar chart indicating the successful displacement of B4F molecules by biotins on the magnetic beads confirming the biotinylation labelling with 87% yield.

2.5.5 Ferritin-avidin Network

Section 2.4.6 presented the experimental setup employed to investigate the protein network formation. The capsule protein that was used as a building block for the network is the horse spleen ferritin, which is an excellent choice due to possessing an iron core that makes the network feasible to be visualized under the scanning electron microscope without sample staining treatment, as the core exhibits a bright spherical entity. Biotinylated ferritin was prepared using the biotin-PEG₂₄-TFP reagent to label the ferritin surface with biotins that bind non-covalently to biotin-binding sites on avidin. To visualize the dimensions of the network, the Figure 2.14 illustrates a two-dimensional bond of two ferritins mediated by avidin. The assembly is facilitated by biotins attached to two opposite sides of the avidin molecule. A fully extended form of this linkage in the network will have a total of 49 nm distance (Figure 2.14) between each two ferritin capsules within the biomaterial. Since the PEG spacers used are flexible in aqueous solutions, the reported length could be less.

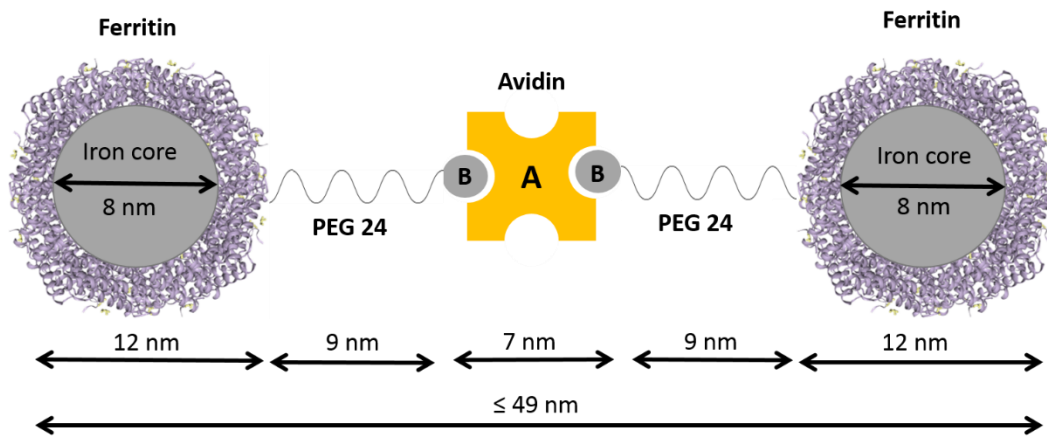


Figure 2.14. Chemical assembly of biotin-PEG₂₄-ferritin capsules through an avidin mediator creates a flexible space of 49 nm.

The discussed protein scaffolds could be engineered with multiple levels of structural porosity. As elaborated earlier, the ferritin protein was targeted with variable biotin-PEG_n linkers such as; PEG₂₄, PEG2K, PEG5K, and others. When completely extended in solution, these molecular attachments that contain terminal biotins have a length of 9 nm, 18.5 nm, and 46.6 nm, respectively (Figure 2.15). Figure 2.15 is an illustration of a saturated avidin protein establishing a tetravalent attachment with four ferritin capsules cross-linked with PEG spacers of variable nano-dimensions.

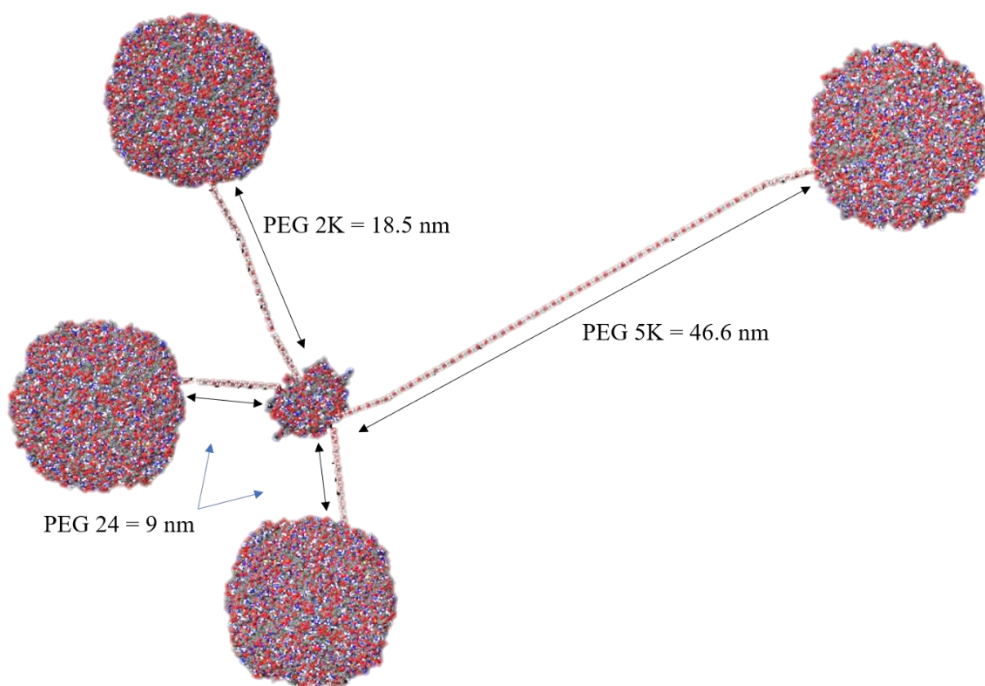


Figure 2.15. Four biotinylated ferritin capsules with different PEG linker lengths are attached with an avidin through the biotin-binding sites. The figure utilized the structures of avidin (PDB: 1AVD), horse spleen ferritin (PDB: 5ERK) and the chemical structure of the various PEG linkers.

As Table 1 indicates, three different biotin-binding proteins; avidin, streptavidin, and neutravidin were utilized as mediators to form protein networks following the same procedure. All

experiments used a stoichiometric ratio of 1:18, Biotinylated ferritin:biotin-binding protein. Figure 2.16A-D, presents a comparison between networks that were made using the three biotin-binding proteins. Vial A presents the control experiment. The control is a mixture of unbiotinylated ferritin and avidin. The figure shows a soluble mixture of both proteins. Vial B contains a complex of biotinylated ferritin with avidin that resulted in the development of aggregates of amorphous material which is believed to be an indication of the network components assembly due to the avidin-biotin complexation. This result is consistent with what has been found by other researchers, that avidin forms visible aggregates with biomolecules that have multiple biotinylations (Heitzmann & Richards, 1974). A further study has shown the formation of extended complexes using biotinylated protein and avidin, which subsequently created large visible aggregates (Garanger et al., 2009). Therefore, it was concluded that the previously obtained research is in line with our findings.

To expand on the protein scaffold assembly, the same experiment was carried out using the biotin-binding protein, streptavidin (Figure 2.16C). Interestingly, the protein network shows a soluble complex (Vial C). The mixture was monitored over the next 7 days to detect possible aggregation development; however, no visible change was noticed. Further exploration of the network self-assembly involved the addition of the neutravidin protein with biotinylated ferritin, which resulted in a soluble material, Figure 2.16D. Vial D shows no amorphous material. The observations in Vial C and D indicated that both neutravidin and streptavidin, do not form insoluble networks.

In contrary to our results, the streptavidin protein has demonstrated the formation of aggregates in many studies, by which controllably aggregated materials were observed by using the streptavidin-biotin interaction as well (Aslan et al., 2004). Moreover, another study reported

that a mixture of biotinylated ferritin and streptavidin incubated for 10-15 minutes results in the formation of observable yellow aggregates (Li et al., 1999).

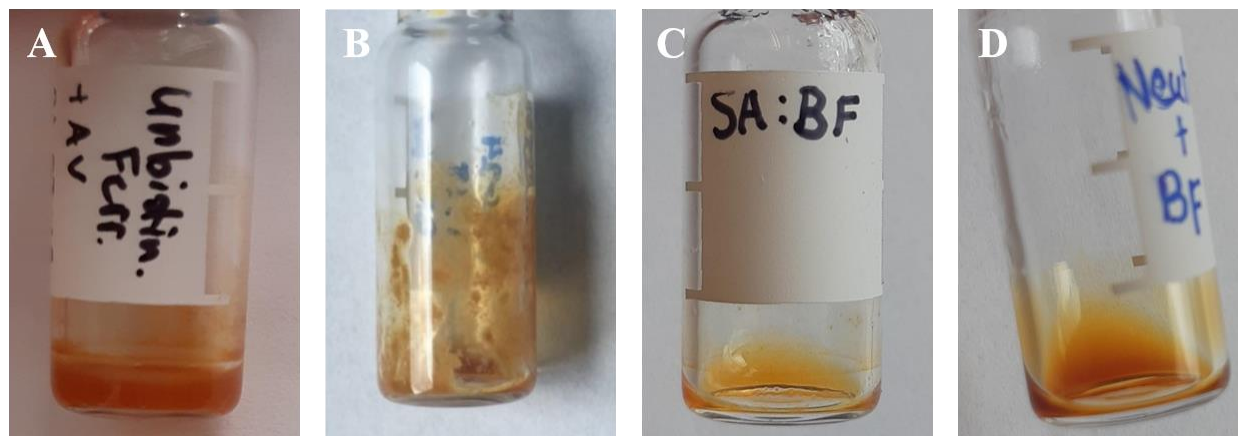


Figure 2.16. Protein networks. A) Control: unbiotinylated ferritin with avidin. B) Biotinylated ferritin with avidin. C) Biotinylated ferritin with streptavidin D) Biotinylated ferritin with neutravidin.

It was hypothesized that electrostatic interactions could play a role in the network assembly and aggregate appearance. This assumption was raised based on the isoelectric point (pI) values of the mediator proteins; avidin (pI = 10.5), streptavidin (pI = 5.0), neutravidin (pI = 6.3), in addition to the ferritin (pI = 5.0-6.0). For example, there might be an electrostatic attraction between modified ferritin and avidin, and repulsion among ferritin and streptavidin/neutravidin. The explanation of why the biotinylated ferritin would show electrostatic attraction with avidin (Vial B) while the unbiotinylated ferritin would not (Vial A), could be referred to the degree of biotinylation on the protein surface. The biotinylated ferritin utilized here was modified with biotin reagent at several lysine residues, which would result in less positive charge density on the surface. Perhaps electrostatic attraction between the modified ferritin displaying biotins and the avidin enhances the complexation phenomenon.

Further experimentation was carried out to learn more concerning the fabricated avidin-based networks. The network with avidin was constructed in a solution of 0.3 M and 1 M NaCl. The electrolyte concentration in the reaction mixture could reduce the protein surface charge contribution to the electrostatic interaction. Figure 2.17A & B show the network prepared in a 0.3 M and 1 M salt solution respectively. It was noticed that the presence of salt has a slight contribution to the solubility of the network with ionic concentration, however, clear populations of tiny aggregates were still observed (indicated with an arrow).

The ease of reversibility of formation of the network assembly upon adding free D-biotin molecules (244.3 g/mol) was investigated. It was hypothesized that if the network was not extremely tight and compact, the addition of free biotin might be able to exchange out the biotin-containing cross-linkers and dissolution of the solid complexes might result. The result of this experiment is shown in Figure 2.17C. The addition of 4-fold of D-biotin relative to avidin molar quantity has resulted in a more soluble network within 30 minutes, in comparison to the network in Figure 2.16A, which shows that the biotin-avidin complex of the protein network may have been replaced with free D-biotin-avidin.

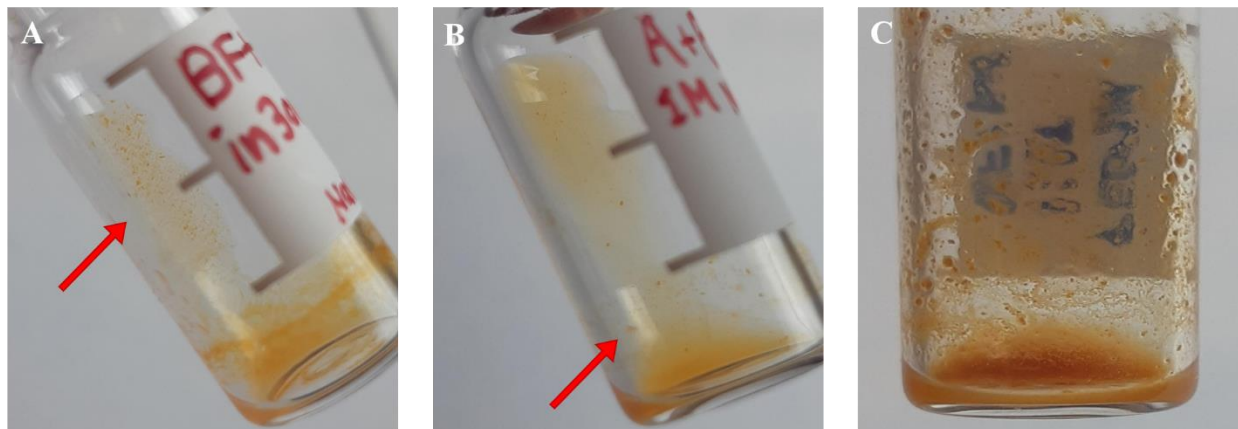


Figure 2.17. Ferritin-Avidin networks. A) A network assembled in 0.3 M NaCl. B) A network assembled in 1 M NaCl. C) A pre-assembled network with free D-biotin molecules added in a 4:1, biotin:avidin ratio.

Additional experiments are to be carried out in order to further draw a full view of the ferritin-avidin protein networks. A proposed experiment would include the network formation using a biotin-free TFP-ester cross-linking reagent (mPEG₂₄-TFP ester) and the reaction of this modified ferritin with avidin.

In addition to observing the material in solution, a solid form was visualized as well. The biotinylated ferritin, produced by reaction with the biotin-PEG₁₂-TFP reagent, was added directly (10 mg/ml) to avidin (50 mg/ml) on a glass slide and allowed to dry at room temperature. The formation of a thin film of solid amorphous biomaterial was noticed (Figure 2.18B). Figure 2.18A shows a control of the same ratios of unbiotinylated ferritin and avidin. This mixture had dissolved readily upon adding water to it, whereas the second mixture shown in Figure 2.18B, did not readily dissolve. Instead, it exhibited the shape of flakes when dried.

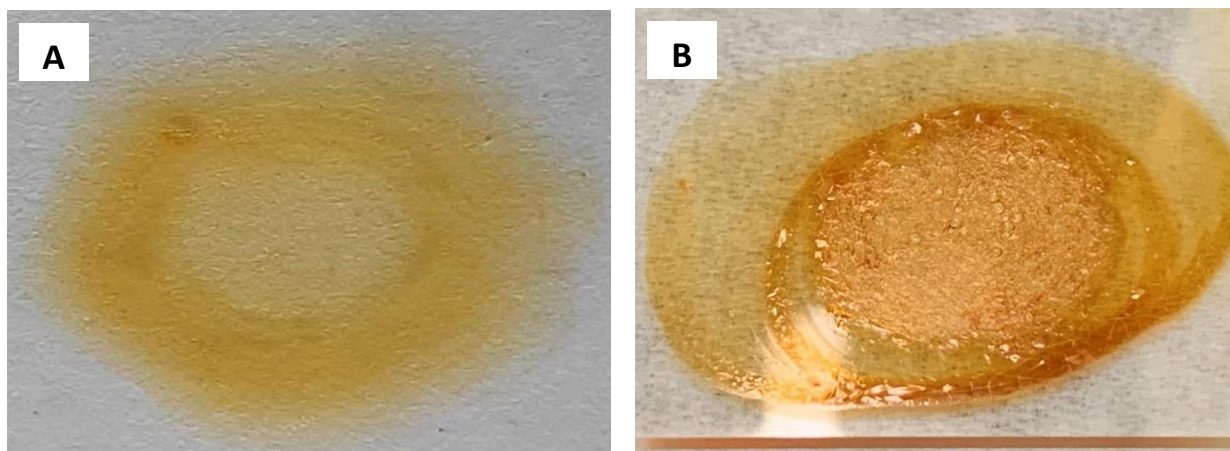


Figure 2.18. A) Control of unbiotinylated ferritin and avidin on a glass slide. B) A thin film of a solid amorphous material made of biotinylated ferritin and avidin.

2.5.6 SEM Characterization

The protein networks made of biotinylated ferritin (biotin-PEG₂₄-TFP), and avidin proteins were visualized using SEM microscopy. The image depicted in Figure 2.19A was set to a resolution of 20 nm. It is clearly possible to observe white dots that correspond to the ferritin iron core of the protein network. Additionally, the EDX technique was used in conjunction with SEM to report the chemical elemental composition of the sample being characterized (Figure 2.19B). The EDX analysis reveals the identity of the bright dots to be iron, as the Fe signal was detected (Figure 2.19B). Distance analysis was done to measure the average distances between ferritin molecules using the “Fiji – ImageJ” software (Schindelin et al., 2012). The average distance between the particles was found to be approximately 18 nm in length. This length suggests that the PEG spacers between ferritin molecules are not fully extended to the maximum length of 45 nm. Another explanation would involve the imaging dimensions of the SEM. SEM shows a two-dimensional image, and as the material being characterized has three dimensions, any two neighboring ferritin iron-cores shown in the image, might be in a different layer/plane of the three-

dimensional structure. This results in a measurement that is not specifically reflective of the distance between two ferritin capsules.

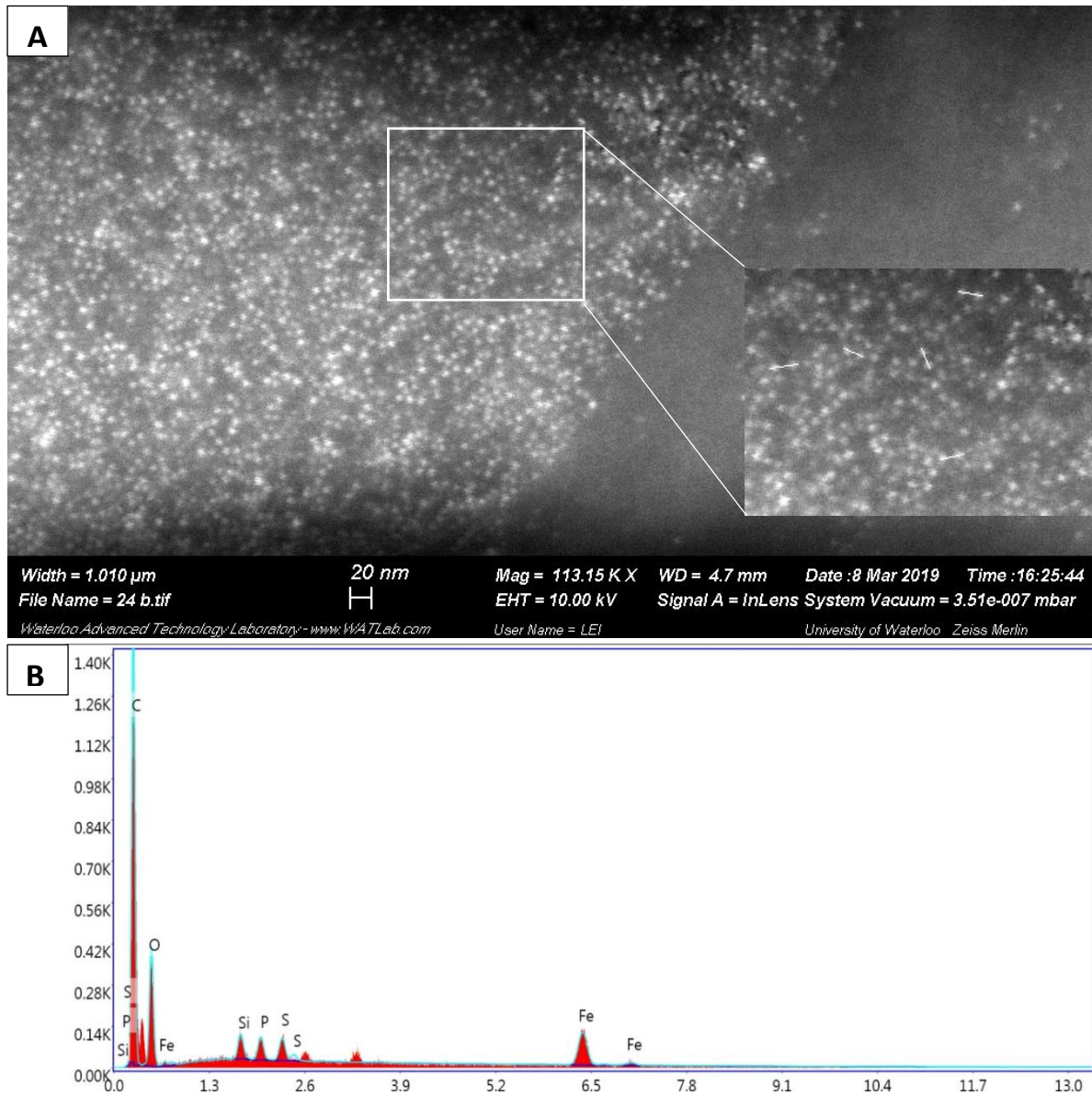


Figure 2.19. A) SEM image of biotinylated ferritin (PEG₂₄-TFP)-avidin material B) EDX analysis shows the chemical elements of the material.

2.5.7 The Effect of Enzyme-bound Ferritin-avidin Network on PET Degradation

An enzymatic-bound ferritin-avidin scaffold was prepared and washed as described in Section 2.5.10. The use of BSA was required in the washing step in order to exclude the protein-protein non-specific van der Waals interactions that emerge upon mixing the biotinylated HiC enzyme with the ferritin-avidin scaffold. To explore the non-specific interactions, the Schrodinger software was employed to map the hydrophobic patches on the surface of HiC cutinase (PDB: 4OYY) and avidin (PDB: 1AVD), both illustrated in Figure 2.20. Significant regions of hydrophobic residues on the HiC enzyme surface appear in green in Figure 2.20A, which are believed to contribute to the surface adsorption to the avidin in the scaffold, which also contains some hydrophobic surface residues (Figure 2.20B).

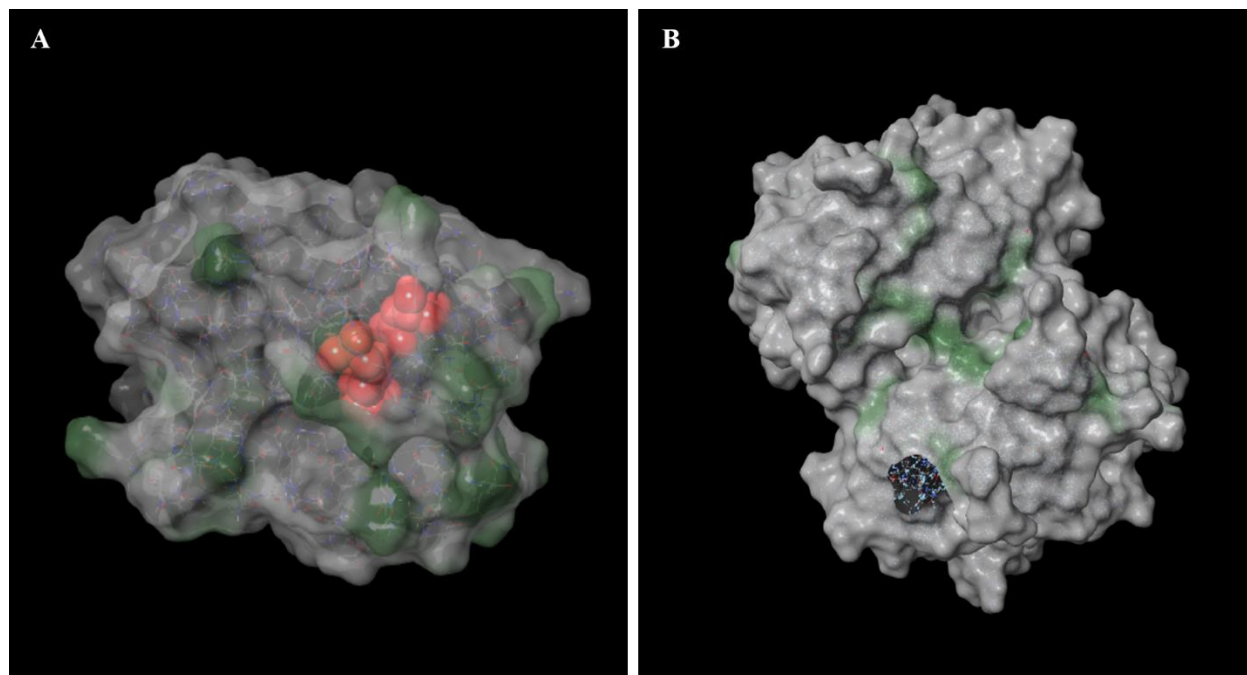


Figure 2.20. Surface mapping of the hydrophobic patches responsible for non-specific interactions between: A) HiC enzyme (PDB: 4OYY) and B) avidin protein (PDB: 1AVD). Hydrophobic regions are shown in green. Images were generated using Schrödinger software. (Schrödinger Release 2020-2: BioLuminate, Schrödinger, LLC, New York, NY, 2020).

Excluding non-specific interactions helped in keeping only the enzymes that were affixed to the material through the biotin-avidin interaction. The presence of BSA and Tween 20 detergent in the solution helped in improving the dispersity and in reducing the non-specific interactions between proteins. Moreover, the HiC enzyme molecules were also found to adhere to surfaces such as tubes or pipette tips, as was previously determined by Jameson Pfeffer (Pfeffer, 2019). Therefore, the washing step was also used to avoid the participation of free enzyme molecules during the enzymatic activity assay that were initially bound to the tube and not to the protein scaffold.

In the control experiment with no enzymatic scaffold, the results obtained from scanning electron microscopy experiments from PET plastic incubation with free HiC enzyme solution at 55 °C and room temperature are shown in Figures 2.21 and 2.22, respectively. The micrographs in Figure 2.21B & D show the PET section with severe digestion as a result of 19 days incubation with the HiC enzyme at 55 °C. While Figure 2.22B & D show no evidence of enzymatic damage when incubated with HiC solution for the same duration at room temperature. These results were obtained by Jameson Pfeffer (Pfeffer, 2019).

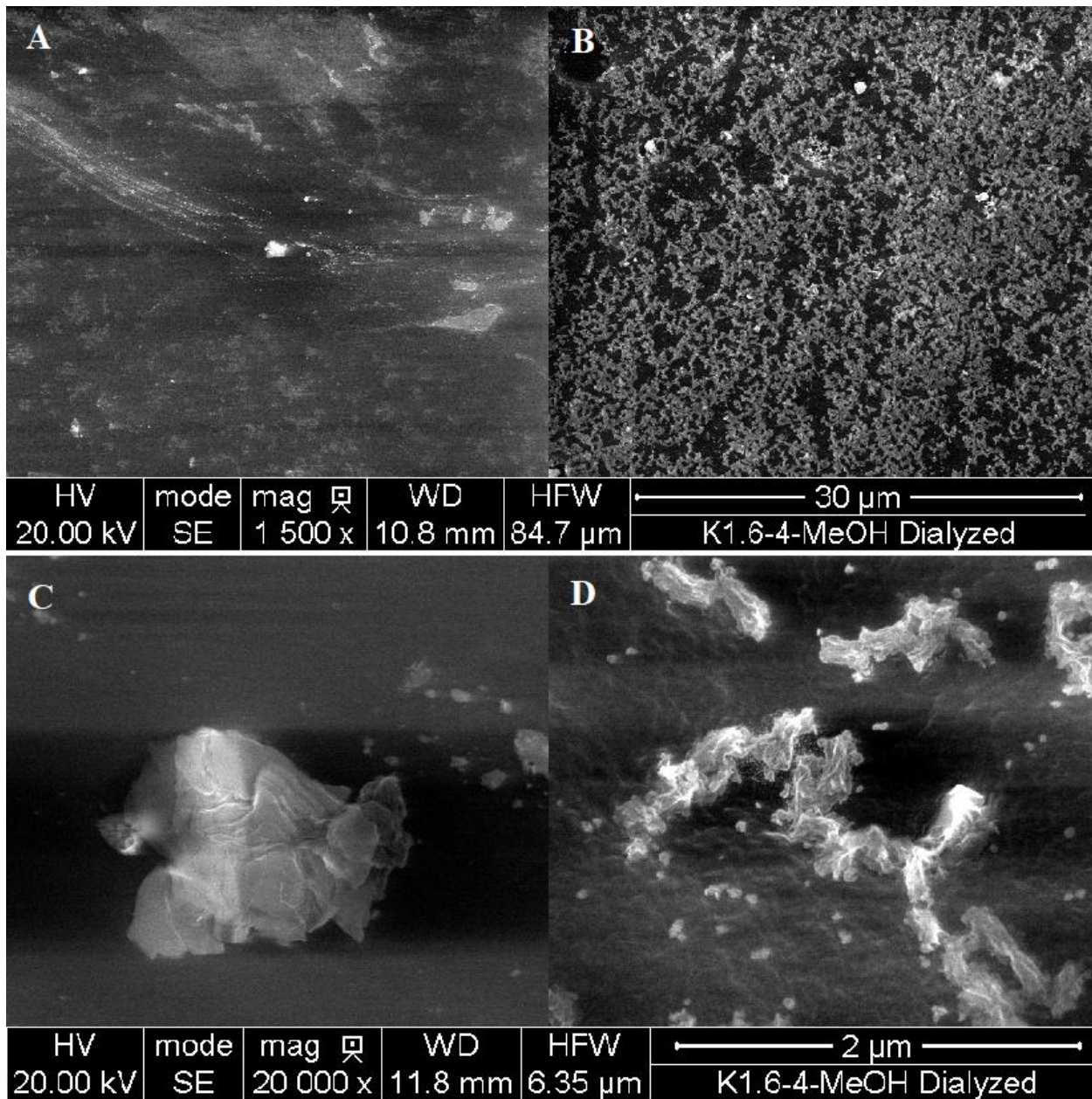


Figure 2.21. A, C) SEM micrographs of PET plastic exposed to 200 mM sodium phosphate buffer at pH 7.0. at 55 °C for 19 days. B, D) SEM micrographs of PET plastic exposed to 20 mg/ml HiC enzyme solution. Images A/B and C/D were taken with 1500 x and 20,000 x magnification, respectively.

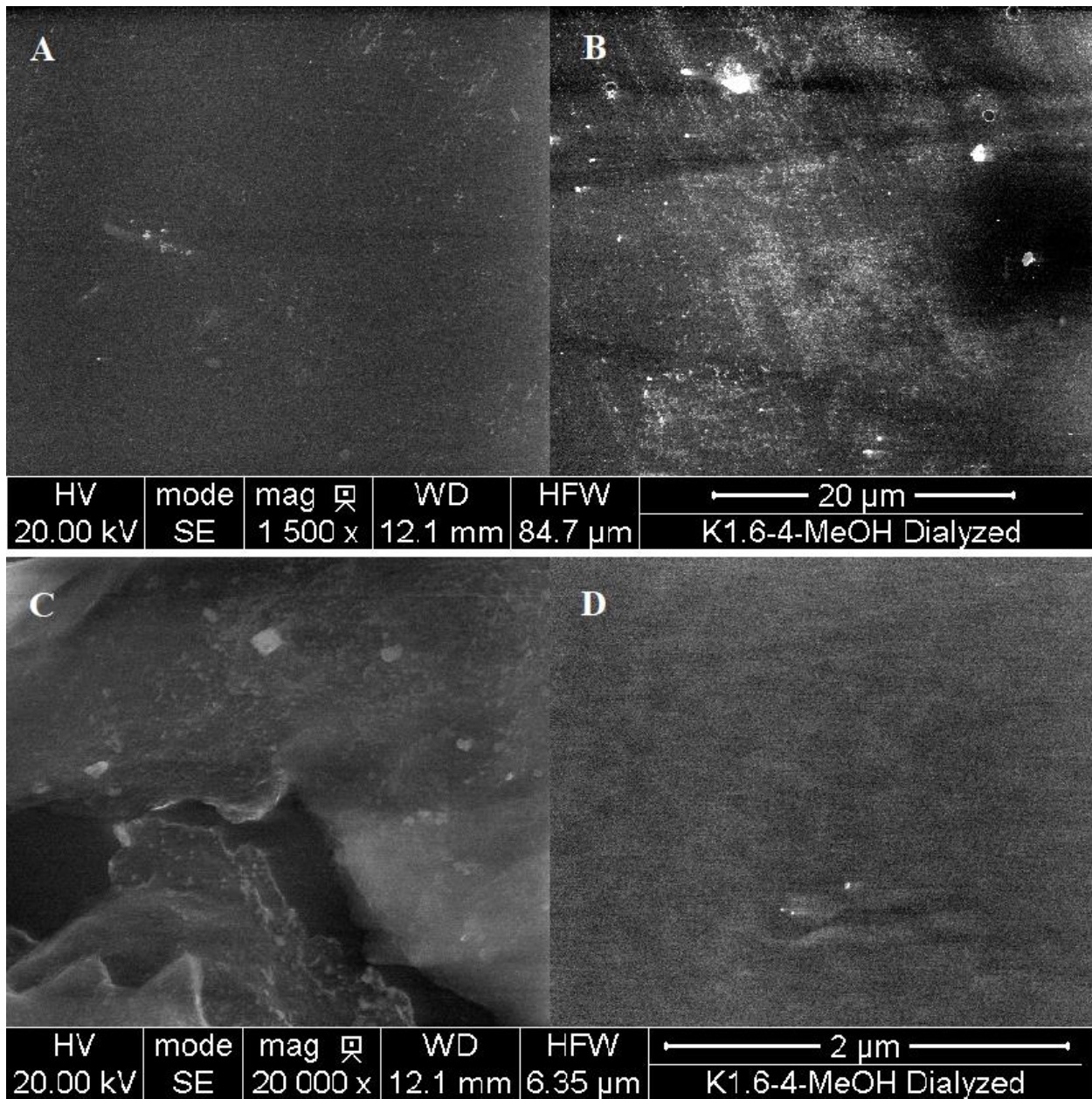


Figure 2.22. A, C) SEM micrographs of PET plastic exposed to 200 mM sodium phosphate buffer at pH 7.0. at room temperature for 19 days. B, D) SEM micrographs of PET plastic exposed to 20 mg/ml HiC enzyme solution. Images A/B and C/D were taken with 1500 x and 20,000 x magnification, respectively.

The effect of the fabricated enzyme scaffold on digesting PET plastic was also examined by monitoring the surface morphology of PET. The PET segments were incubated with the enzyme-bound scaffold at room temperature for 15 days. The subsequent PET surface damage as a result of HiC digestion of PET polymers was visualized using SEM to monitor the evidence of PET surface damage as a result of digesting PET polymers, caused by the esterase activity of the enzymatic scaffold during incubation. First, control samples were prepared for comparison.

The next figure presents a set of control images on untreated PET with 1500x and 20,000x magnification. Figure 2.23A & C shows a sample of dry PET with no enzyme exposure, and Figure 2.23B & D is for a sample was exposed to 200 mM sodium phosphate buffer, pH 7.0 buffer with no enzyme exposure.

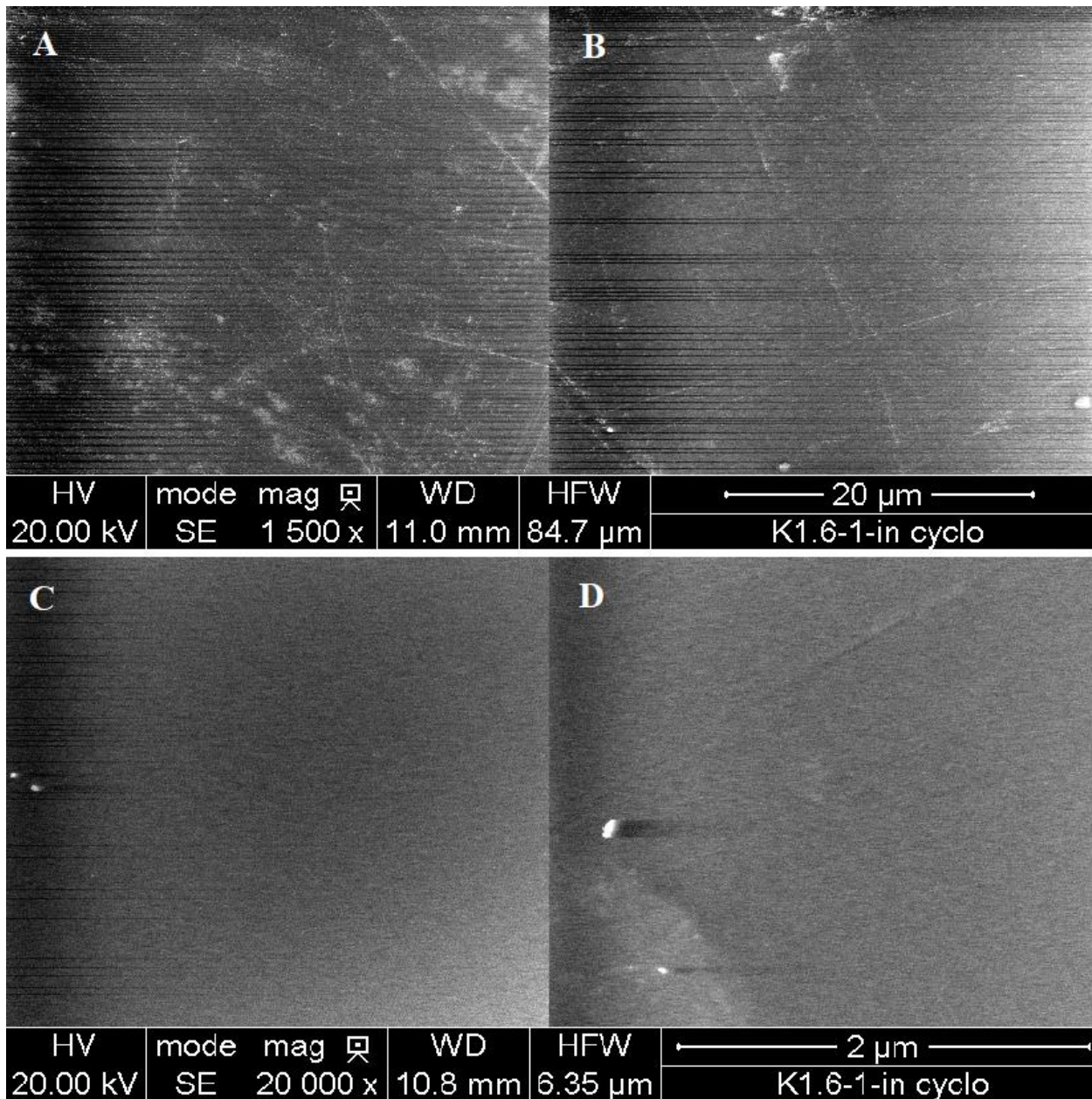


Figure 2.23. SEM images of PET samples incubated at room temperature for 15 days. A, C) Image of untreated dry PET section taken with 1500 x and 20,000 x magnification. B, D) Untreated PET section exposed to 200 mM sodium phosphate buffer, pH 7.0 with 1500 x and 20,000 x magnification.

Next, the enzymatic scaffold exposure effect was tested on the PET sections. Figure 2.24 displays the hydrolysis effects of exposure to an enzyme-bound scaffold over 15 days of room temperature incubation. The images obtained exhibit obvious instances of damage to the studied sample of PET plastic. More notably, is the observation of an apparent hole in the PET section caused by the HiC scaffold. The micrographs in Figure 2.24 A, C & E correspond to one spot on the PET section and present subsequent magnification. These images were generated by a secondary electron (SE) detector. While the micrographs in Figure 2.24 B, D & F that correspond to a second spot in the same PET sample, were generated by a backscattering (BS) electron detector. BS detector can be more useful in providing more topographic information by the maximized contrast, which is clearly noticed in the micrograph, since it relies on the elastic reflection interaction between the sample and the electron beam.

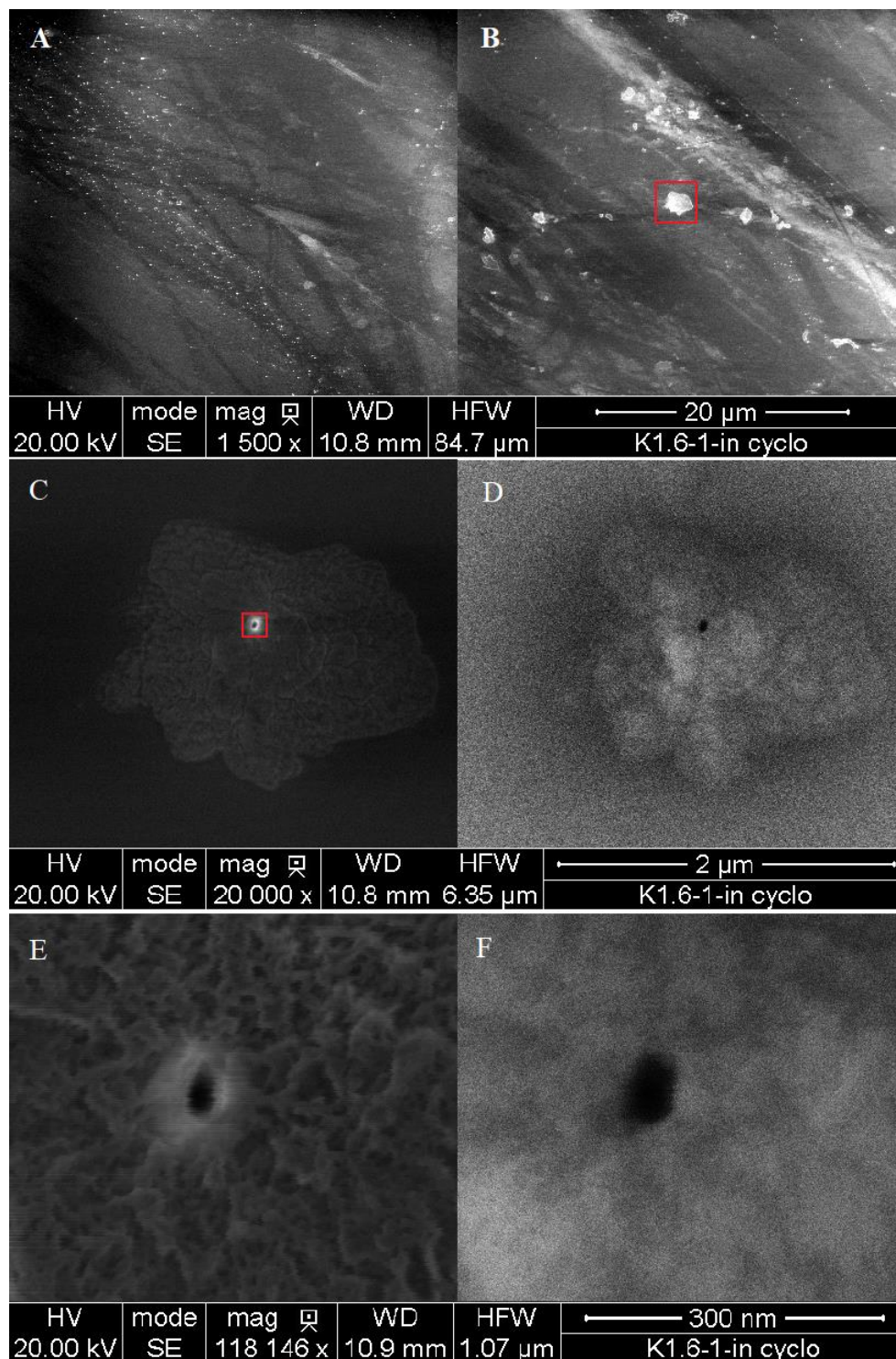


Figure 2.24. SEM images of PET after digestion by the enzyme-bound scaffold over the duration of 15 days at room temperature. The micrographs were taken with 1500 x, 20,000 x, and 118,146 x magnification. Images A, C, and E were taken using an SE detector, and images B, D, and F were taken using a BE detector.

The scanning electron microscopy imaging of PET plastic incubated with the enzymatic-scaffold was consistent with degradation similar to that observed by the enzyme alone. However, the enzymatic scaffold was more successful than the soluble free enzyme in causing PET degradation at room temperature, while the soluble enzyme required elevated temperature to exhibit a damaging effect.

2.5.8 Photolytic Behavior of PC biotin-PEG₃-NHS Carbonate Ester Containing Protein Network

In this part of the project, we explored the use of a photo-responsive PEG spacer in the design of the ferritin-avidin network. HSF was modified using the PC biotin-PEG₃-NHS carbonate ester, a known labile photocleavable cross-linker. The ferritin-avidin network containing ferritins modified with the photocleavable linker was then exposed to UV light at 365 nm for 0, 30, and 45 min (Levalley et al., 2020). Initial attempts were performed by pipetting the sample in a closed plastic centrifuge tube; however, this way did not result in chemical bond photolysis due to the presence of a physical barrier, the plastic tube. Therefore, a polystyrene microplate was used, which substantially improved the PEG reagent photolysis process.

The results of the MALDI-TOF analysis for the ferritin-avidin photocleavable protein network after undergoing UV radiation exposure at 365 nm for 0, 30, and 45 minutes are shown in Figure 2.25. Spectrum A is the mass peak of the unexposed network control corresponding to a peak at 15981 m/z, which is the avidin monomeric mass, and a second peak at 20066 m/z. This peak exhibits a significant widened peak base creating a shoulder at a mass corresponding to the PC biotin cross-linker, evidence that this mass peak was comprised of two components, that concludes a successful conjugation. Both spectra B, and C, which belong to samples with 30 and

45 min UV light exposure, respectively, show that the shoulder peak has completely disappeared.

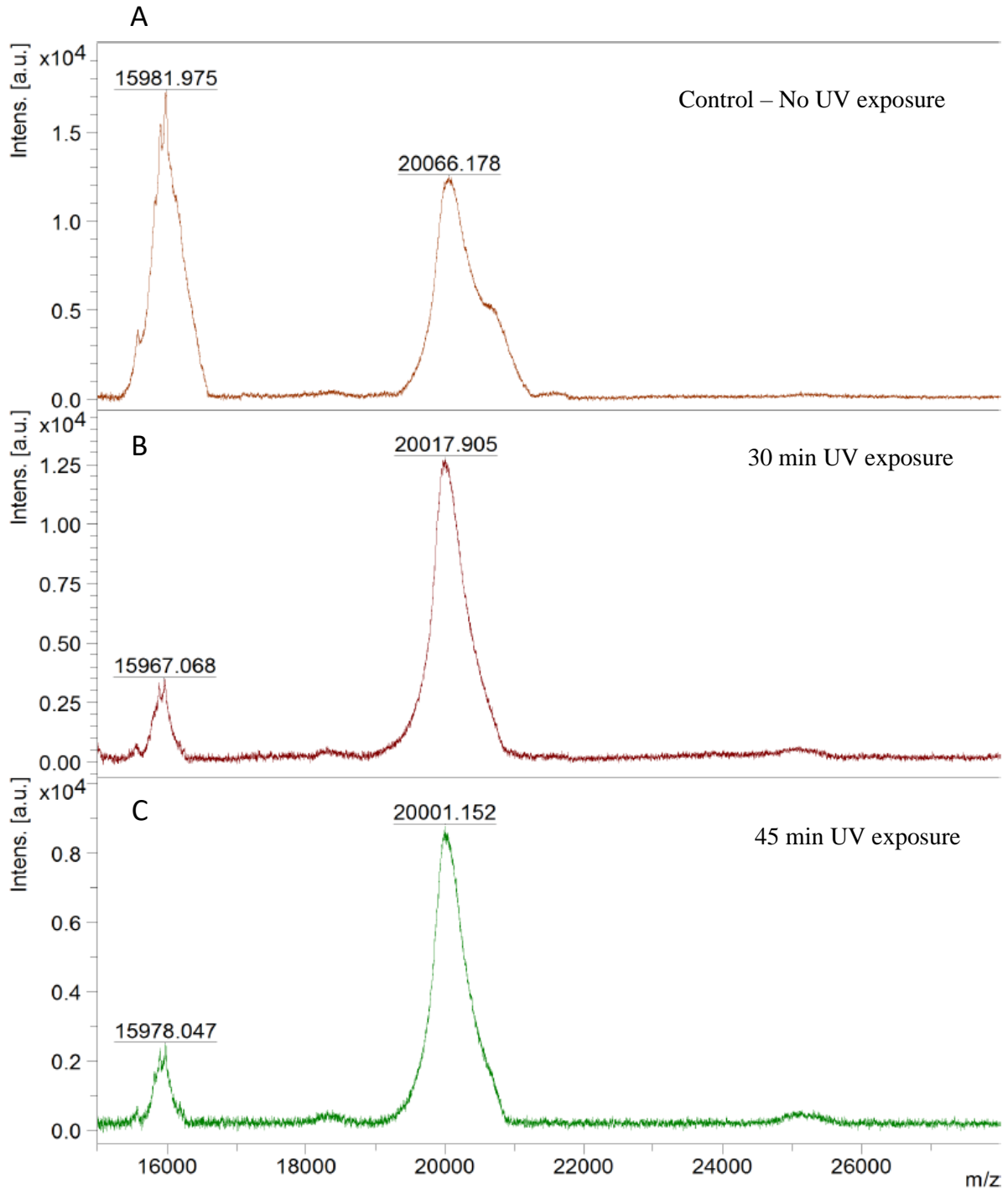


Figure 2.25. Results of MALDI-TOF for the photolytic protein network. A) Protein network with no exposure to UV light. B) 30 min UV light exposure. C) 45 minutes UV light exposure.

The absence of the shoulder increment in the biotinylated ferritin mass peak is an implication of the full photolysis of the ferritin-avidin network. The photolysis of the network is expected to follow the Norrish type II photocleavage mechanism (Figure 2.26), where the cleavage occurs at the carbamate moiety of the reagent (Dalal et al., 2018).

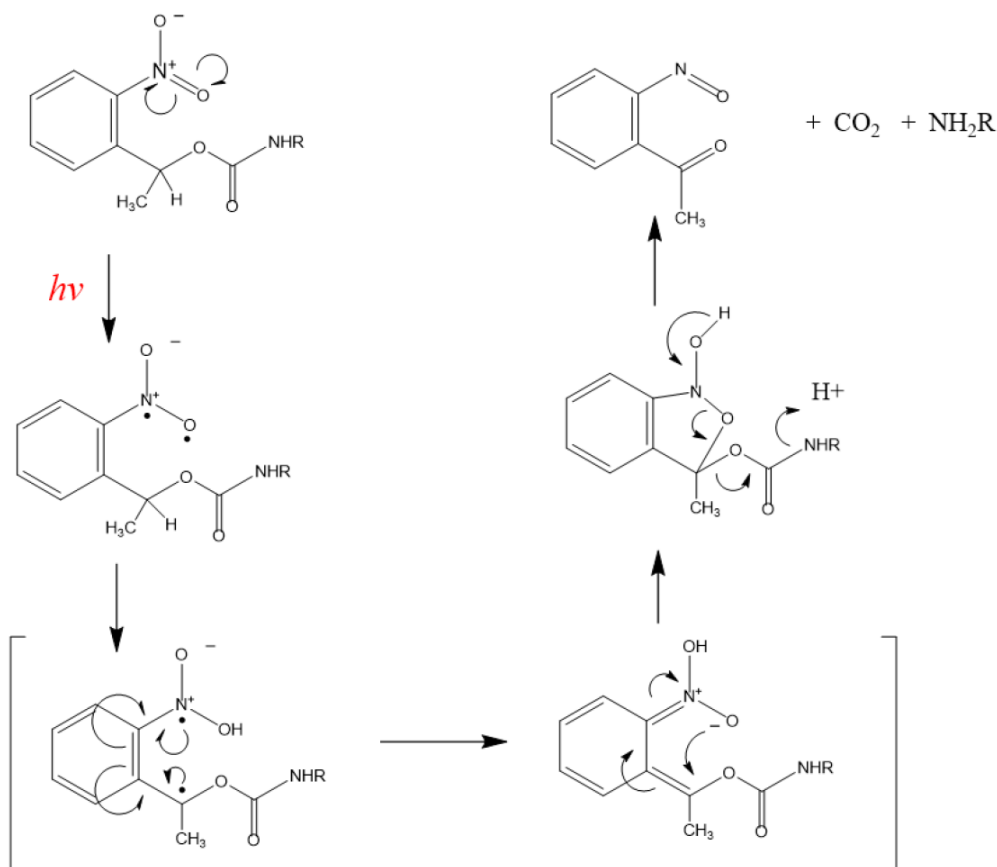


Figure 2.26. The mechanism of Norrish type II photocleavage at the carbamate moiety.

As the PC biotin reagent attachment is released from ferritin, the ferritin-avidin bond through the biotin linker will be freely liberated in the solution causing the subsequent degradation of the protein network. The mass spectrometry results in Figure 2.25 confirm that the network was successfully photocleaved within 30 minutes of UV light exposure. An image of this photolyzed

network is presented in Figure 2.27, which shows a dissolved material as a result of the UV light exposure that triggered the carbamate moiety cleavage.

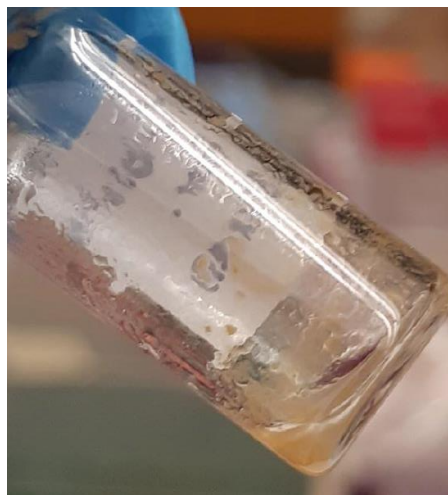


Figure 2.27. Ferritin-avidin network exposed to UV light at 365 nm for 30 minutes.

Based on these findings, the strategy of exploiting a controlled labile drug compound in the ferritin-avidin network seems to be a promising approach that can be pursued to for medical applications to fabricate a self-healing protein nanomaterial bandage. Figure 2.28 is a scheme for the design of a protein-based smart bandage that releases the drug Besifloxacin.

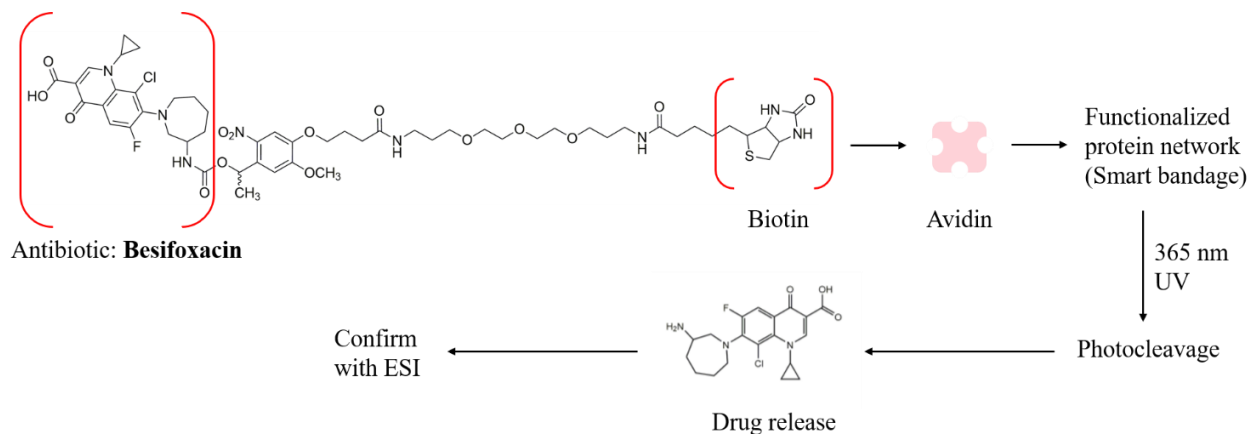


Figure 2.28. The design of functionalized protein networks with photocleavable drug molecules for medical applications (e.g. Smart bandages).

3 Chapter 3: Development of a New Bioconjugation Strategy

3.1 Introduction

Tris-2-carboxyethyl phosphine (TCEP) (Figure 3.1A) is a water-soluble reducing agent used in protein modification and organic synthesis preparatory steps to reduce even the most stable disulfide bridges between cysteine residues and sulfhydryl alkyl molecules (Liu et al., 2010). This reducing agent is a mandatory step prior to protein bioconjugation reactions to produce free-thiol nucleophilic cysteines, making them ready for alkylation via a cross-linking compound, typically with a maleimide-containing molecule in a bioconjugation reagent. The double bond of the maleimide ring (Figure 3.1B) undergoes alkylation by sulfhydryl residues to form a stable thioether bond, occurring through a typical Michael addition reaction.

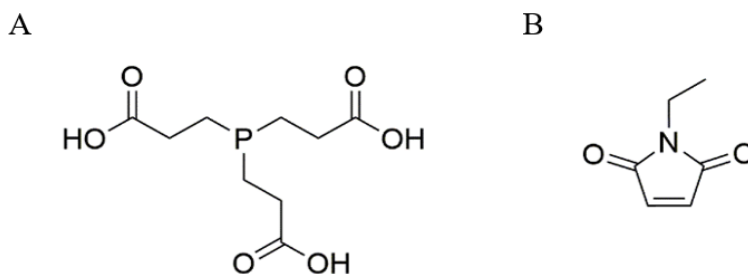
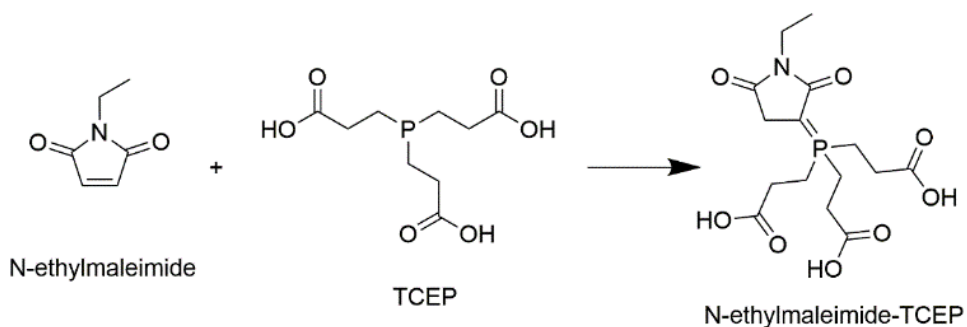


Figure 3.1. Chemical structure of A) Tris-2-carboxyethyl phosphine (TCEP) reducing agent, and B) N-Ethylmaleimide.

TCEP is odorless, and it is more stable as a reducing agent than dithiothreitol (DTT) or β -mercaptoethanol (BME), in addition to being more effective over a wider pH range (Liu et al., 2010). Using phosphine-based reducing agents as a replacement to the thiol-based agents is more favorable as they interact more rapidly, have a physiological pKa (i.e. 7.4) suitable for a wide range of bioconjugation reactions, in addition to their reaction being irreversible when reducing

the disulfides, unlike thiol-based reducing agents that can oxidize the sulfhydryl groups back to disulfide bridges in a reaction mixture (Kantner et al., 2017).

A different aspect of TCEP functionality is considered in this chapter. The common protocols for disulfide reduction suggest that there is no need to remove TCEP from the reaction mixture before introducing the maleimide-based conjugation reagent (Kantner & Watts, 2016). Contrary to this, some articles in the literature have demonstrated that the nucleophilic phosphorous atom of TCEP is reactive towards the Michael acceptor, maleimide, producing a stable TCEP-MAL ylene incapable of interacting with the cysteinyl thiols (Mthembu et al., 2020). A model interaction of N-ethylmaleimide (NEM) and TCEP is shown in (Scheme 3.1).



Scheme 3.1. Reaction of N-ethylmaleimide and TCEP agent to form a stable ylene adduct.

This hypothesis was evidenced by the decrease of maleimide-conjugation yields in addition to the formation of an unreactive side product resulting from the reaction between both compounds, suggesting that the maleimide reagent is being neutralized in the presence of the reducing reagent, TCEP (Kantner & Watts, 2016). Several techniques were utilized to support these observations. Moreover, the Honek group has encountered similar findings. A former student, Dr. Hawa Gyamfi, noticed that upon using TCEP reagent to reduce the disulfide bonds in *Archaeoglobus fulgidus* ferritin (AfFtn) protein, that TCEP inhibits the reaction between protein

cysteine residues and maleimido-C3-NTA, where the cysteines remained unmodified after incubation at different time points (Gyamfi, 2019). The mass spectrometry chromatograms of the AfFtn incubated with the N-substituted maleimide reagent exhibited an unmodified protein signal, in the presence of TCEP. Whereas, upon removing the TCEP from the reaction, all the cysteine residues were 100% modified with the maleimide reagent on all the subunits of the protein, showing that indeed there is a competitive reaction between both species.

Another study by Kantner and his group suggested developing a method to compromise the reactivity of TCEP towards maleimide without having to remove the TCEP from the reaction. This strategy employed the PEG-azide reagents to quench the TCEP activity towards maleimide, which helped in retaining the protein conjugation efficiency of the cysteine-maleimide reactions as shown in Figure 3.2. PEG-azides were shown to be capable of oxidizing the trialkylphosphine molecules to constrain the phosphorous nucleophilic attack. Figure 3.2. shows an SDS gel with and without PEG-azide quenching of TCEP (Kantner et al., 2017).

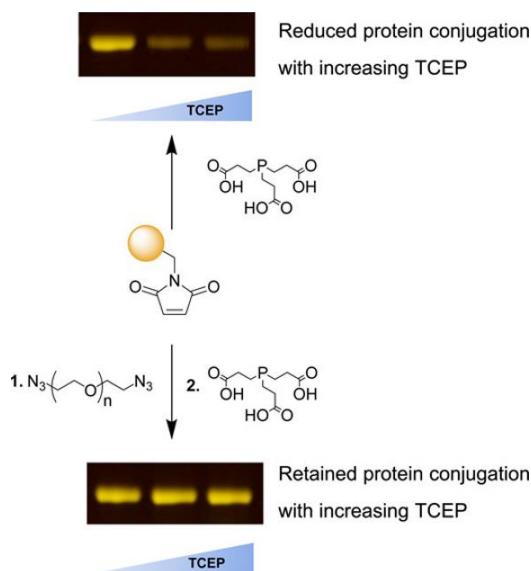
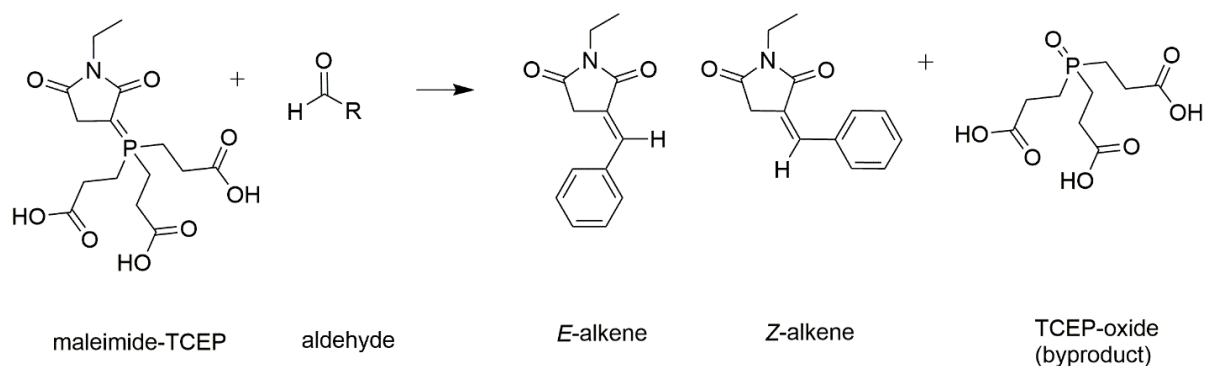


Figure 3.2. Reaction of maleimide and TCEP in the presence of PEG-azides that resulted in retaining the protein conjugation. Reproduced with permission under CC license from (Kantner et al., 2017).

Wittig olefination is an important organic reaction which allows for the production of an alkene by the reaction of a carbonyl moiety of a ketone or an aldehyde with a phosphonium salt, namely an ylide, which is a zwitterion compound that produces phosphine oxide as a byproduct (Scheme 3.2). The Wittig reaction has been extensively used in the pharmaceutical area. A common use is the synthesis of tetraterpenoid compounds, e.g. carotenoids, via the carbonyl olefination of a symmetrical or asymmetrical C_x-dialdehyde with two equivalences of an appropriate C_x-phosphonium salt (Bogacz-Radomska et al., 2020). The generalized N-substituted maleimide-alkyl phosphorous adducts were demonstrated to undergo Wittig reaction with aldehyde derivatives under certain conditions (Bogacz-Radomska et al., 2020). Literature reviews have reported a diverse range of organic synthesis conditions that require a heating step at a temperature in the range 50-100 °C, over a 1-12 hour period, and the required use of different concentrations of base catalysts, while other articles reported no use of a base catalyst (Kim et al., 2017) (Bayat et al., 2017) (Brackman et al., 2013). This reaction with an aldehyde produces a mixture of *E*- and *Z*-olefins (Thiemann, 2007) (Scheme 3.2), with the *E* configuration to be more dominant (Bayat et al., 2017) and thermodynamically more favorable isomer.



Scheme 3.2. Wittig reaction mechanism of an N-Ethyl maleimide-TCEP adduct with an aldehyde that produces *E*- and *Z*- alkenes, with the *E*-isomer being more thermodynamically favorable, and phosphine-oxide as a byproduct.

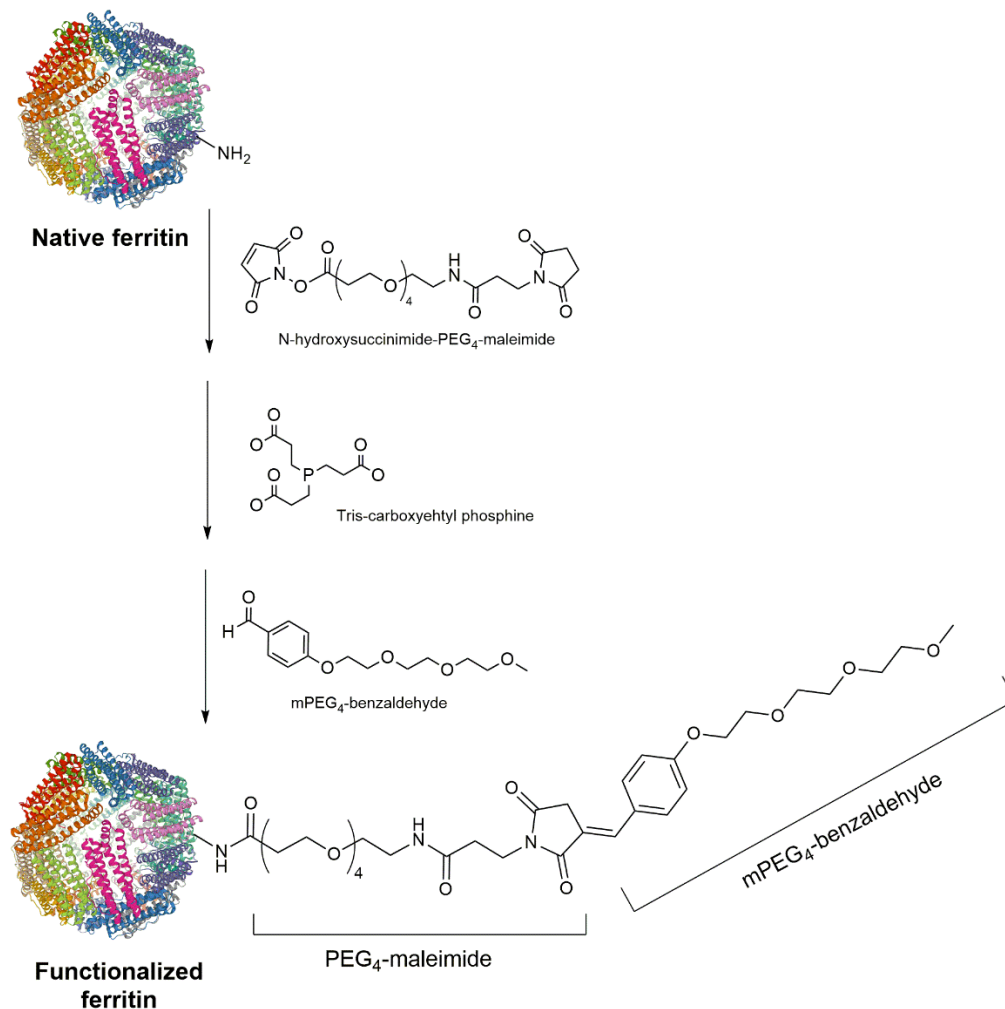
With respect to protein modification reactions, a wide array of functional groups can be covalently and irreversibly introduced site-specifically to a protein of interest via a Wittig reaction. The traditional method is the olefination of an existing aldehyde group on a protein. Aldehydes are not naturally available within proteinogenic amino acids, however, incorporating an aldehyde handle within the amino acid sequence of a protein can be achieved through different strategies, such as the chemical installation of tags, the enzymatic incorporation of probes, or the site-specific incorporation for non-native carbonyl-containing amino acids (Agten et al., 2016). Nevertheless, the carbonyl's electronic properties will differ according to the employed strategy (Spears & Fascione, 2016). Recent bioconjugation studies on enabling the Wittig olefination reaction on aldehyde-tagged proteins reported a 65% yield determined by ESI- and MALDI-MS (Han et al., 2012). This approach has shown promising applications, by which studies have demonstrated tangible potential for protein tracking in live cells via Wittig enhanced fluorescence tagging (Spicer & Davis, 2014). Other applications were described by the successful streptavidin-mediated affinity isolation of proteins, through the Wittig conjugation of a biotin-phosphonium salt on an aldehyde-functionalized FKBP12 protein (Lum et al., 2013).

Wittig reactions are commonly performed and work well with solvated adducts in an organic-aqueous environment. On the other hand, performing Wittig reactions employing polymer supported resins containing trialkylphosphines instead of the free phosphines can result in a more efficient strategy as it can be considered more environmentally and economically friendly. Moreover, a resin-based approach has been reported to afford purer olefin products and eliminates the sometimes-difficult removal of the phosphine oxide byproduct by having it remain attached to a polymer, which is easily separated from the desired product (Moussa et al., 2019). More advantages offered by the utility of solid supported resins might also be realized if they were

employed in strategies to immobilize target enzymes onto these resins, providing enzyme-attached resins capable of possibly increased stability and ease of recycling from a reaction mixture (Mohamad et al., 2015).

3.2 Objectives

This chapter outlines the detailed methodology that was followed to investigate the viability of a multi-step strategy to achieve a new approach to protein bioconjugation. The approach will be to attach a maleimide-based functionality to the surface of a protein, reacting this maleimide with TCEP to form a reactive ylide, and then to attempt to utilize this functionality to perform a Wittig reaction with an aldehyde to finally produce a modified protein. We decided to exploit former research findings in this area, supported by our group's observations, in order to generate a strategic approach to indirectly bioconjugate PEG-aldehyde-containing molecules to a ferritin surface, further allowing to incorporate a select aromatic aldehyde to protein networks. The protein used in this project, ferritin, is not rich with cysteine amino acids and contains only one unexposed residue. Our previous trials in modifying this cysteine were not fruitful, therefore we decided to employ a heterobifunctional cross-linking reagent, NHS-PEG₄-maleimide, that might be expected to be bioconjugated to lysine residues -which are abundant on the surface of ferritin- at one end and will expose a solvent-accessible maleimide group on the protein surface at the other end. To the best of our knowledge, no studies have been undertaken that employ this strategy. If successful, the approach would allow a protein to be modified with a maleimide functional group and allow for a wide array of aldehydes to be attached to the protein for applications in biophysics, drug delivery, and immobilization (Scheme 3.3).



Scheme 3.3. A novel bioconjugation strategy on ferritin proteins aims to attach a wide array of aldehyde molecules via Wittig olefination.

3.3 Materials

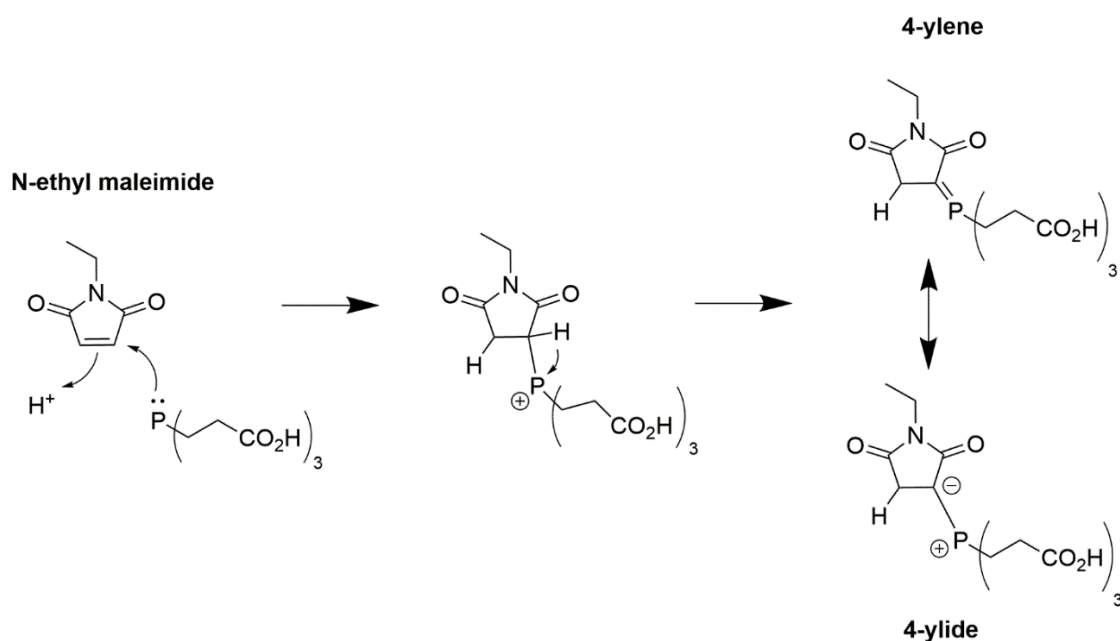
The following compounds were obtained from the noted commercial resources: Tris(2-carboxyethyl)phosphine hydrochloride, (TCEP.HCl; <= 100%; Sigma-Aldrich, Canada). *N*-Ethylmaleimide (NEM) (J. T. Baker Chemical Co. NJ, US). *p*-Anisaldehyde (98%; Sigma-Aldrich, Canada). MAL-dPEG®₄-NHS ester (90%; Quanta BioDesign, Ltd, USA), mPEG₄-benzaldehyde

(98%; BroadPharm, San Diego, CA, USA), Sephadex G-25 resins. Nickel His-TrapTM HP column (GE Healthcare, Chicago, USA).

3.4 Methodology

3.4.1 Reaction of N-ethylmaleimide with Tris-2-carboxyethylphosphine

Initial investigations were performed under mild conditions similar to protein conjugation reaction conditions. NEM (8.0 mg, 0.064 mmol) and TCEP (1 equiv., 18.3 mg, 0.064 mmol) were dissolved in 1 mL of doubly distilled water purged with argon gas for 10 min, then incubated while stirred for 1 hour at room temperature. The reaction mechanism is described in Scheme 3.4. The mixture was completely dissolved showing a clear solution with a concentration of 66 mM. After incubation, the adduct was analyzed and detected on ESI-MS instrumentation.



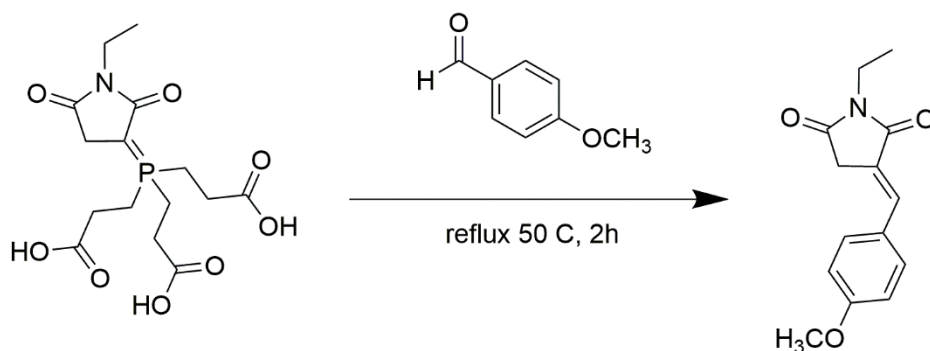
Scheme 3.4. Reaction mechanism of N-ethylmaleimide with tris-2-carboxyethylphosphine incubated for 1 hour at room temperature.

3.4.2 ^{31}P NMR

Phosphorous Nuclear Magnetic Resonance (^{31}P NMR) spectroscopy was employed to verify the formation of the synthesized adduct. A sample of the NEM-TCEP adduct (7.2 mg, 300 μL) described above, was diluted with deuterium oxide, D_2O , and transferred to a new 7" NMR tube (NE-HL5-7"). The sample was analyzed using a 500 MHz high resolution UltraShieldTM Bruker spectrometer for 2-4 hours. The pulse program used was zgpg30 with pulse delay of 3 seconds.

3.4.3 Optimization of Wittig Olefination Reaction Conditions

Various attempts were pursued to react an aldehyde moiety to the TCEP-NEM adduct (Scheme 3.5). The *p*-anisaldehyde was chosen as simple aromatic model to achieve the Wittig product, before conducting this reaction on a protein. All of the preliminary conducted experiments were unfruitful, until we eventually could optimize a successful procedure that yielded the desired product.



Scheme 3.5. Reaction scheme of NEM-TCEP adduct with *p*-anisaldehyde results in the alkene product with the *E*-isomer.

p-Anisaldehyde (136 g/mol) was chosen and first attempted as a model aldehyde to test the viability of an NEM-TCEP Wittig olefination with a simple aldehyde. *p*-Anisaldehyde (1.123 g/mL, 0.033 mmol, 4 μ L, 5 equiv.) was added to the previously prepared and verified TCEP-NEM adduct (6.6×10^{-3} mmol, 100 μ L) in 20% HPLC grade ethanol solution (400 μ L) as the organic solvent. A strong base, sodium hydroxide; NaOH (2 M, 6.6×10^{-3} mmol, 3.3 μ L) was added to the reaction mixture with an adduct:base molar ratio of 1:1. The organic reaction was refluxed for 4 hours at a temperature between 50-60 °C. The reaction was then permitted to cool to room temperature, followed by solvent evaporation to remove ethanol under reduced pressure using rotary evaporator (Rotovap) prior to analysis.

Moving forward through the aldehyde conjugation plan, the reagent *m*-PEG₄-benzaldehyde, 268.3 g/mol, which is the aldehyde of interest, was purchased from BroadPharm® (95% purity; BroadPharm, San Diego, USA). To test the validity of the purchased aldehyde derivative in undergoing a Wittig olefination, a reference standard compound of NEM-*m*-PEG₄-benzaldehyde was prepared and analyzed by following the previously optimized procedure, the same that utilized the *p*-anisaldehyde.

3.4.4 HSF Protein Surface Modification

3.4.4.1 Conjugation of Maleimide Linkers to the HSF Surface

Horse spleen ferritin (10 mg/mL) was incubated with an approximately 200-fold molar excess of NHS-PEG₄-MAL reagent (Figure 3.3) to the capsule protein in 150 mM potassium phosphate buffer at pH 7.4 for 1 hour at room temperature. After incubation, the sample preparation was performed according to MALDI-TOF MS protocols and sent for analysis.

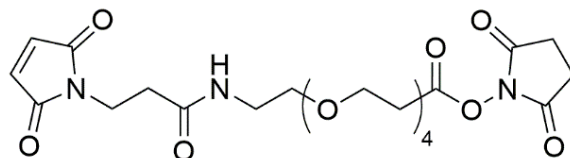


Figure 3.3. The chemical structure of the bioconjugation reagent MAL-dPEG₄-NHS ester

3.4.4.2 MAL-TCEP Adduct Formation on HSF surface

TCEP (3.6 μg , 1.248×10^{-5} mmol, 40 μL , 1 equiv.) was added to the HSF protein sample (0.5 mg, 1.248×10^{-5} mmol, 10 μL). This protein sample contained 1.248×10^{-5} mmol of conjugated PEG₄-maleimide linker. A stock solution of TCEP (1.26 mg, 14 mL) was first prepared in DDH₂O for serial dilutions. The TCEP stock was degassed by argon purging for 10 minutes prior to adding to the reaction vial to lower the chance of TCEP oxidation with air molecules in water, since the product of oxidation, TCEP-oxide has the potential to decrease the yield of TCEP-MAL adduct formation. The reaction vial was kept at room temperature, 25 °C, for 1 hour before MS analysis.

3.4.5 Modified-HSF Sample Preparation for MS Analysis

3.4.5.1 C₁₈ ZipTips: Reverse Phase Chromatography

Labelled PEG₄-MAL-TCEP protein samples were prepared prior to the ESI-MS run by using reverse phase chromatography, C₁₈ ZipTips (Millipore Sigma, Oakville, Canada). The starting concentration of the modified protein sample was 50 μM . With a micropipette set to 10 μL , the ZipTip was installed and wetted by aspirating for 7 times using a solution of 100% acetonitrile and 7 more times using 0.1% (v/v) formic acid. The pipetted solution was discarded each time. Then the protein sample was slowly loaded onto the ZipTip by aspirating for 15 times and expelling the sample back into the tube each time. Afterwards, a sample washing step was

employed. This was performed by aspirating in 0.1% formic acid for 7 times and discarding the liquid into waste each time. Finally, to elute the purified protein, it was aspirated into a 50 μ L solution of 1:1 MeOH:H₂O containing 0.1 % formic acid (FA) and expelled in the tube. The desalted sample was injected into the ESI-MS instrument in a positive mode setting.

3.4.5.2 Centrifugal Spin Filtration

A second sample preparation protocol was optimized using spin filters (Amicon® Ultra-0.5; 10 kDa MWCO) to assist in gaining a sufficiently pure and concentrated sample prior to mass spectrometric analysis. To first verify the validity of this method and to avoid loss of the modified HSF protein sample, a native unmodified HSF was tested first. Horse spleen ferritin (55 mg/mL) was incubated in a 5% formic acid solution with a volume ratio of 1:10, acid:protein, in a total volume of 10 μ L. This concentration of formic acid is needed to dissociate the protein capsule and to protonate the subunits. The washing step started with pipetting the 10 μ L sample in an Amicon® filter with 400 μ L of 0.1% formic acid which was then spun in the centrifuge for 10 min at 8960 x g. This step was repeated twice. Two more spins were done using a solution of 1:1 MeOH/H₂O:0.1% formic acid. After the last round, the filtrate was collected and diluted to the desired concentration with a solution of 1:1 MeOH/H₂O:0.1% formic acid, then injected into the electrospray mass spectrometer with a voltage setting of 4.6 kV, temperature of 300 °C, and a resolution of 17,500.

3.4.5.3 Gel Filtration Purification of Ferritin-MAL-TCEP Conjugate

The column was equilibrated with filtered and degassed fresh 0.1% formic acid solution at pH 2.64. A 100 μ L sample of ferritin-MAL-TCEP was diluted in 400 μ L of 0.1% formic acid. The diluted sample was then injected onto the column, then isocratically eluted. The protein sample

was collected and concentrated using the SpeedVac Vacuum concentrator. The overall process of purification and concentration required 48 hours before injecting in ESI-MS, while the sample remained in 0.1% formic acid throughout the procedure.

3.4.6 Expression and Purification of Pfftn

Another member of the ferritin superfamily was explored in this project, the His-tagged *Pyrococcus furiosus* ferritin, which was designed by Dr. Honek and synthesized commercially by Genescript Inc. The Pfftn plasmid (Pfftn-pET-22b) that encodes for the C-terminal His6-tagged Pfftn construct was transformed into bacterial BL21 *Escherichia coli* (*E. coli*) cells via heat shock (Gyamfi, 2019)

Luria Bertani (LB) agar plates were prepared using 2.5 g Bio-Tryptone, 1.3 g yeast extract, 2.5 g NaCl, 3.75 g agar. The media was autoclaved for 45 minutes (25 min/25 min “dry”), liquid cycle. Once cooled to 50 °C, ampicillin (100 µg/mL) was added to the media. LB-broth-amp was poured in six petri dishes and kept at room temperature until complete solidification. A bacterial stab culture was made by introducing a pipette tip of BL21 *E. coli* cells deep into a 5 mL solution of LB-amp broth, then incubated overnight in a 37 °C, 220 rpm/min shaker until a cloudy broth was visible. The cloudy bacterial broth was streaked on the agar plates in a zig-zag fashion using a wire inoculating loop. The agar plates were incubated for 16 hours in a 37 °C incubator. A single colony from the plate was inoculated in a 100 mL LB-amp broth then incubated overnight in a 37 °C, 220 rpm/min shaker to grow the bacterial culture. An aliquot (20-50 mL) of the overnight grown culture (100 mL) was inoculated in a 1 L solution of LB media (10 g Bio-Tryptone, 5.2 g yeast extract, 10 g NaCl) containing 100 µg/mL of ampicillin. The optical density (OD₆₀₀) of the inoculated large media started at 0.05, and was measured using a UV-vis spectrophotometer. The media was re-incubated a 37 °C, 220 rpm/min shaker until 1.2 OD₆₀₀, where the expression of

PfFtn protein was induced by adding isopropyl β -d-1-galactoside, (IPTG; 1 mM, 238.3 mg) which is known to bind to the *lac* repressor to trigger the transcription of *lac* operon genes to encode the protein of our interest. The culture was incubated again for 4 hours. The bacterial cells were harvested by centrifugation for 30 min using the “Beckman” JA14 rotor at 6000 x g. The harvested cell pellets weighed 5.15 g. The harvested cells were suspended in a 50 mL lysis buffer (150 mM NaCl, 50 mM MOPS, pH 7.5). Meanwhile, a protease inhibitor, 1 mM of phenylmethylsulphonyl fluoride (PMSF), was added in the suspension to inhibit the activity of cell proteases upon their release from the cells. Afterwards, the cells were physically homogenized in a manual Dounce glass tissue grinder while placed in an ice bucket. The suspended cells were lysed under high pressure to break open the cells using an Avestin Emulsiflex-C5 (Mannheim, Germany) at 17000 psi. The lysate was heat shocked in an 80 °C water bath for 10 min to destroy all the biomolecules that cannot tolerate this elevated temperature. Cell debris and heat damaged, or insoluble proteins were pelleted down by centrifugation using Beckman JA25.5 rotor at 18,000 g for 40 min and the supernatant was pipetted out and filtered through a 0.45 μ m nylon syringe filter prior to column purification.

Immobilized metal affinity chromatography (IMAC) purification method was chosen to purify the polyhistidine-tagged PfFtn via the affinity interaction of histidine to immobilized Ni²⁺. The 1 mL Nickel His-TrapTM HP column (GE Healthcare, Chicago, USA) was attached to a Bio-Rad chromatography system (BioLogic Duo Flow instrument). The column was equilibrated with binding buffer (150 mM NaCl, 5 M GdnHCl, 20 mM imidazole, 50 mM MOPS, pH 7.5). The cleared lysate was loaded onto the IMAC column, then washed by pumping 10 column volumes (CV) of binding buffer to allow unbound proteins to flow through the column. The bound protein was eluted with 150 mM NaCl, 5 M GdnHCl, 300 mM imidazole, 50 mM MOPS, pH 7.5. The

purity of the eluted fractions was later tested using 15% sodium dodecyl sulfate polyacrylamide gel electrophoresis (SDS-PAGE). Positive-ion mode ESI-MS was used to validate the mass of the PfFtn protein subunit. The expected monomeric mass of PfFtn is 21,374 Da, obtained using the Expasy Compute pI/Mw tool. The protein sequence is shown in Figure 3.4.

10	20	30	40	50	60
MLSERMLKAL	NDQLNRELYS	AYLYFAMAAY	FEDLGLEGFA	NWMKAQAEED	IGHALRFYNY
70	80	90	100	110	120
IYDRNGRVEL	DEIPKPPKEW	ESPLKAFAAA	YEHEKFISKS	IYELAALAEED	EKDYSTRAFL
130	140	150	160	170	180
EWFINEQVEE	EASVKKILDK	LKFAKDSPQI	LFMLDKELSA	RAPKLPGLLM	QGGELEHHHH HH

Figure 3.4. The amino acid sequence of His6-PfFtn construct.

3.4.7 Preparation of PfFtn-MAL Conjugate

Expressed and purified His6-tagged *Pyrococcus furiosus* ferritin (PfFtn) was utilized to pursue capsule protein modifications with a soluble maleimide reagent. PfFtn stock solution was stored in 25 mM HEPES buffer and 150 mM NaCl in a -20 °C freezer. A 3 mg/mL fresh stock solution of MAL-PEG₄-NHS ester reagent (513.5 g/mol) was prepared and dissolved in ≥ 99.9% DMSO solvent. PfFtn aliquot (0.8 mg/mL or 1.5 μM, 1.48×10⁻⁷ mmol, 95 μL) was incubated with MAL-PEG₄-NHS ester reagent (0.015 mg, 2.96×10⁻⁵ mmol, 200 equiv., 5 μL) and kept overnight in a 4 °C fridge. It was vital to keep a low concentration of DMSO in the reaction mixture, as low as 5%, to maintain the protein's native state and avoid unfolding. After incubation, the sample was desalted using Amicon[®] spin filters, 10 kDa MWCO, by adding 400 μL of DDH₂O to the protein-conjugate sample over 5 rounds of filtration at 6720 x g. The sample was retrieved from the filter membrane and diluted with DDH₂O to a concentration of 0.3 μM. An aliquot of this sample was then diluted to 0.03 μM using an acidic solution of 1:1 MeOH/H₂O:0.1% FA, as a preparatory step

for ESI analysis to protonate and decluster the protein sample. The sample was injected into the ESI instrument employing the positive-ion mode.

3.4.8 Preparation of PfFtn-MAL-TCEP Conjugate

The previously prepared PfFtn-MAL sample ($0.3\ \mu\text{M}$, $1.36\times 10^{-7}\ \text{mmol}$, $440\ \mu\text{L}$) was used. A $1\ \text{mg/mL}$ stock solution of TCEP was prepared in DDH_2O and further diluted to $4.5\times 10^{-4}\ \text{mg/mL}$, where a sample ($10\ \mu\text{L}$, $1.63\times 10^{-6}\ \text{mmol}$) of the dilute TCEP solution was added to the PfFtn-MAL. The molar excess of TCEP used in this reaction was quantified to be 1 equivalent to a protein capsule and 12 equivalents to maleimide molecules cross-linked on the capsules, since each capsule was modified with an estimation of 12 molecules of PEG₄-MAL, according to MALDI-MS analysis. The reaction mixture of PfFtn-MAL-TCEP was incubated overnight at $4\ ^\circ\text{C}$ and desalted the next day with DDH_2O for further analysis by mass spectrometry.

3.4.9 Reaction of mPEG-benzaldehyde with PfFtn-MAL-TCEP Conjugate

The sample of PfFtn-MAL-TCEP conjugate that remained in DDH_2O after the previous MS analysis ($0.3\ \mu\text{M}$, $1.49\times 10^{-10}\ \text{mmol}$, $410\ \mu\text{L}$) was mixed with the mPEG₄-benzaldehyde reagent (1 equivalent) and sodium hydroxide base (1 equivalent). This reaction mixture was pipetted in a round bottom flask, size 19/22, attached to a Liebig condenser over a hot water bath of $60\ ^\circ\text{C}$. The reaction was heated for four hours. Subsequently, the heated sample was cooled before employing the sample preparation protocols for ESI MS as previously described. Next, the sample was injected in ESI-MS positive mode for mass analysis.

3.5 Results and Discussion

3.5.1 Characterization of the Reaction of N-ethylmaleimide with Trialkylphosphine

ESI MS was used in the positive ion mode. The ESI MS analysis revealed the adduct (375.11 g/mol) identity as one distinctive high intensity mass peak at 376.1172 m/z (Figure 3.5), which belongs to the $[M+H]^+$ mass of the protonated product. This reaction is a rapid chemical reaction, as the spectrum shows no mass peaks of any trace starting material, NEM (MW: 125 g/mol) nor TCEP (MW: 250 g/mol). Reference standards of these compounds, NEM and TCEP, were run to confirm that indeed they do appear in the mass spectrum of these compounds.

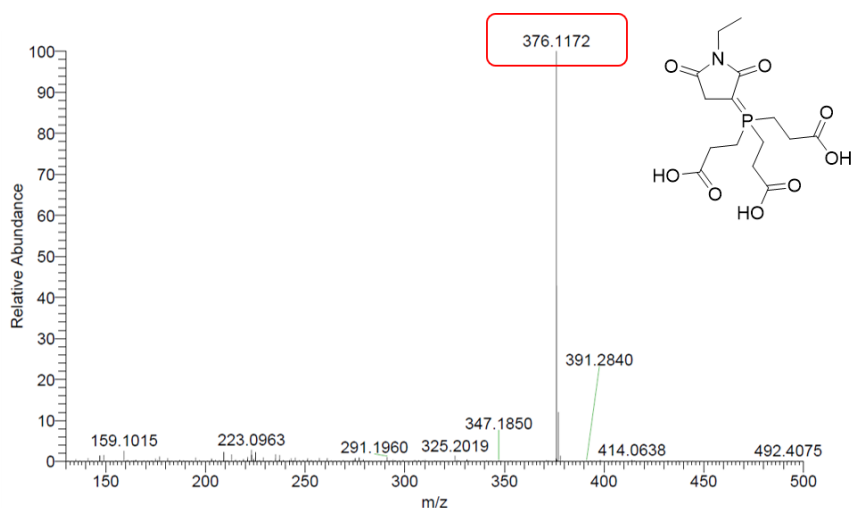


Figure 3.5. The product of the TCEP and NEM reaction exhibiting a mass peak at 376.1172 m/z on ESI MS.

3.5.2 ^{31}P NMR Evaluation

The synthesis of the desired compound was verified using ^{31}P NMR (500 MHz) in D_2O . The analysis of the ^{31}P NMR spectrum exhibited two doublet phosphorous ^{31}P resonance signals (Figure 3.6), one of which is a characteristic of the ylide product of the NEM-TCEP adduct chemical shift at $\delta = 39.89\text{-}39.97$ ppm. The second peak corresponds to the phosphorous resonances

of the TCEP-oxide compound at $\delta = 57.43\text{-}57.69$ ppm. The signal ^{31}P resonance of the adduct that was synthesized is consistent with the literature data reported previously by Kantner et al (2016). Similarly, the byproduct signal peak is consistent with earlier findings reported by Martindale et al (2016). The presence of doublet peaks suggests two forms of the desired product, which is explained by the incomplete deuteration of the NEM-TCEP compound in the reaction vial, where it contains a mixture of monodeuterated species and methine protonated species are incompletely decoupled.

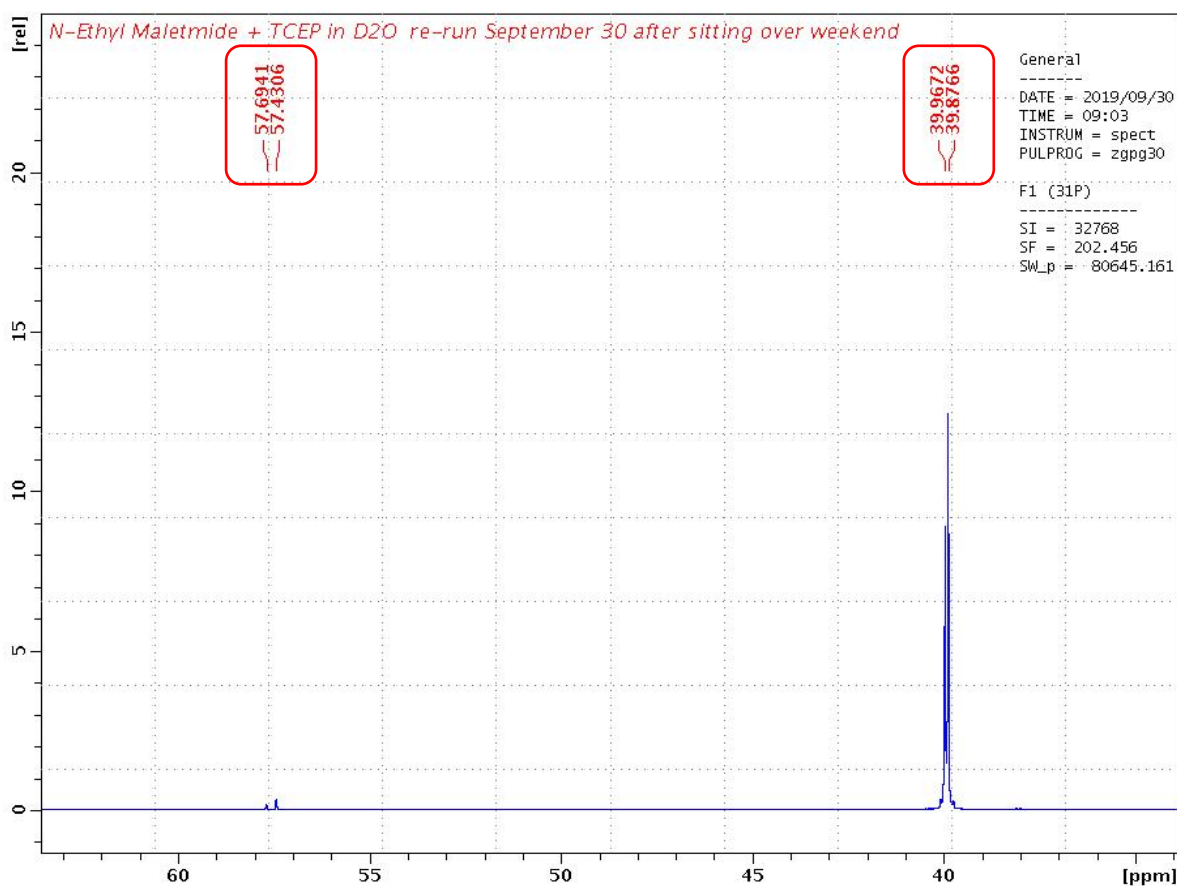


Figure 3.6. The ^{31}P NMR spectrum of the NEM-TCEP product at chemical shift $\delta = 39.89\text{-}39.97$ ppm, and the TCEP-oxide byproduct at $\delta = 57.43\text{-}57.69$ ppm.

3.5.3 Wittig Olefination Reaction of the TCEP-MAL Conjugate with Aldehyde Derivatives

To optimize the Wittig olefination procedure of TCEP-MAL with aldehyde compounds, a simple model reaction using *p*-anisaldehyde was pursued to validate the reaction before moving forward with the aldehyde-protein conjugation, as described in Section 3.3.3. The addition of the base may be critical in this type of reaction since it works as a catalyst by deprotonating the phosphorous ylide intermediate to allow the positively-charged phosphorous ion, which is a strong electron withdrawing group, to stabilize the adjacent carbanion, to attack the aldehyde.

Attention was paid to the concentration of NaOH and ethanol used in this reaction model. The concentration of NaOH needed for catalysis was lowered to the minimum possible quantity, a 1:1 molar ratio of adduct:base, because this protocol will be applied subsequently to a protein. The presence of an excess amount of a base has unfavorable consequences on proteins, such as amino acid deprotonation to form dehydroalanine residues or base-catalyzed racemization causing *L*-amino acids to partially racemize to the *D* enantiomer (Ebbers et al., 1997). Another point to keep in consideration is the concentration of ethanol as the co-solvent. Many organic-based procedures reported using pure anhydrous (99%) ethanol or methanol for a similar reaction (Jung et al., 2013) (Ha et al., 2011). Pure ethanol would denature most proteins so instead, a 20% ethanol solution was employed, and it was found to work as well for this simple model reaction.

ESI MS was used to confirm the product formation. The anticipated mass spectrum that corresponds to the NEM-anisaldehyde product as a result of the Wittig reaction was successfully obtained at 246.1129 *m/z* (Figure 3.7). A second mass peak belonging to the starting material (NEM-TCEP) at 376.11 *m/z* was detected as well.

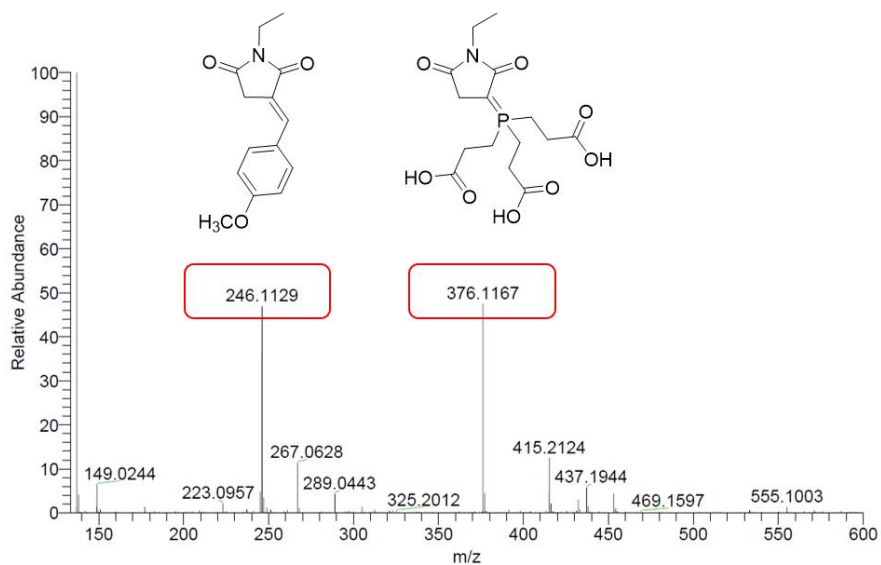
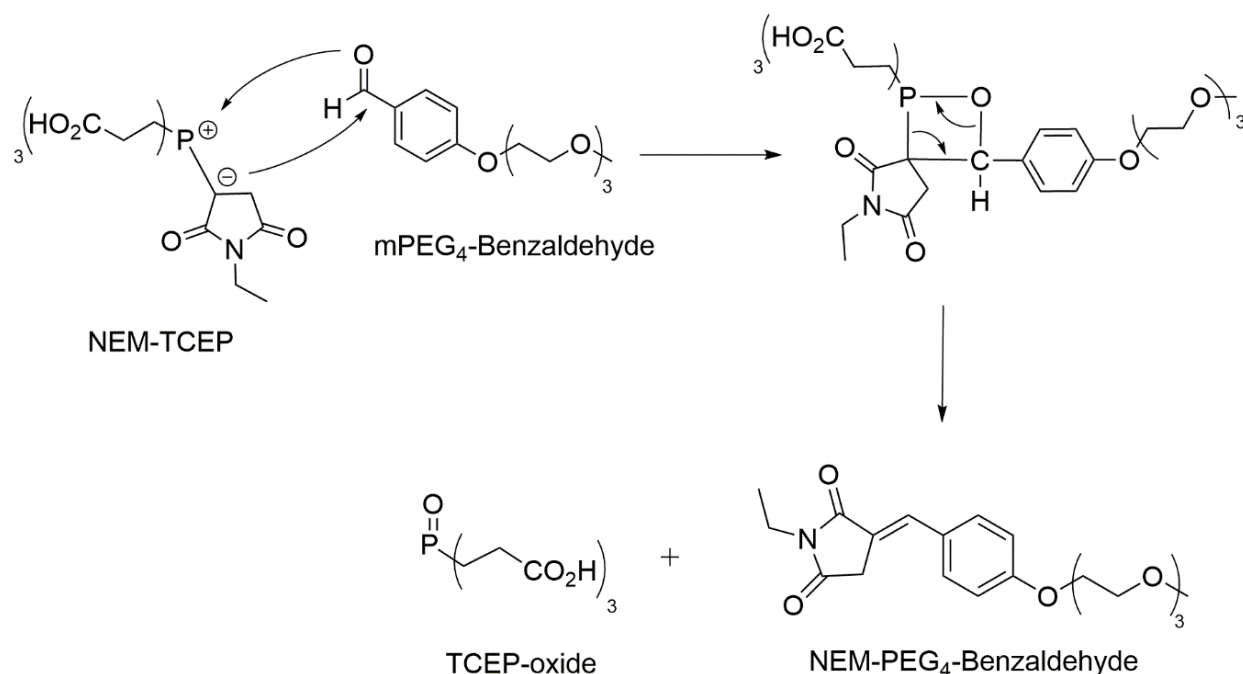


Figure 3.7. MS spectrum shows two distinct peaks of the aldehyde product at 246.11 m/z and the starting material at 376.11 m/z.

After confirming the Wittig reaction product using *p*-anisaldehyde, the same procedure was followed moving forward through the aldehyde conjugation plan. The desired aldehyde reagent to be cross-linked on the target ferritin protein was to be a water-soluble aldehyde with a hydrophilic PEG chain. First, the reaction of the PEGylated aldehyde compound, mPEG₄-benzaldehyde, with NEM-TCEP adduct was confirmed. The detailed reaction mechanism is depicted in Scheme 3.6.



Scheme 3.6. Wittig reaction mechanism of NEM-TCEP and mPEG-benzaldehyde.

As for the model experiment, ESI MS was employed for mass detection. The predicted mass peak for the NEM-mPEG₄-benzaldehyde product as a result of the Wittig reaction was successfully observed at 378.19 m/z (Figure 3.8). Since the PEGylated aldehyde compound showed reactivity towards the ylene adduct, it was employed to further pursue selective conjugation on a protein surface. The mass peak intensities in Figure 3.8 exhibit a qualitative analysis of the analyzed products. Molecules exhibit differences in their ionization properties, where a low intensity mass peak in a certain spectrum is not necessarily proof of a low concentration of the material, but the ionization capability in a certain ESI charge mode, and vice versa.

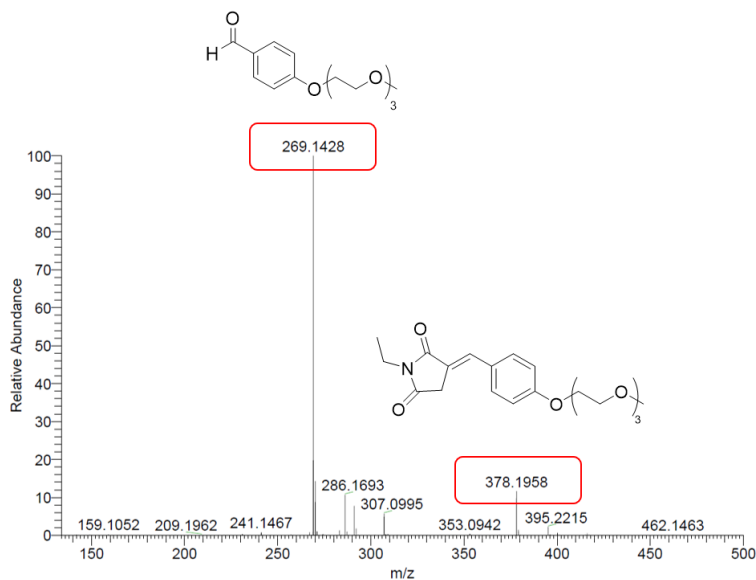


Figure 3.8. ESI spectrum shows two distinct peaks of the aldehyde product at 378.19 m/z and the starting material of the aldehyde reagent at 269.13 m/z.

3.5.4 MALDI Analysis of MAL-TCEP Adduct Formation on the HSF Surface

As it was confirmed that an aldehyde moiety can react with a maleimide-TCEP molecule and replace the trialkyl phosphonium moiety by performing a Wittig olefination reaction, the next step was to implement these findings on a protein. The first step was to modify the protein with a maleimide moiety. Herein, the maleimide groups were attached to the surface of the capsule protein, horse spleen ferritin (HSF), via NHS-PEG₄-MAL reagent that is targeted to attack the surface lysine residues, forming a covalent amide bond with the lysine side chains. As mentioned, this approach was employed due to the lack of the accessible cysteines on the HSF surface which limits the ability to integrate maleimide groups to the protein surface via the sulfhydryl groups of the cysteines directly, which would then have employed a bis-maleimido-containing reagent. MALDI-TOF MS instrumentation was used to generate a protein spectrum of HSF-PEG₄-MAL (Figure 3.9A). After confirming the successful maleimide conjugation with the HSF protein, TCEP

was added to the reaction mixture to form an adduct with free maleimides on the HSF surface. As the reaction of maleimide and TCEP is rapid and thermodynamically favorable, only one molar equivalence of TCEP was added to the HSF-MAL solution. The MALDI result of the HSF-MAL-TCEP product is presented in Figure 3.9B. MALDI-TOF MS was employed to confirm the mass of the products, as the ESI mass spectrometry technique was not successful in detecting ferritin subunits as previously mentioned in an earlier chapter. As shown in Figure 3.9, spectrum A, the HSF-PEG₄-MAL sample, displays two peaks, a ferritin subunit and a maleimide-modified ferritin subunit. Spectrum B of Figure 3.9 shows the peak of the HSF-MAL-TCEP product. Although sample B was treated with TCEP, spectrum B resembles that of spectrum A. The TCEP attachment to the maleimide on ferritin should result in a mass peak at approximately 20648 m/z, but instead, the peak is at 20470 m/z, this is a protein-PEG₄-MAL peak. Therefore, either the TCEP did not attack the maleimide groups or the choice of MALDI-TOF mass spectrometry is not the best choice, since MALDI is not sensitive enough to small mass additions when the linear mode is used, and it provides a low resolution for these additions.

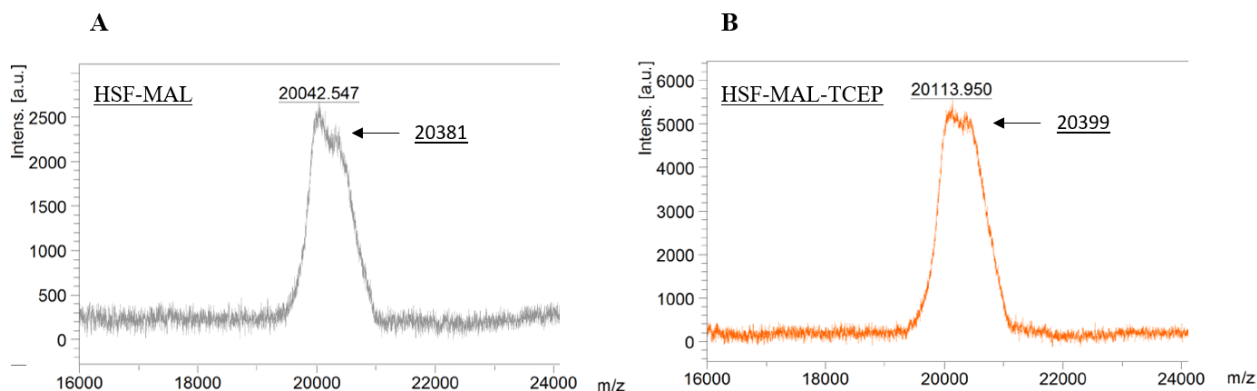


Figure 3.9. MALDI-TOF mass spectra of HSF conjugation. A) Spectrum of a mass peak at 20042 m/z, corresponding to the mass of a single native unmodified ferritin subunit with a side shoulder peak at 20399 m/z suggesting ferritin subunits were labelled with one PEG₄-MAL molecule. B) A mass peak of a single unmodified subunit at 20113 m/z with a shoulder peak at 20470 m/z that corresponds to one PEG₄-MAL modification.

Moreover, the same reaction was replicated, since human error is always possible to take place. Also, following the same procedure, different reaction mixtures with different molar excesses were prepared to accelerate the reaction kinetics. These mixtures were analyzed on MALDI-TOF MS as well. The replicated experiments resulted in spectra that were similar to the earlier ones, which displayed non-resolved peaks of the modification. Furthermore, it was attempted to employ the ESI MS technique for these samples to obtain mass confirmation of the protein conjugate product, where ESI MS is more quantitatively accurate and able to provide a precise mass value for the molecule. The sample preparation of HSF-MAL-TCEP protein samples prior to the ESI MS run utilized the reverse phase chromatography, C₁₈ ZipTips. Ferritin is a water-soluble protein and the reverse phase resin is hydrophobic. However, ferritin possesses hydrophobic patches in its structure (Zhang & Orner, 2011), enabling us to employ this technique. Following the procedure described in Section 3.4.5.1, the sample preparation using C₁₈ ZipTips appeared to be unsuccessful. The protein sample was bound to the tips and poorly recovered after several aspirations, so the sample was minimally sufficient to result in a representative MS spectrum. The sample was injected in the instrument, and again, no successful TCEP attachment was detected during the ESI analysis (spectrum not shown).

HSF protein samples are known to be very hard to be ejected into the gas phase in an ESI MS run. A close look at the literature reveals a lack in utilizing the ESI MS approach to characterize horse spleen ferritin, for the primary reasons that ferritin is a heavily glycosylated and iron loaded protein causing ion-suppression, a common problem in many non-compatible ESI samples, while MALDI-TOF MS is recommended for glycan-containing proteins (Zaia, 2010). Only one work in literature was found that employs ESI MS, with a procedure that required convoluted sample separation and preparation (Plath et al., 2015).

3.5.5 Characterization of HSF Protein

Since difficulties were experienced with MALDI-TOF MS, the choice of employing ESI as an alternative to MALDI-TOF was made for a precise demonstration of the protein mass and further efforts were made to optimize a sample preparation protocol to obtain an ESI-compatible clean sample (Section 3.4.5). A purified native ferritin sample, as per the procedure reported in Section 3.4.5.2 was collected from the Amicon spin filter and injected in ESI MS positive ion mode. The peak series in the total ion chromatogram (TIC) Figure 3.10A exhibits a distribution of multiply charged analyte ions, a definite characteristic of a well-ionized protein sample. Figure 3.10B is the deconvoluted spectrum of an HSF subunit obtained by BioPharma Finder™ Software that shows a predominant peak at 20,098 Da, which is the mass of the HSF subunit. The same mass value was obtained previously by MALDI-TOF MS when analyzing the same sample. The peak at 19,117 Da is believed to be the mass of the L-chain type of subunit, based on the fact that ferritin has two types of chains, H (heavy) and L (light). These results provide a good fit to the data obtained formerly using a different MS technique. It was concluded that the centrifugal spin filtration technique with the use of dilute formic acid (0.1 %) as a washing solution for ferritin instead of DDH₂O was successful to produce a detectable ferritin sample. Exposing the protein sample to diluted formic acid for four consecutive rounds had contributed in a relatively significant protonation that was enough for a difficult sample to fly in the Q-exactive ESI MS orbitrap.

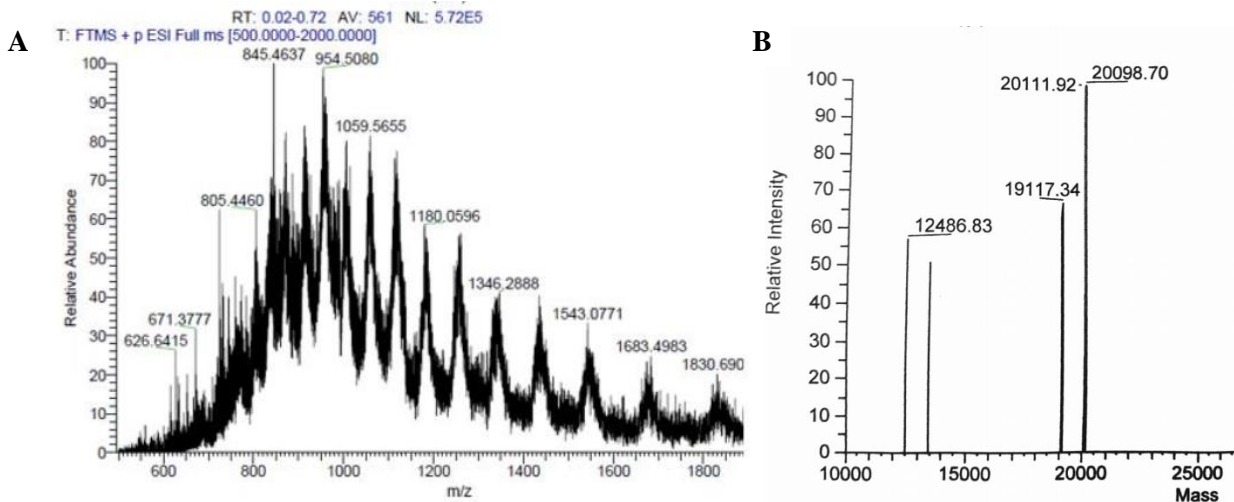


Figure 3.10. A) TIC spectrum of HSF showing multiply charged protein ion peaks. B) The deconvoluted TIC spectrum represents an accurate mass that corresponds to one unmodified HSF subunit.

There are reasons why there is a second mass peak at 20,111 Da along with different peaks around 12-13 kDa in the discussed ESI spectrum, other than the actual protein subunit peaks. As discussed earlier in Section (1.1.2.1), HSF is a glycoprotein, which is a challenging biomolecule to characterize because it contains glycan microheterogeneity in its polypeptide chains. The glycan composition is not equally expressed among all the ferritin subunits and other subunits may not have carbohydrates at all, resulting in heterogenous mixtures of subunits with non-identical masses in the same capsule protein. In addition to microheterogeneity, the sample was not obtained from a recombinant source where the masses of polypeptide chains and carbohydrate composition are identical, instead it was obtained from a commercially available source that was extracted from equine spleen. The commercial protein stock may contain unknown impurity components.

3.5.6 Characterization of the HSF-MAL-TCEP Adduct

The purification of the HSF-MAL-TCEP sample using the C₁₈ ZipTips reverse phase chromatography was not productive in the sample recovery step from the ZipTip. Interestingly, the centrifugal spin filtration method was only successful in recovering samples of unmodified ferritin, and not the TCEP-modified samples, because it was suspected that the TCEP attachments on the protein aid in binding the protein to the filter membranes. Hence this strategy did not yield a pure sample of the ferritin modified with TCEP attachment. Since our findings support the use of dilute formic acid as a washing solution for ferritin instead of DDH₂O, it was decided to seek a different purification method. The gel filtration chromatography using Sephadex G-25 resins was used instead.

The Sephadex G-25 column was equilibrated and the sample isocratically eluted with a very low pH of 2.64 containing dilute formic acid. The isocratic elution means that the mobile phase composition remained constant throughout the run. The very low pH was found to be critical to maintain a declustered ferritin capsule into monomer subunits, which is a requirement for ESI analysis. This condition will trigger the release of the encapsulated elemental iron and eliminate it from the protein subunits.

The ESI MS technique produced a clearly detected protein spectrum (Figure 3.11A), which exhibited a very well resolved set of multiply charged fragments, a perfect chromatogram in comparison to any previously obtained spectrum for ferritin. The deconvoluted spectrum showed a significant peak at 16,950 Da (Figure 3.11B), however, this is not the reported molecular weight for ferritin. To further investigate, the same sample was analyzed using MALDI-TOF MS. MALDI analysis showed two mass peaks, suggesting two species. One distinctive peak at 16,960 Da, which is the same species which appeared in the deconvoluted ESI spectrum (Figure 3.11C), and a second

low intensity peak at 20,707 Da. The ~700 Da increment to the ~20,000 Da ferritin mass, is the value range anticipated for the modification that we are seeking for HSF-MAL-TCEP.

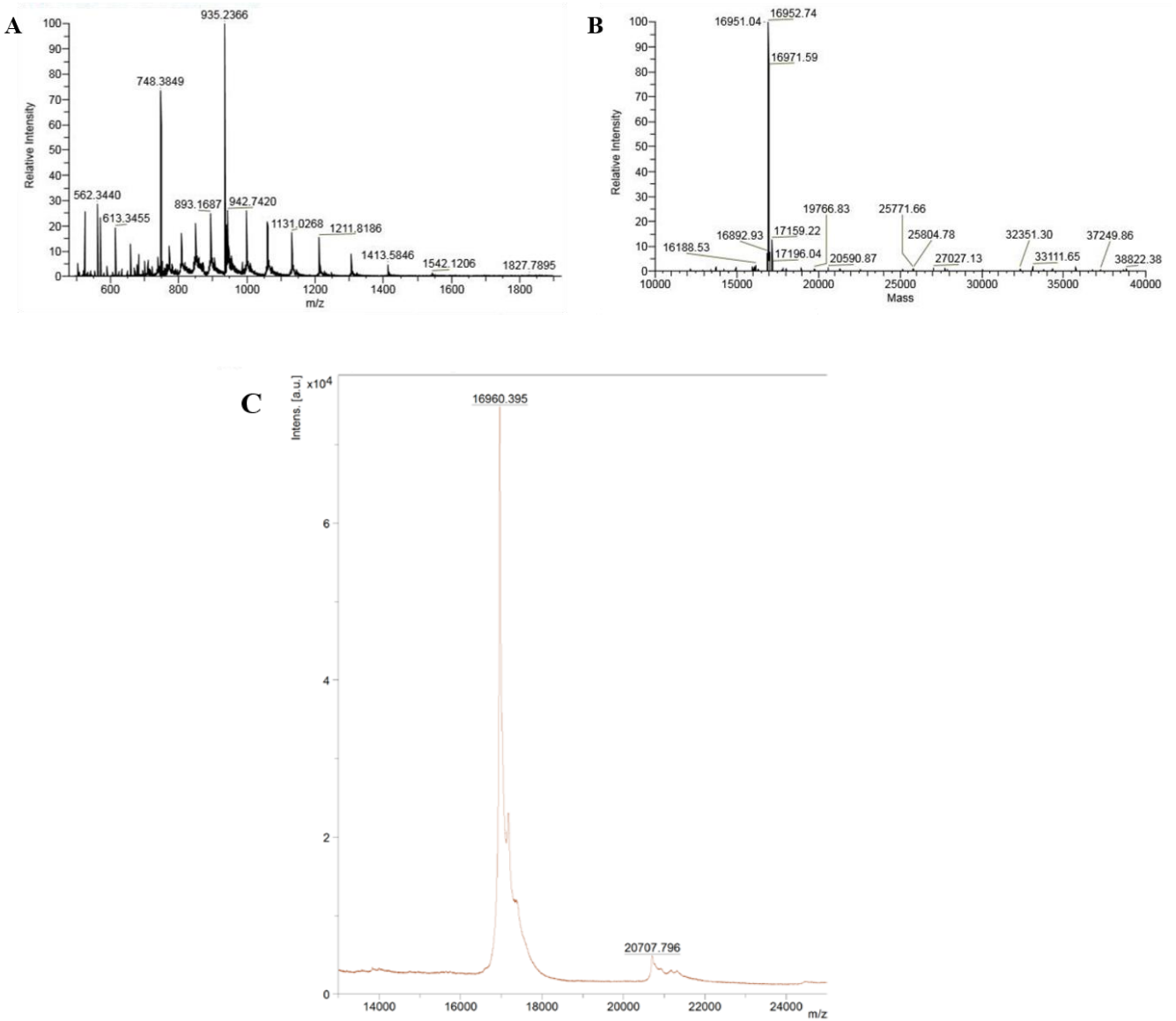


Figure 3.11. A) TIC-ESI spectrum for the HSF-MAL-TCEP sample purified by gel Sephadex G-25. B) The deconvoluted ESI spectrum exhibiting the mass peak of the modified protein. C) MALDI mass spectrum of the same sample.

Yet, to explore the identity of the peak at 16,960 Da, we eliminated the possibility that the species of 16,950 Da protein mass belongs to an unknown component existing in the commercial protein stock, because after the first ferritin modification with NHS-PEG₄-MAL, the sample was washed using a spin filter of 100 kDa MWCO. A membrane with a similar cutoff is enough to rinse proteins of 16.9 kDa molecular weight through the filter. A more reasonable argument to consider is the possible effect of formic acid being the solution surrounding the ferritin throughout the purification and concentration procedures. We suspected that the 0.1% formic acid solution possesses chemical cleavage activity towards the ferritin polypeptide chains. Given that the dilute formic acid was at pH 2.64, ferritin is known to survive acidic conditions down to pH 3.0 and retain the intact capsule structure. A complete declustering of the ferritin subunits was recorded at pH 2.0. Dilute solutions of 2% formic acid were found to be used for chemical cleavage at aspartyl residues of proteins (Li et al., 2001). The mentioned information indicates that ferritin capsules in 0.1% formic acid solution should be declustered, but with no denatured or cleaved polypeptide chains. However, as mentioned in the methods Section 3.4.5.3, the sample remained in the diluted acid for a relatively long period, in addition to being exposed to heat while in the SpeedVac instrument. It was suspected that the combination of both conditions, time duration and temperature, have contributed to the likely protein damage. To support and investigate the theory of formic acid cleavage effect, ExPASy peptide cutter tool (Gasteiger et al., 2003) was employed to determine if the estimated fragmentation is consistent with our findings. The tool predicted 12 possible cleavage sites. Fontana & Gross stated a possible polypeptide cleavage at the aspartate-histidine at the C-terminus of proteins in dilute formic acid (Fontana & Gross, 1986). This is consistent with ferritin cleavage at position 146 (Figure 3.12).

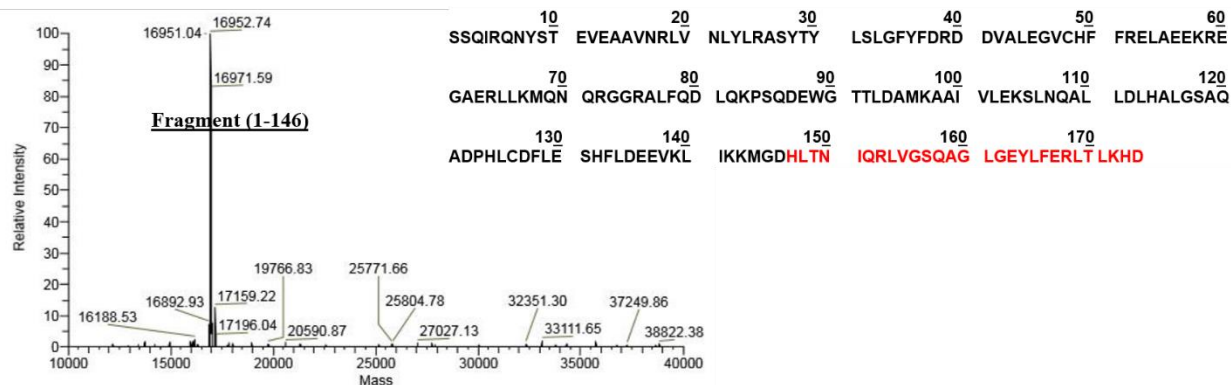


Figure 3.12. Deconvoluted ESI spectrum that exhibits a mass peak corresponding to a cleaved HSF fragment after an extended treatment with 0.1% FA. Beside the spectrum is the amino acid sequence of HSF. The black label is the sequence corresponding to the mass in the spectrum. The red labelled sequence indicates the cleaved fragment.

The mass of the cleaved red labelled fragment in (Figure 3.12) equals to 3208 Da, as per the ExPASy PeptideMass tool. This mass subtracted from the native ferritin mass (~20,000 Da) gives that total of 16,792 Da. A value very close to that shown by the spectrum in Figure 3.11, being larger by approximately 160 Da. This mass is very likely to belong to different branched or linear N-glycan residues distributed unevenly on the capsule surface.

3.5.7 Surface Modification of *Pyrococcus furiosus* Ferritin (PfFtn)

3.5.7.1 Characterization of the PfFtn-MAL-TCEP Adduct

Detection of the commercial HSF protein was problematic and time consuming. Although numerous attempts were made to characterize HSF in mass spectrometry, however, those attempts were unfruitful. As a result, it was decided to pursue the project with a different ferritin capsule protein. The HSF protein was substituted with the thermophilic *P. furiosus* ferritin (PfFtn) protein. The PfFtn was proved to be more feasible for mass analysis and more compatible with ESI.

His6-tagged PfFtn was expressed and purified by other members of the Honek laboratory and stocks of 0.8 mg/mL of PfFtn in 25 mM HEPES, 0.1 NaCl, pH 7.4 were stored and available in the -80 °C fridge. A sample of the PfFtn stock solution was desalted using DDH₂O using an Amicon® filter, 10 kDa MWCO, and analyzed by ESI MS (Figure 3.13). This protein was readily detected using the MS technique. Unlike HSF, no difficulties were associated with the sample preparation, handling, or ionization of the recombinant His-tagged PfFtn. The multiply charged protein ions appeared in the TIC chromatogram (Figure 3.13A) of the detected sample, which were deconvoluted to their masses using BioPharma Finder™ Software. Figure 3.13B reveals a mass of 21,374 Da for the PfFtn monomer. After conjugating PfFtn with NHS-PEG₄-MAL, the ESI sample analysis detected a high intensity mass peak at 21,772 and 22,171 Da (Figure 3.13C), a result of one and two subunit modifications with the maleimide linker respectively. This spectrum showed a sensitive and accurate detection of a double-maleimide modification peak. The next conjugation that was performed was with the nucleophilic phosphorous compound, TCEP, attacking the free maleimide rings and generating MAL-TCEP adducts on the protein. This adduct was successfully detected using ESI MS. A substantial mass peak at 22,021 Da is observed in Figure 3.13D, matching the expected mass of the PfFtn-MAL-TCEP conjugate.

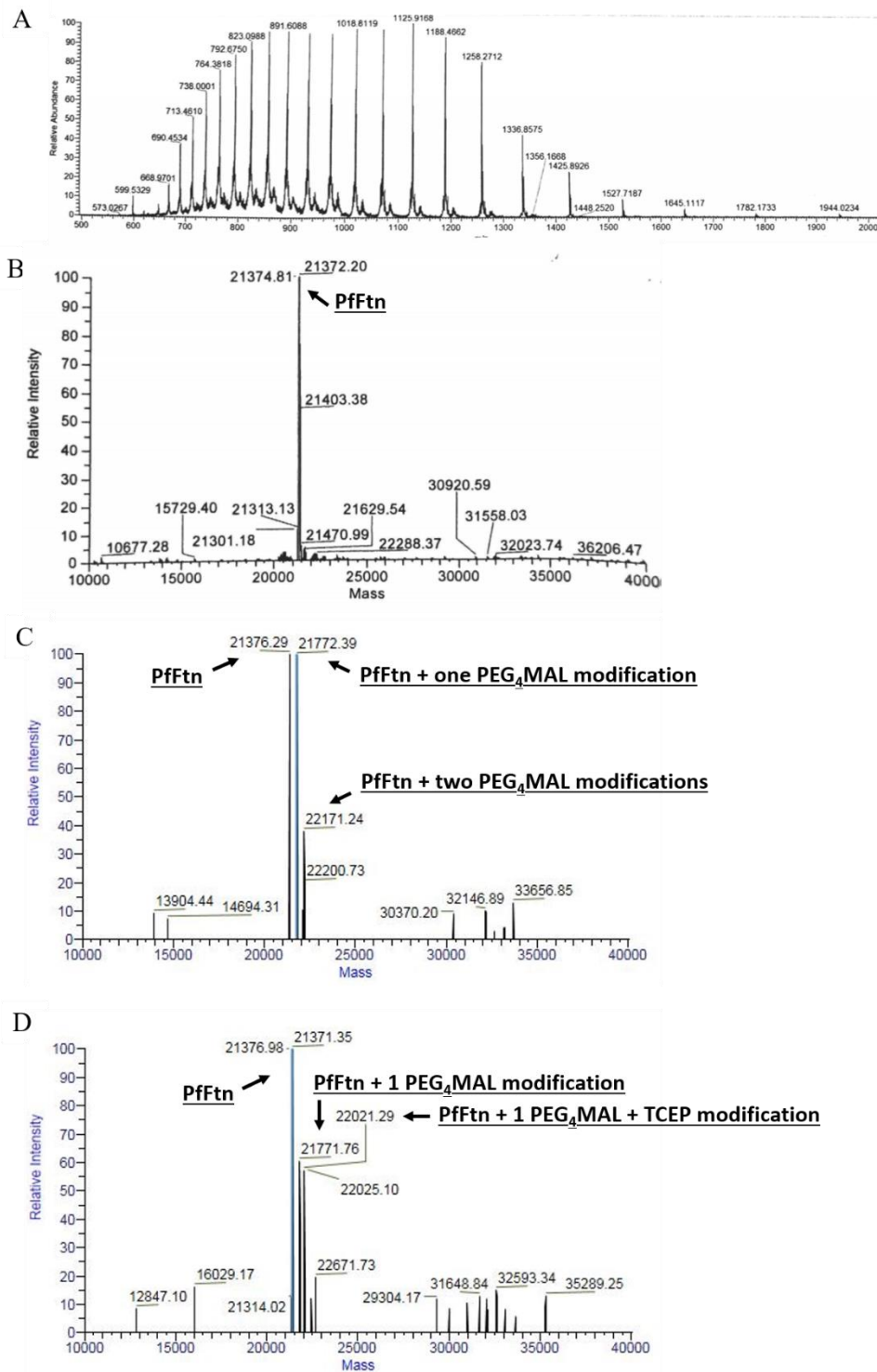


Figure 3.13. A) TIC-MS chromatogram of PfFtn. B) Deconvoluted ESI MS mass spectrum of one PfFtn subunit. C) Deconvoluted ESI MS spectrum shows two additional mass peaks correspond to one and two MAL modifications. D) Deconvoluted ESI MS spectrum of the PfFtn-MAL-TCEP product.

3.5.7.2 Characterization of the Pfftn-MAL-aldehyde Adduct

The mPEG₄-benzaldehyde compound was chosen as the first aldehyde to react with a MAL-TCEP-modified protein as this aldehyde has a hydrophilic PEG functionality, which increased aqueous solubility of this aldehyde over the simple aromatic aldehyde *p*-anisaldehyde. The reference standard of NEM-mPEG₄-Benzaldehyde compound was first synthesized successfully as mentioned in Section 3.5.3 to affirm the validity of the commercial reagent to undergo Wittig olefination with the ylide adduct (Figure 3.8). Since the olefination reaction of the aldehyde moiety with the NEM-TCEP ylide was reproducible when attempting reactions with both *p*-anisaldehyde and mPEG₄-benzaldehyde, therefore, we anticipated a positive result on the Pfftn. His-Pfftn capsule protein was adopted in this part of the project after confronting real challenges in acquiring representative protein spectra and mass measurements with the HSF capsule protein, whereas no difficulties with handling or detecting the Pfftn capsule protein were found. Another key reason that motivated us to alter the protein template from HSF to Pfftn is that Pfftn is a thermally stable protein. It is very crucial that the conjugated protein is resistant to moderately high temperatures, since the Wittig olefination reaction requires a refluxing environment up to 60 °C to yield the desired product. A sample of a previously prepared Pfftn-(PEG₄-MAL-TCEP)_x was reacted with the commercially provided compound, mPEG₄-benzaldehyde, according to the reaction conditions determined as per Section 3.4.3. Analysis of the resulting ESI mass spectrum revealed a successful conjugation of the aldehyde moiety on the surface of the monomeric subunit of Pfftn (Figure 3.14). The spectrum revealed a peak at 22,036 Da that corresponds to the identity of the target Pfftn-aldehyde product (Figure 3.15).

Utilizing His-Pfftn was a felicitous choice of a compatible capsule protein, enabling a successful demonstration of the original proof-of-concept of a new protein bioconjugation strategy.

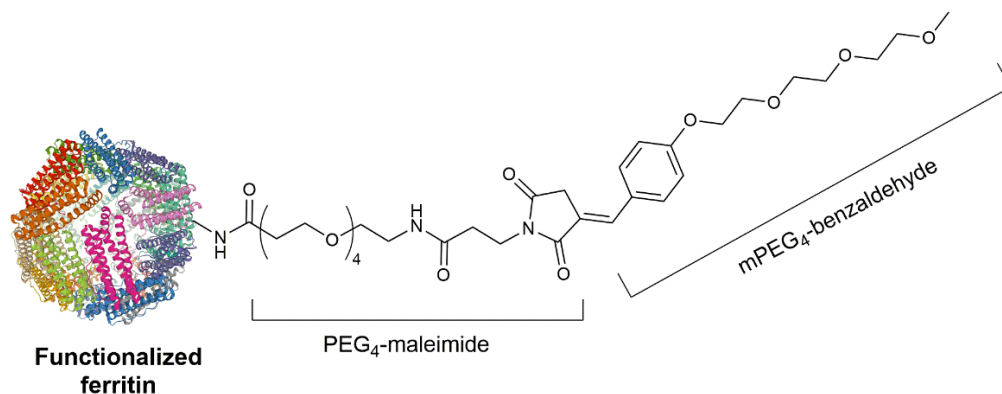


Figure 3.14. The final product the surface functionalized ferritin. An (E)-isomer of a Wittig olefinated benzaldehyde, cross-linked on His-PfFtn capsule protein through a lysine targeted maleimide reagent.

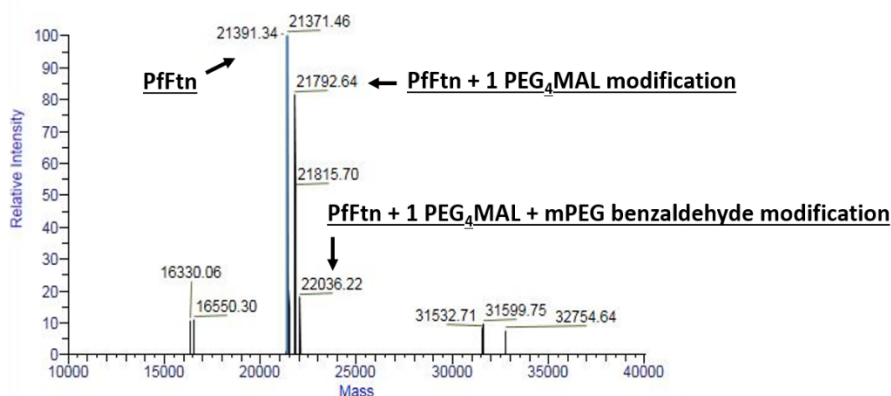


Figure 3.15. Deconvoluted ESI MS spectrum exhibits mass peaks corresponding to the final product formation with the mPEG₄-benzaldehyde attachment.

3.5.8 Purification of *Pyrococcus furiosus* Ferritin (PfFtn)

The recombinant PfFtn protein was engineered to have His₆-tag at the C-terminal that points towards the interior of the capsule protein. His-PfFtn was purified using an IMAC purification column that exposes immobilized divalent metal cations (Ni²⁺) that interacts with the histidine side chains of the target protein. The purification protocol of PfFtn was elaborated in the

methods section (Section 3.4.6). It was expected that a protein peak in the elution chromatography profile (Figure 3.16B), would be observed, but instead of a peak, the elution profile was observed as a plateau, which was fractionated into multiple tubes, an indication that the protein was not purified. Fractions from the flow-through and the plateau imidazole gradient were collected and inspected using 15% SDS-PAGE. It was expected to observe protein bands at the imidazole gradient at around 21 kDa, where the imidazole should bind to the column replacing the bound protein. However, the gel did not reveal protein bands (Figure 3.16A). The gel reveals dark bands around the mass of the PfFtn, which suggested that the protein was not bound to the IMAC column. Although the lysate was boiled for 10 min before purification but that seemed to not be sufficient to decluster the 24-mer capsule to expose the His-tagged subunits. Therefore, the protein was further boiled for 30 min and purified again with IMAC. Fractions from the second purification were examined with SDS-PAGE (Figure 3.16C) and it also showed no fractions of pure PfFtn. Previous work done by a former student (Hawa Gyamfi; PhD thesis) was reviewed for a verified purification procedure. She reported that to obtain a complete declustering of PfFtn capsules, a 6 M concentration of GdnHCl is needed in the binding buffer, while our procedure used 5 M GdnHCl, which was found to be insufficient. A third purification round using a higher GdnHCl concentration will be attempted in the future as soon as the time frame permits.

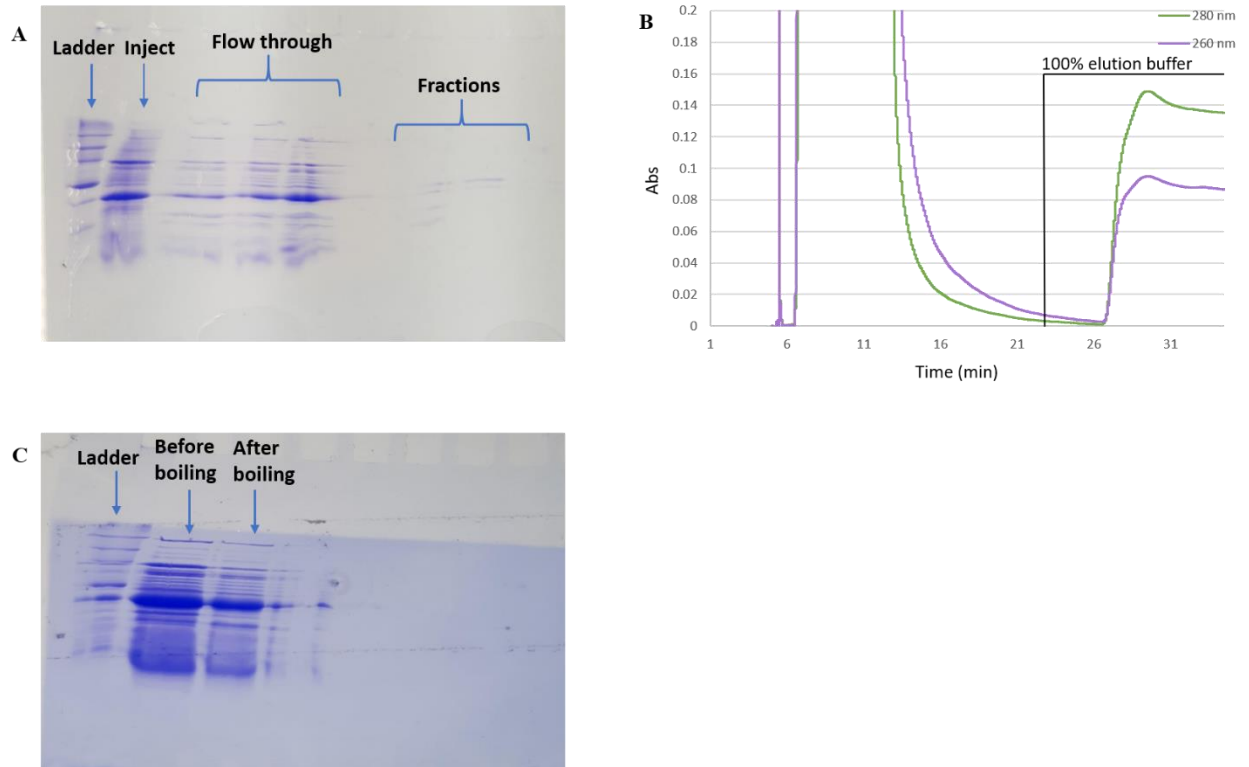


Figure 3.16. A) SDS-PAGE gel of PfFtn protein after purification with IMAC column. B) The elution profile for His-PfFtn purified using IMAC. C) SDS-PAGE gel of two PfFtn protein samples, before and after boiling.

3.6 Conclusion

This project has explored a new methodical strategy to enable functionalized ferritin for protein networks. Here it has been shown, employing mass spectrometry techniques, that a supramolecular ferritin protein can be tagged with aldehyde-containing molecules, by employing the Wittig olefination reaction in the presence of the nucleophilic phosphorous adduct NEM-TCEP covalently cross-linked on the protein surface and site-specifically at the lysine residues. Implementing this organic reaction on a protein under harsh temperature conditions was demonstrated to be completely viable and safe when using the *Pyrococcus furiosus* ferritin (PfFtn) protein. No denaturation of the PfFtn monomeric subunit was observed. The choice of the conjugated protein is vital, especially when employing an analytical mass measurement technique such as mass spectrometry. Further research to be pursued in the future will employ a diverse range of interesting aldehydes to be conjugated to proteins and to attempt this strategy on proteins that are not capsule proteins but still thermally stable, in order to determine the limitation of this labelling strategy.

4 Chapter 4: Computational Studies on the Energetics of Bioconjugation Reactions

4.1 Overview

Different bioconjugation reactions employing TFP and NHS reactive ester groups were carried out in the Honek laboratory and discussed in Chapter 2 of this thesis. It has been shown in the literature (Lockett et al., 2008), and demonstrated in this research that the TFP ester has higher stability in aqueous solution, as opposed to the NHS ester.

To further expand the current understanding in regard to these observations, and during Covid-19 outbreak, it was decided to undertake a thermodynamic study by running theoretical calculations during the lockdown period away from the university. For this purpose, the molecular modeling and computational chemistry application, Spartan, from Wavefunction was employed in this study to calculate the reaction energies for bioconjugation reactions. Also, there are different reactive functional groups that have been used in bioconjugate techniques (e.g. nitrophenyl, methyl esters, sulfo-NHS, thiocyanate, carbonate, and others), besides TFP and NHS, so a range of reactions was studied by modeling their hydrolysis and simple amine reactions (aminolysis). The hydrolysis and aminolysis reactions are to mimic the reactions of these groups in empirical experiments with water and the nucleophilic amine from lysine residues, respectively.

Quantum chemical computations were implemented to calculate the energies of these functional groups. Initially, all these reactions were modeled in the gas phase. Likewise, the computational calculations are feasible to be performed with aqueous environment as well, but it will be more complicated which could be further looked at in future theoretical computations. Choosing the gas phase to model the reactions will assist in gaining an insight about the inherent

properties of the molecules by removing the extraneous complexity associated with theoretical water molecules.

In this project, thermochemical recipes and density functional models were employed in the Spartan software. Thermochemical recipes are a combination of quantum chemistry methods that calculate and reproduce empirical heats of formation (Ohlinger et al., 2009). Density functional models (DFT) evaluate and describe the energy of the molecules as a universal function of their electron charge density (Bagayoko, 2014). The DFT models are supported with a wide range of basis sets for multiple demands.

4.2 Methods

4.2.1 Thermochemical recipes

Thermochemical recipes were employed to calculate the heat of formation (kJ/mol) energy values for this set of reactions, by which the calculations were performed in the gas state. The widely used calculations models in thermochemical recipes, both T1 and G3(MP2) were selected. Only uncharged molecules were accommodated when using the T1 model. The molecular geometry was taken into consideration, where the “equilibrium conformer” setting was assigned in the T1 calculations, as this option is not applicable with the G3(MP2) model. The T1 method as incorporated in Spartan consists of:

- A) HF/6-31G* optimization
- B) RI-MP2/6-311+G(2d,p)[6-311G*] single point energy with dual basis set
- C) An empirical correction using atom counts, Mulliken bond orders, HF/6-31G* and RIMP2 energies as variables

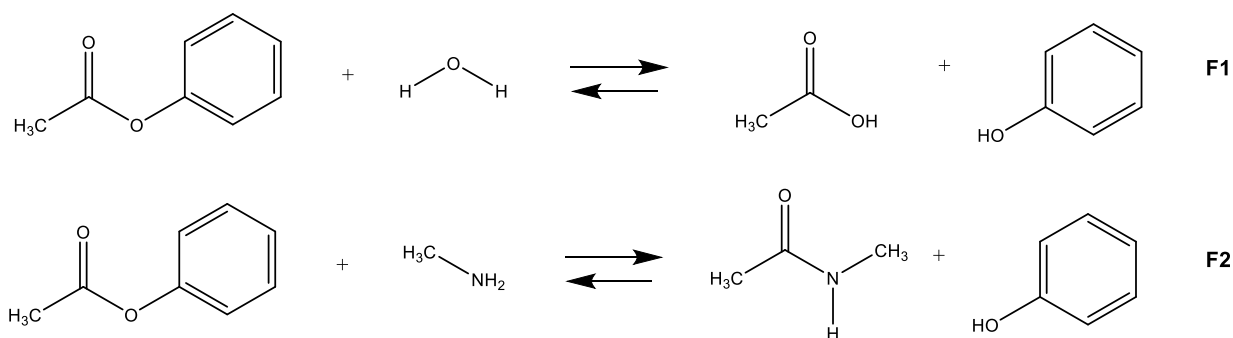
4.2.2 Density Functional Models

DFT calculations were carried out employing the functionals; M06-2X with the basis set 6-311+G(2df,2p) for single point calculations, and B3LYP with the basis set 6-31G* for geometry optimization. Likewise, the DFT calculations were implemented in the gas phase as well, and the “equilibrium conformer” setting was specified for each reaction.

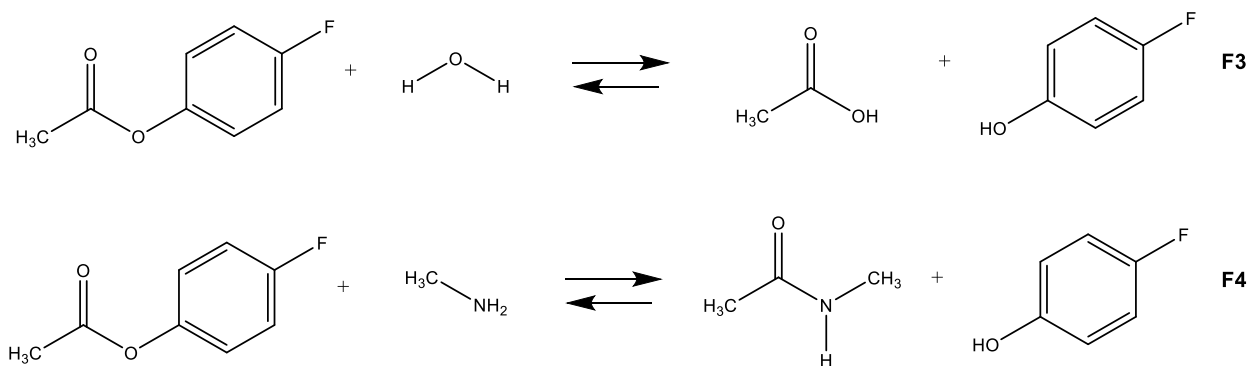
4.3 Results and Discussion

The complexity of the molecular system of interest dictates the type of calculations employed in a theoretical chemistry project. Herein, a set of reactions involving molecules with relatively small atomic mass units were studied, therefore, the thermochemical recipes and the DFT calculations that are applicable to small molecular weight molecules, were employed. A combination of various functional groups involved in bioconjugation reactions is presented in the reaction schemes below.

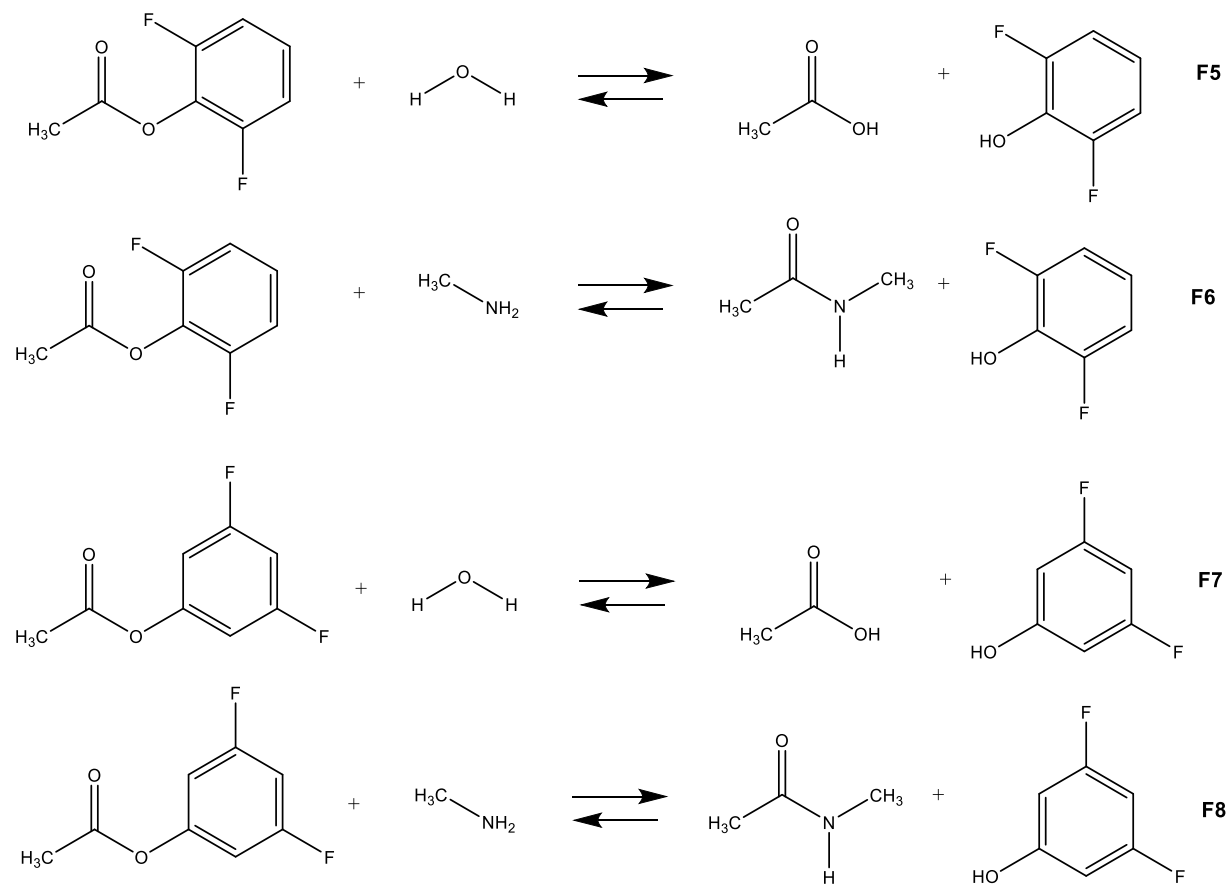
The results shown in this section are of the following groups; phenyl ester (F1-F2), fluorine substituted phenyl esters (F3-F16), acetyl chloride (Cl1-Cl2), sulfo-NHS (SO₃H-1, SO₃H-2), nitrophenyl (NO₂-1, NO₂-2), methyl acetate (MA-1,MA-2), thioester (TE1-TE2), and N-hydroxysuccinimide ester (NHS-1, NHS-2). The theoretical computations involved energy calculations of the hydrolysis and aminolysis of these molecules, mimicking the nucleophiles; water and amines. Other reactions of interest to this project were considered as well. Schiff base formation (OR1), methyl maleimide reactions with tris-2-carboxyethyl phosphine (TCEP) and tris-hydroxypropyl phosphine (THPP) (OR2-OR5), methyl maleimide-TCEP adduct with benzaldehyde (OR6-OR7). These reactions are depicted in Schemes 4.1-4.17.



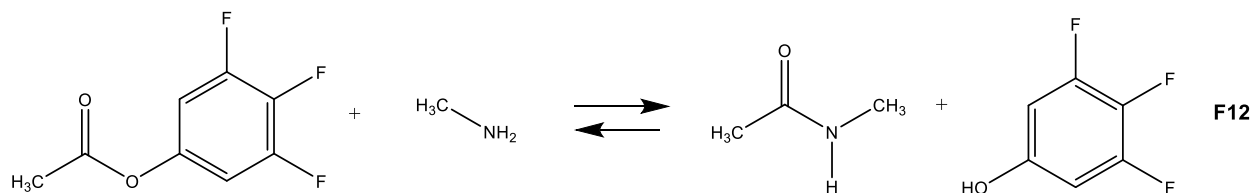
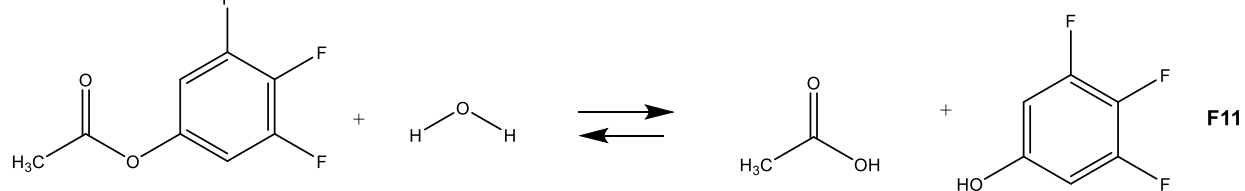
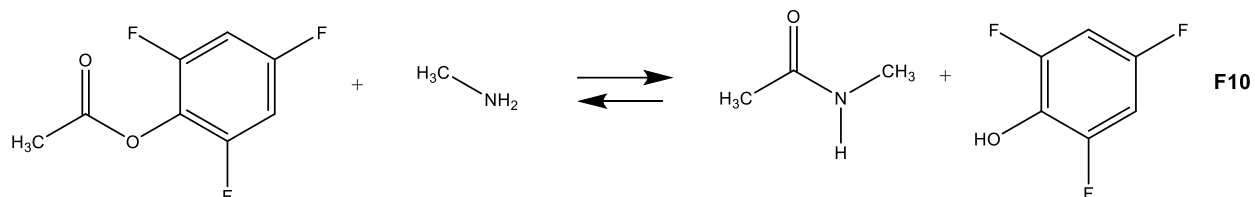
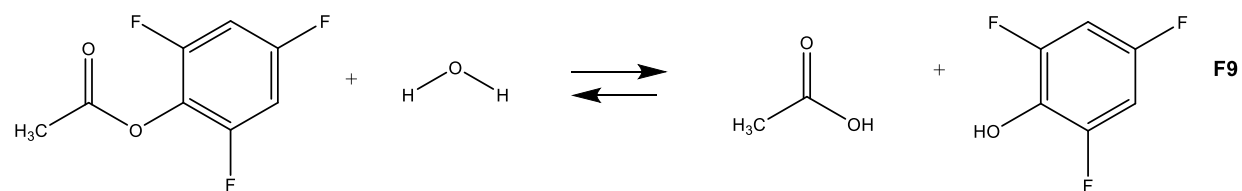
Scheme 4.1. Reactions of phenyl esters.



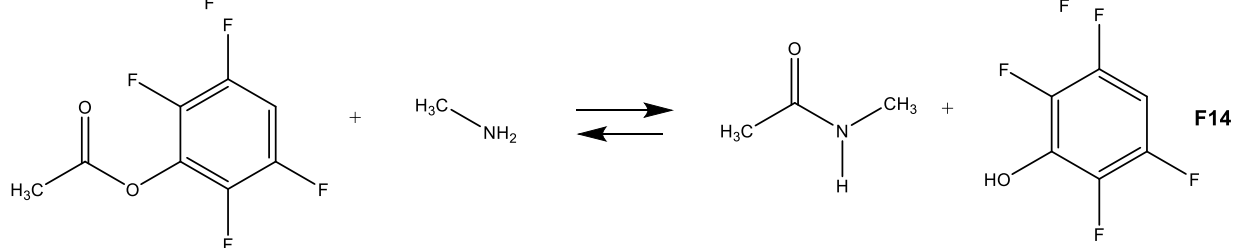
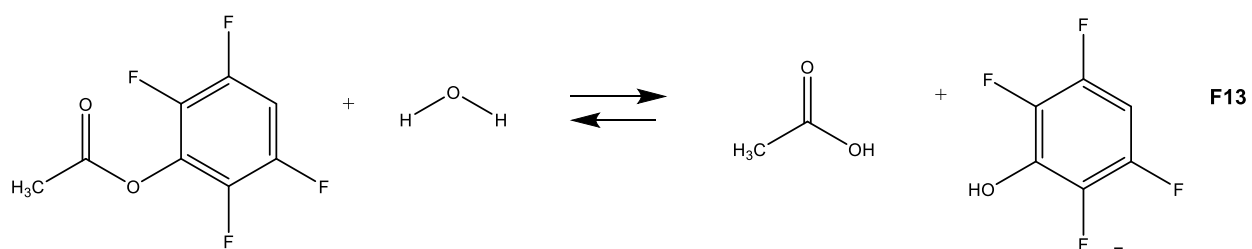
Scheme 4.2. Reactions of monosubstituted fluorophenyl esters.



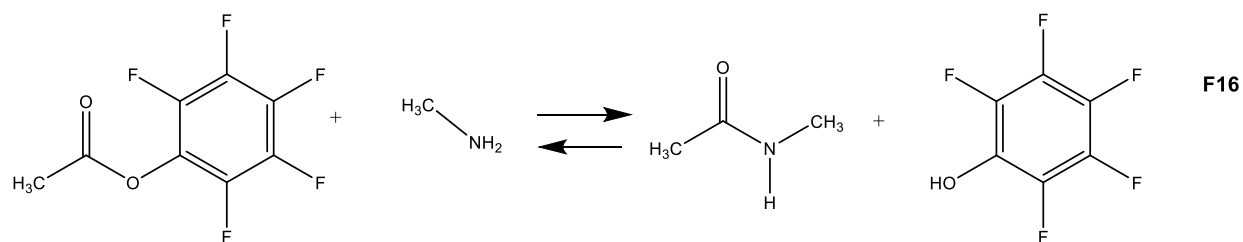
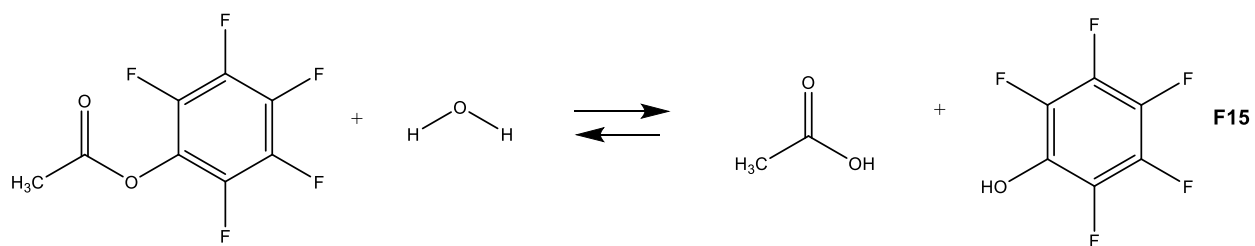
Scheme 4.3. Reactions of difluorephenyl esters.



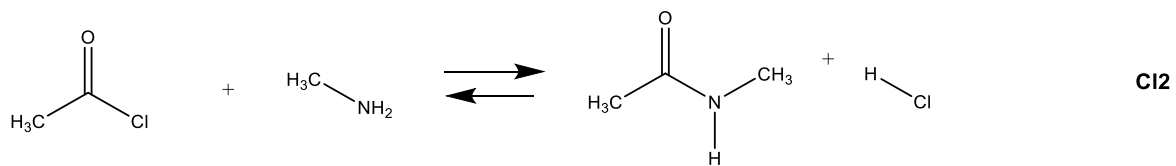
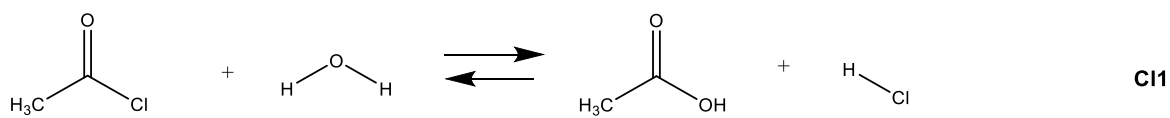
Scheme 4.4. Reactions of trifluorophenyl esters.



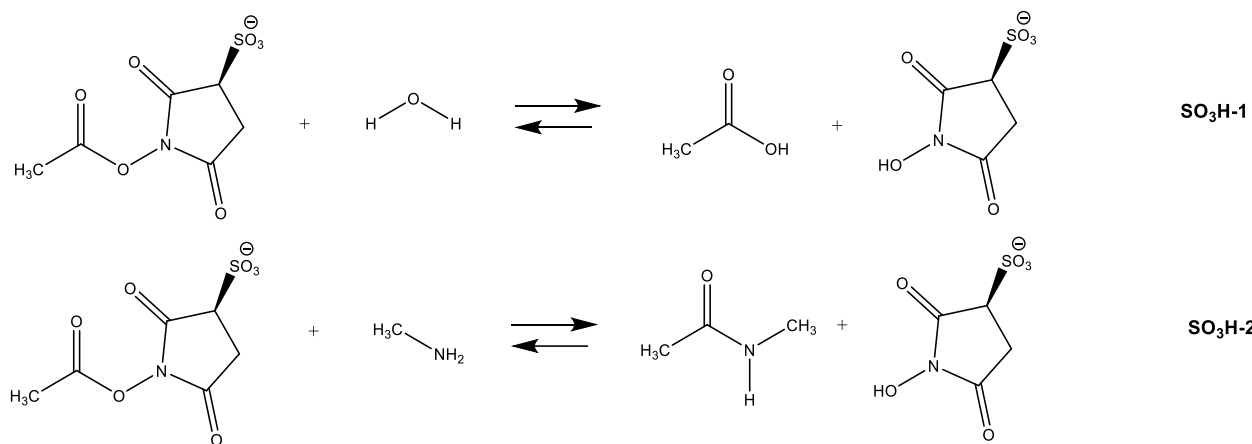
Scheme 4.5. Reactions of tetrafluorophenyl esters.



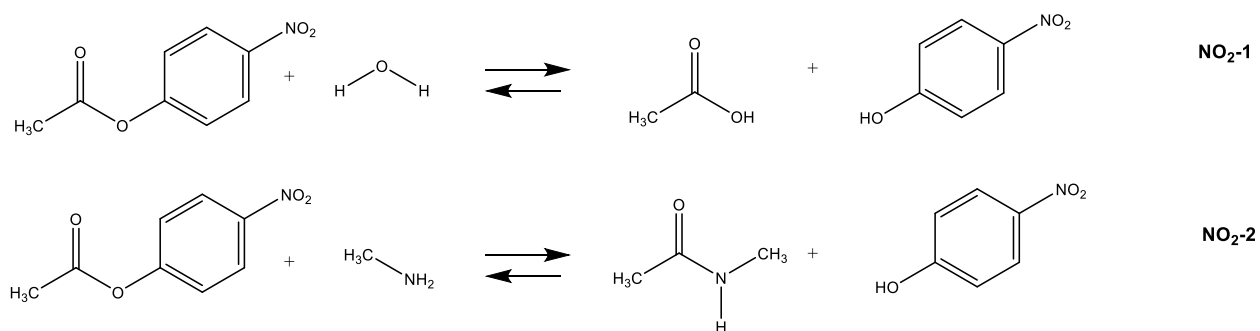
Scheme 4.6. Reactions of pentafluorophenyl esters.



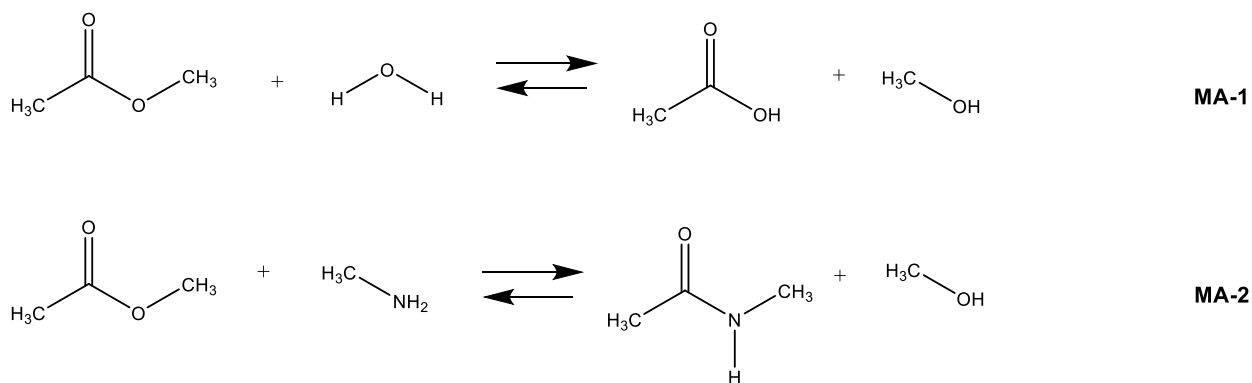
Scheme 4.7. Reactions of acetyl chlorides.



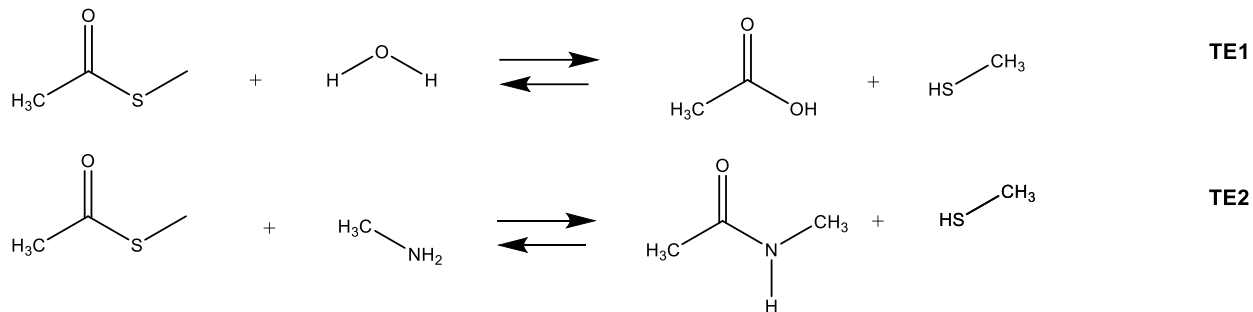
Scheme 4.8. Reactions of sulfo-NHS esters.



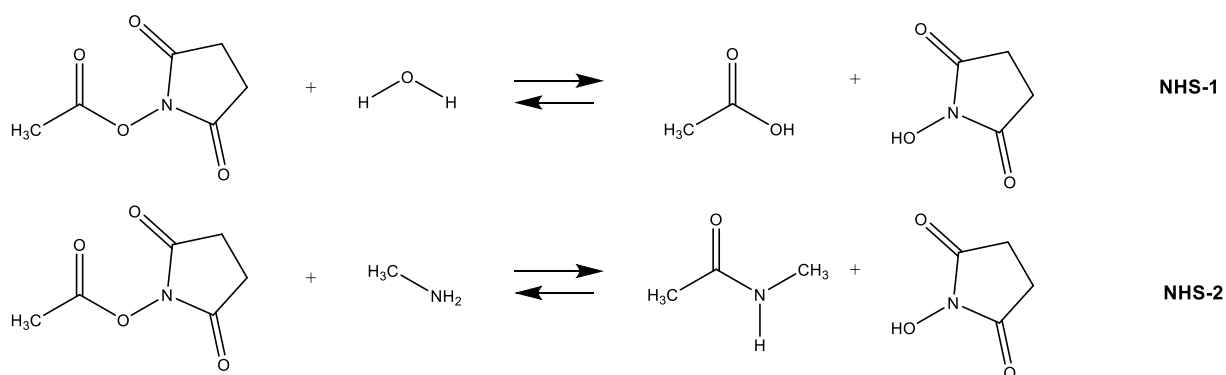
Scheme 4.9. Reactions of p-nitrobenzyl esters.



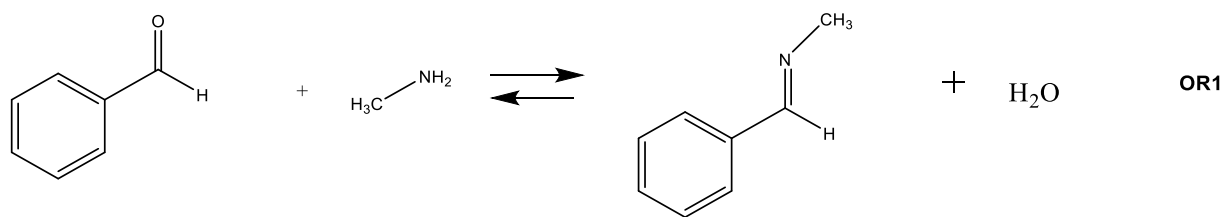
Scheme 4.10. Reactions of methyl acetates.



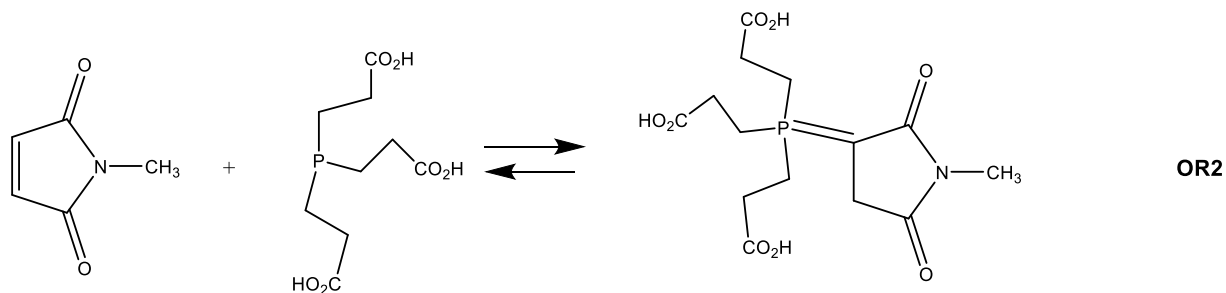
Scheme 4.11. Reactions of thioesters.



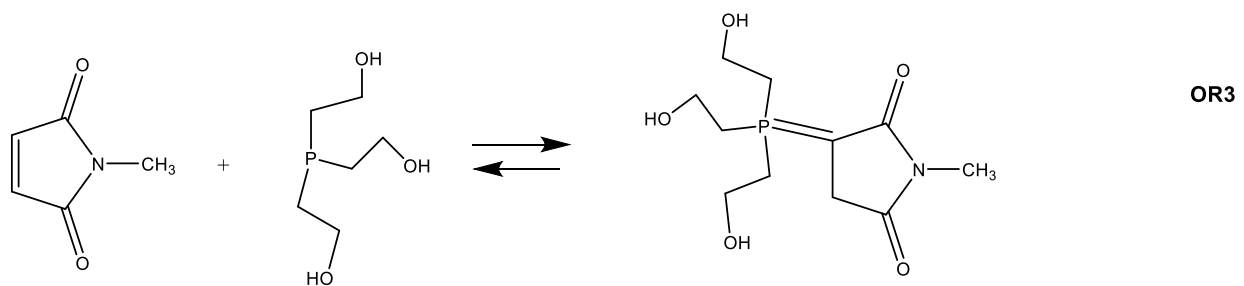
Scheme 4.12. Reactions of N-hydroxysuccinimide esters.



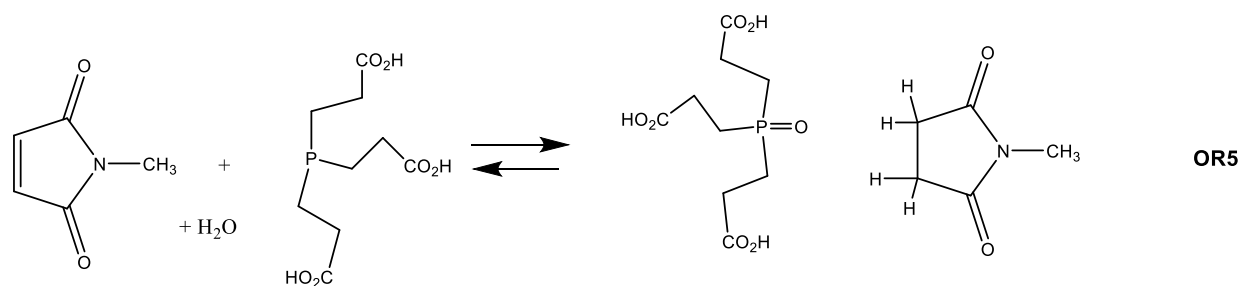
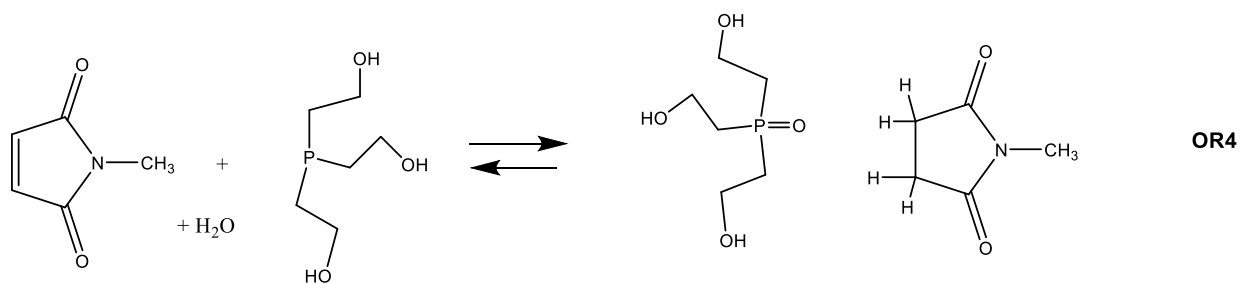
Scheme 4.13. Schiff base formation.



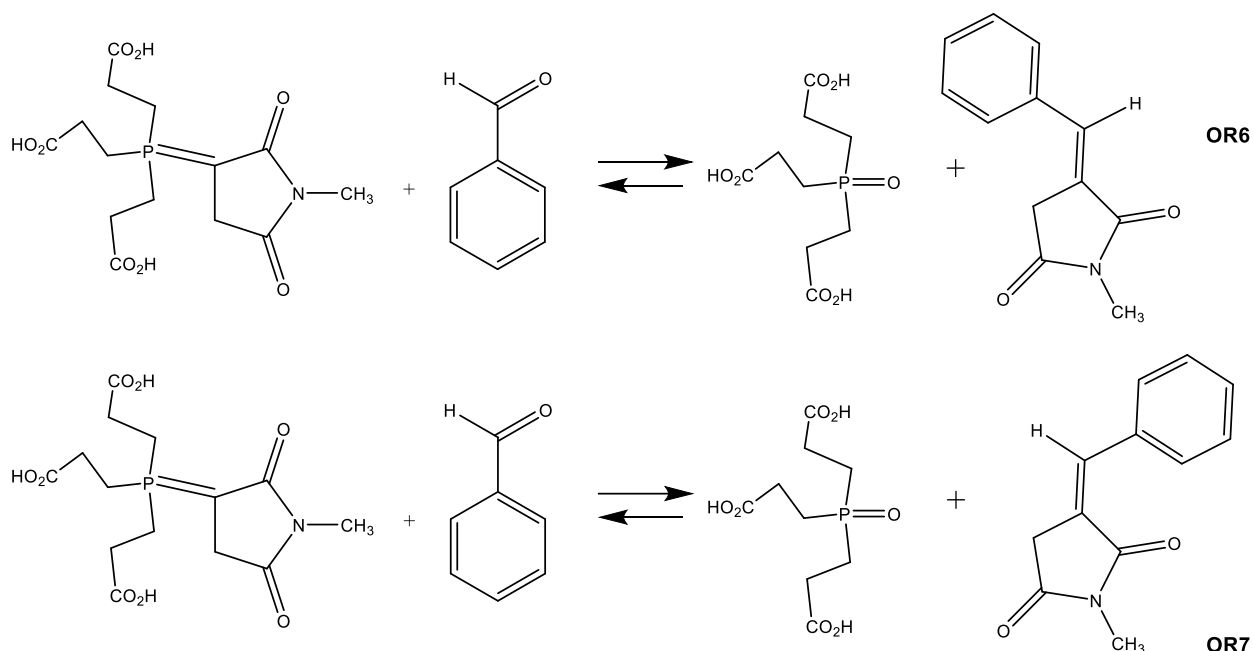
Scheme 4.14. NEM-TCEP adduct formation.



Scheme 4.15. NEM-THPP formation.



Scheme 4.16. NEM-TCEP and THPP reactions in H₂O.



Scheme 4.17. Wittig reaction forming *E*- and *Z*-alkenes.

First, the T1 and G3(MP2) calculations were performed. The calculations using the T1 recipes have a reduced computational cost and time compared to the G3(MP2) protocol, but the energy values exhibited similar accuracy. This is determined in the comparison presented in Table 5. It was important to assign the best molecular conformation before starting the calculations. The equilibrium conformer setting in T1 calculations performed a systematic search for possible conformations in order to choose the lowest energy conformer and used that to calculate the heat of formation. Whereas, G3(MP2) used the existing conformer and optimizes its geometry before starting the calculations.

Table 5. Calculated energy values using the thermochemical recipes models

Reaction	T1	G3(MP2)
	ΔE (kJ/mol)	ΔE (kJ/mol)
F1	-3.89	-2.35
F2	-25.58	-27.87
F3	-2.45	-0.18
F4	-24.14	-25.7
F5	-7.15	-4.67
F6	-28.84	-30.19
F7	-6.83	-5.35
F8	-28.52	-30.87
F9	-5.03	-1.84
F10	-26.72	-27.36
F11	-4.87	-3.13
F12	-26.56	-28.65
F13	-8.01	-5.64
F14	-29.7	-31.16
F15	-5.81	-3.25
F16	-27.5	-28.77
Cl1	-43.00	-38.25
Cl2	-64.73	-63.77
SO ₃ H-1	8.47	15.91
SO ₃ H-2	-13.22	-9.61
NO ₂ -1	-7.89	-6.05
NO ₂ -2	-29.68	-31.57
MA-1	19.45	22.65
MA-2	-2.28	-2.87
TE1	-10.29	-5.82
TE2	-32.02	-31.34
NHS-1	5.38	9.67
NHS-2	-16.35	-15.85
OR1	-14.26	-17.6
OR2	-86.03	NA
OR3	-99.95	NA
OR4	-223.74	NA
OR5	-245.45	NA
OR6	-146.21	NA
OR7	-129.06	NA

The DFT calculations were carried out next. The density functionals offer and employ a variety of different data sets in the model's database. For this part of the study, the M06-2X functional was chosen as it provides a good performance for calculations of reaction energies and thermochemistry (Mardirossian & Head-Gordon, 2016). Energy values are shown in Table 6.

Table 6. Calculated energy values using the DFT models

Reaction	DFT: M062X/6-311+G(2df,2p) - B3LYP/6-31G*		
	ΔE (kJ/mol)	ΔG (kJ/mol)	ΔH (kJ/mol)
F1	-17.88	-14.68	-12.18
F2	-36.13	-31.03	-35.20
F3	-15.19	-11.16	-9.42
F4	-33.44	-27.51	-32.43
F5	-21.21	-20.56	-14.48
F6	-39.46	-36.91	-37.50
F7	-23.23	-20.91	-16.26
F8	-41.48	-37.26	-39.27
F9	-18.28	-19.27	-11.64
F10	-36.48	-43.13	-34.48
F11	-20.56	-20.62	-13.94
F12	-38.76	-44.47	-36.78
F13	-23.72	-24.67	-16.87
F14	-41.95	-47.41	-39.51
F15	-20.57	-23.08	-13.89
F16	-38.8	-45.82	-36.53
Cl1	-43.74	-41.72	-45.17
Cl2	-61.99	-58.07	-68.19
SO ₃ H-1	-7.58	-6.84	-1.77
SO ₃ H-2	-25.83	-23.19	-24.78
NO ₂ -1	-25.68	-25.75	-18.69
NO ₂ -2	-43.93	-42.10	-41.71
MA-1	15.04	19.26	18.74
MA-2	-3.21	2.90	-4.28
TE1	-17.17	-26.96	-15.46
TE2	-35.41	-43.31	-38.48
NHS-1	-6.53	-7.48	0.28
NHS-2	-24.78	-23.84	-22.74
OR1	-3.47	-2.3	-9.8
OR2	-94.39	-10.41	-85.17
OR3	-104.7	-35.32	-96.92
OR4	NA	NA	NA
OR5	NA	NA	NA
OR6	-148.87	-152.89	-146.58
OR7	-130.58	-130.85	-127.8

Based on the energy calculations shown in Table 5 and 6, these computational data conclude that the thioester (TE2, $\Delta E = -32.02$ kJ/mol) is the most thermodynamically favorable reactive ester group, and that NHS ester (NHS-2, $\Delta E = -16.35$ kJ/mol) is less thermodynamically favorable than the TFP ester (F14, $\Delta E = -29.7$ kJ/mol), which is in a good alignment with our experimental observations. Additionally, it is noticed throughout the data set that the reactions with the nucleophilic amines are more thermodynamically favorable than the reaction with water. A comparison between the energies of the activated esters is shown in Figure 4.1.

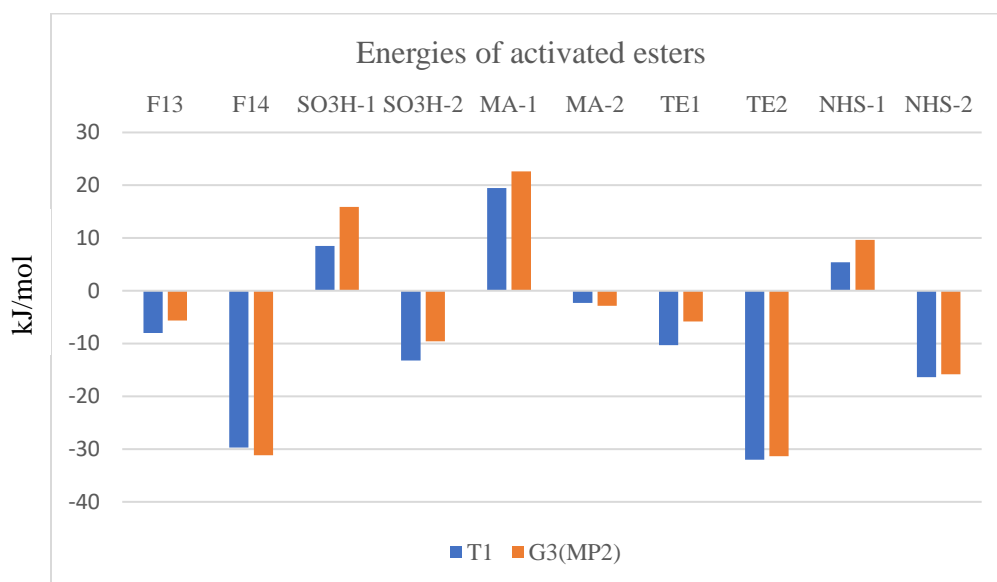


Figure 4.1. The energies of activated esters (kJ/mol).

The results also show that the *E*-isomer is of lower energy and is more likely to be the product of Wittig olefination than the *Z*-isomer, in the reaction of maleimide-TCEP and benzaldehyde. This is consistent with the literature discussed in Chapter 3 concerning the type of the product isomer. Further work would be necessary to calculate the energies for the discussed reactions in water to see how they compare with those of the gas phase energy values.

5 Chapter 5: Summary and Future Directions

Over the course of this thesis research, multiple subprojects were conducted to expand the current knowledge on the protein networks functionalities and bioconjugation strategies. The protein network material we designed aim to expand the scope for industrial and medical applications. Figure 5.1 illustrates the full picture of the thesis project's methodical plan. The project hypothesized that using these protein networks would provide enzymatic, photocleavable, and magnetic functionalities. Throughout the project, the materials have demonstrated substantial results, enabling them to serve as an efficient plastic degrading material and a smart bandage.

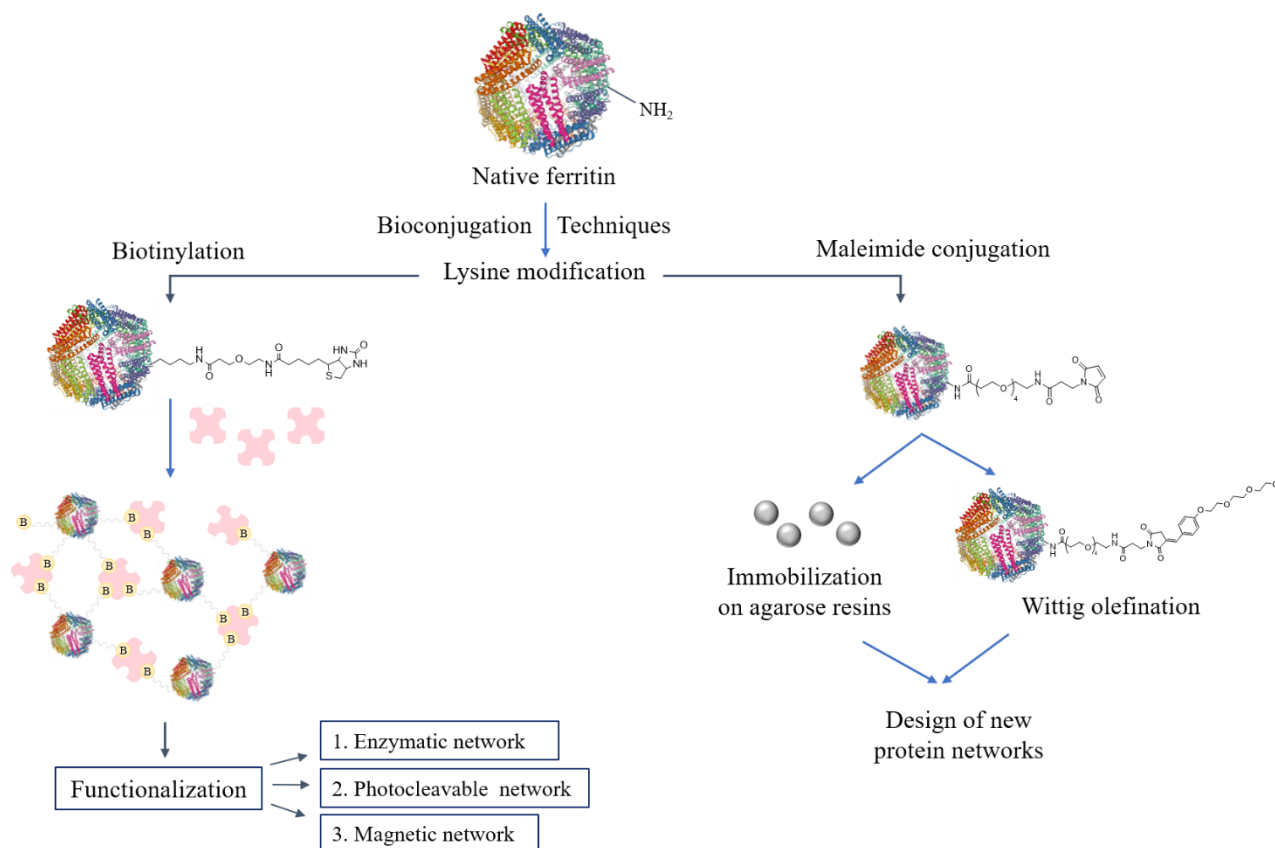


Figure 5.1. Schematic summary of the thesis project.

An array of countless creative approaches could be pursued via the maleimide conjugation for immobilization applications. Figure 5.2 displays three potential advantages of conjugating a maleimide containing molecule (e.g. protein, enzyme, or small molecule) on a polymer-supported TCEP resin.

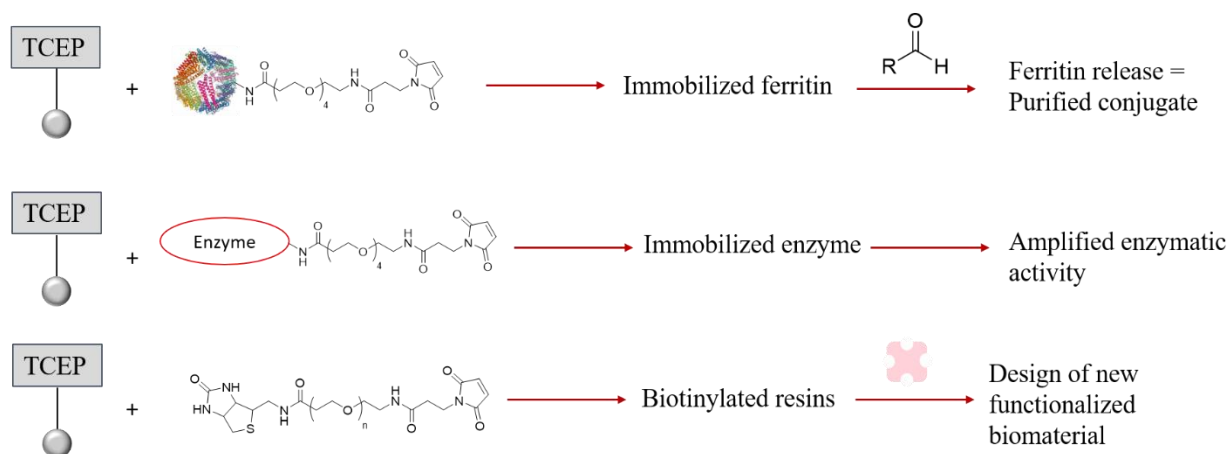


Figure 5.2. The maleimide conjugation approach for immobilization applications.

Two ferritin capsule proteins, horse spleen ferritin (HSF) and *Pyrococcus furiosus* ferritin (PfFtn) were investigated in this work as the major building blocks for the protein networks. In the first part of the project, the HSF was successfully bioconjugated at the exposed lysine residues with various potential bifunctional PEG cross-linkers that contain an activated ester (e.g. TFP or NHS ester) on one end and a biotin molecule on the second end that will be displayed on the exterior surface of the protein. The modified HSF capsules with biotins were subsequently cross-linked with the avidin through the strongest non-covalent complexation in nature. Utilizing the strength and durability of the biotin-avidin interaction, in addition to the compatible choice of the cross-linker, these networks could demonstrate an enzymatic activity when loaded with various molecules. The options include but are not limited to; enzymes, photocleavable drug release when

choosing a corresponding linker moiety, filtration biomembrane characteristic with tunable pores when adjusting the expanded PEG spacer, and a lot more to be counted. Moreover, the sophistication of this biomaterial could be increased through occupying the empty biotin binding sites with biotinylated species (e.g. fluorophores, enzymes, magnetic particles, drug molecules).

The second part of the project has investigated and successfully accomplished a novel bioconjugation strategy, which aimed to modify the surface lysine residues of the ferritin employing a multistep conjugation process that incorporated an aldehyde-containing molecule exploiting the Wittig reaction. The strategy utilized a small molecular weight adduct, TCEP-MAL that is difficult to detect a high-resolution mass peak for. Therefore, the thermally stable PfFtn protein was utilized in this part, since determining an accurate mass of the small molecular modifications in ESI-MS technique was a real challenge when using the HSF as the capsule protein. Pursuing this bioconjugation strategy should provide more interesting characteristics to the protein networks.

Despite all the work that has been undertaken, and the promising results obtained in both parts of the project, there is much more to explore about the novelty of these supramolecular proteinaceous nanomaterials and the plethora of strategies that could be pursued to tailor the properties of the scaffold in order to attain the desired application.

5.1 Optimizations and Bioconjugation with Functional Aldehydes

Milder conditions that require lower temperatures to drive the Wittig olefination of mPEG₄-benzaldehyde with PfFtn will be optimized. The mild conditions will include eliminating the use of NaOH catalyst, because bases are not advised to be used in a proteinaceous environment. An alternative would be using a basic buffer solution (e.g. EPPS buffer). Furthermore, two

additional water-soluble aldehydes are to be labelled to proteins to add functionality. These are; PEG₁₂-benzaldehyde with dansyl group that exhibits a fluorescence activity, and PEG₁₂-benzaldehyde with biotin group that can attach with high affinity to avidin proteins (Figure 5.3).

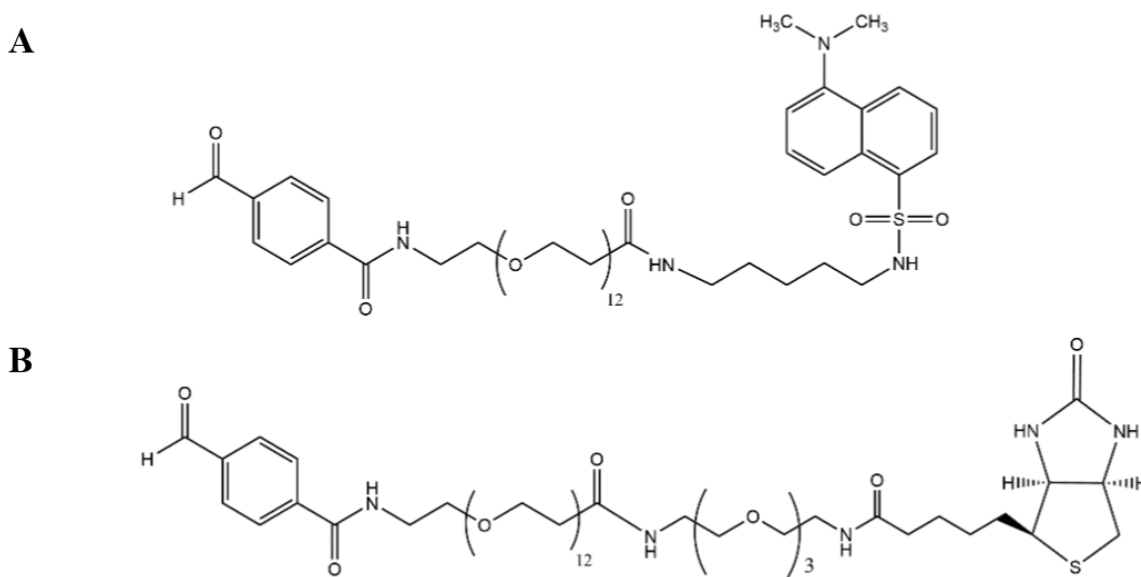


Figure 5.3. Two aldehyde reagents for bioconjugation with proteins. A) PEG₁₂-benzaldehyde with dansyl group that exhibits a fluorescence activity. B) PEG₁₂-benzaldehyde with biotin group that can attach robustly with avidin proteins.

5.2 Immobilizations on Polymer-supported TCEP Resins

An array of various approaches could be pursued by utilizing the TCEP-MAL reaction strategy to make new biomaterials. The future work will include the immobilization of proteins using “Immobilized TCEP Disulfide Reducing Gel” (Thermo Fisher Scientific, Rockford, IL, US), a polymer-supported TCEP-containing resin made of cross-linked agarose gel. A protein modified with maleimide can react with the TCEP forming the adduct to be attached to the resin. An aldehyde molecule will be used to release the protein from the resin. Not only capsule proteins

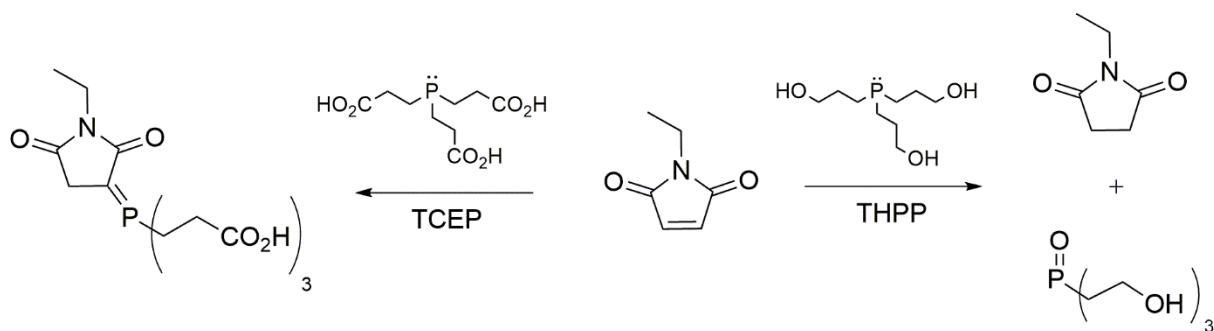
could be incorporated in this direction, but also non-capsule proteins would add a new dimension to the proposed idea. The enzyme bovine carbonic anhydrase (BCA) that catalyzes the conversion of carbon dioxide and water to bicarbonate ions (Saito et al., 2004), will be modified with maleimide groups and attached to the TCEP resins. In addition to its common function, BCA has been found to catalyze the hydrolysis of *p*-nitrophenyl ester to *p*-nitrophenol (Pocker et al., 1974) that absorbs 405 nm wavelength, so this functionality will be exploited in this context. The immobilization method should increase the concentration of the catalytic molecule and perhaps increase the stability of the immobilized enzyme. This new bioconjugation technique is to be enabled by employing the agarose resins to serve as a biorenewable platform for the formation of new materials with sustainable building blocks.

5.3 Computational Studies

Future work will include transition state modelling. The plan is to compare the energies of the substrates and the transition states to be able to explain what is contributing to the capability of the TFP esters to remain intact longer in aqueous solution. Transition state modeling was carried out by our group intensively using Spartan (Wavefunction Inc.) and AutoTS (Schrodinger, LLC) software. Some challenges were faced in the preliminary work, so the future work will include further studies to successfully calculate transition state energies. Previous literature reported comparative studies on the hydrolysis rates between TFP and NHS, however, no studies on the thermodynamics of the functional groups were found in the literature.

In regard to the transition state modeling, there is a second aspect that our group is interested in revealing in the future work. Tris-2-carboxyethyl phosphine (TCEP) and Tris-hydroxypropyl phosphine (THPP) are both soluble reducing agents, however, each one has been shown to produce different products (Scheme 5.1). As this research states, TCEP was determined

to produce a stable adduct when reacted with maleimide. On the other hand, THPP tends to reduce the maleimide to succinimide (Kantner & Watts, 2016). The reason for yielding different products has not been uncovered yet. It is difficult to interpret this observation in terms of the charge and the induction differences between the carboxyl and hydroxyl functional groups, since both compounds have a very similar pKa value for the phosphorous atoms of the TCEP and THPP (pKa = 7.7 and 7.2, respectively) (Kantner & Watts, 2016). The Honek group will be working on the computational study to model the transition state of both reagents, hoping that will provide some insight.



Scheme 5.1. The reaction of N-ethylmaleimide with TCEP produces an ylene, while its reaction with THPP results in reduction of the maleimide ring.

References

- Agten, S. M., Dawson, P. E., & Hackeng, T. M. (2016). Oxime conjugation in protein chemistry: from carbonyl incorporation to nucleophilic catalysis. *Journal of Peptide Science*, 22(5), 271–279. <https://doi.org/10.1002/psc.2874>
- Alp, D., Kuleaşan, H., & Altıntaş, K. (2020). The importance of the S-layer on the adhesion and aggregation ability of Lactic acid bacteria. *Molecular Biology Reports*, 47, 3449–3457. <https://doi.org/10.1007/s11033-020-05430-6>
- Andrews, S. C. (2010). The Ferritin-like superfamily: Evolution of the biological iron storeman from a rubrerythrin-like ancestor. *Biochimica et Biophysica Acta - General Subjects*, 1800(8), 691–705. Elsevier. <https://doi.org/10.1016/j.bbagen.2010.05.010>
- Annesley, T. M. (2003). Ion suppression in mass spectrometry. *Clinical Chemistry*, 49(7), 1041–1044. <https://doi.org/10.1373/49.7.1041>
- Arosio, P., Adelman, T. G., & Drysdale, J. W. (1978). On ferritin heterogeneity. Further evidence for heteropolymers. *The Journal of Biological Chemistry*, 253(12), 4451–4458. <http://www.ncbi.nlm.nih.gov/pubmed/659425>
- Ashton, L., Brewster, V. L., Correa, E., & Goodacre, R. (2017). Detection of glycosylation and iron-binding protein modifications using Raman spectroscopy. *Analyst*, 142(5), 808–814. <https://doi.org/10.1039/c6an02516a>
- Aslan, K., Luhrs, C. C., & Pérez-Luna, V. H. (2004). Controlled and reversible aggregation of biotinylated gold nanoparticles with streptavidin. *Journal of Physical Chemistry B*, 108(40), 15631–15639. <https://doi.org/10.1021/jp036089n>
- Attwood, S. J., Cortes, E., Haining, A. W. M., Robinson, B., Li, D., Gautrot, J., & Del Río Hernández, A. (2016). Adhesive ligand tether length affects the size and length of focal adhesions and influences cell spreading and attachment. *Scientific Reports*, 6(1), 1–11. <https://doi.org/10.1038/srep34334>
- Bagayoko, D. (2014). Understanding density functional theory (DFT) and completing it in practice. *AIP Advances*, 4(12), 127104. <https://doi.org/10.1063/1.4903408>
- Baneyx, F., & Matthaëi, J. F. (2014). Self-assembled two-dimensional protein arrays in bionanotechnology: From S-layers to designed lattices. *Current Opinion in Biotechnology*, 28, 39–45. <https://doi.org/10.1016/j.copbio.2013.11.001>
- Bayat, M., Hosseini, S. R., & Asmari, E. (2017). Simple synthesis of (E) and (Z)-2-(arylmethylidene)-N-phenyl succinimides via Wittig olefination by using PS-TPP resin. *Phosphorus, Sulfur and Silicon and the Related Elements*, 192(1), 98–102. <https://doi.org/10.1080/10426507.2016.1225739>
- Bogacz-Radomska, L., Harasym, J., & Piwowar, A. (2020). Commercialization aspects of carotenoids. In *Carotenoids: Properties, Processing and Applications* (pp. 327–357). Elsevier. <https://doi.org/10.1016/b978-0-12-817067-0.00010-5>
- Brackman, G., Al Quntar, A. A. A., Enk, C. D., Karalic, I., Nelis, H. J., Van Calenbergh, S.,

- Srebnik, M., & Coenye, T. (2013). Synthesis and evaluation of thiazolidinedione and dioxaborocane analogues as inhibitors of AI-2 quorum sensing in *Vibrio harveyi*. *Bioorganic and Medicinal Chemistry*, *21*(3), 660–667. <https://doi.org/10.1016/j.bmc.2012.11.055>
- Carniel, A., Valoni, É., Nicomedes, J., Gomes, A. da C., & Castro, A. M. de. (2017). Lipase from *Candida antarctica* (CALB) and cutinase from *Humicola insolens* act synergistically for PET hydrolysis to terephthalic acid. *Process Biochemistry*, *59*, 84–90. <https://doi.org/10.1016/j.procbio.2016.07.023>
- Cengiz, N., Gevrek, N., Sanyal, R., & Sanyal, A. (2020). Fabrication of Patterned Hydrogel Interfaces: Exploiting the Maleimide Group as a Dual Purpose Handle for Cross-Linking and Bioconjugation. *Bioconjugate Chemistry*, *31*(5), 1382–1391. <https://doi.org/10.1021/acs.bioconjchem.0c00108>
- Chen, S., Su, L., Chen, J., & Wu, J. (2013). Cutinase: Characteristics, preparation, and application. In *Biotechnology Advances*, *31*(8), 1754–1767. <https://doi.org/10.1016/j.biotechadv.2013.09.005>
- Clapper, J. D., Pearce, M. E., Guymon, C. A., & Salem, A. K. (2008). Biotinylated Biodegradable Nanotemplated Hydrogel Networks for Cell Interactive Applications. *Biomacromolecules*, 1188–1194.
- Clark, A. E., Kaleta, E. J., Arora, A., & Wolk, D. M. (2013). Matrix-Assisted laser desorption ionization-time of flight mass spectrometry: A fundamental shift in the routine practice of clinical microbiology. *Clinical Microbiology Reviews*, *26*(3), 547–603. <https://doi.org/10.1128/CMR.00072-12>
- Dai, Y., Wang, C., Chiu, L. Y., Abbasi, K., Tolbert, B. S., Sauvé, G., Yen, Y., & Liu, C. C. (2018). Application of bioconjugation chemistry on biosensor fabrication for detection of TAR-DNA binding protein 43. *Biosensors and Bioelectronics*, *117*, 60–67. <https://doi.org/10.1016/j.bios.2018.05.060>
- Dalal, A., Khanna, R., & Kamboj, R. C. (2018). Photochemical Transformation of some 3-benzyloxy-2-(benzo[b]thiophen-2-yl)-4H-chromen-4-ones: A Remote Substituent Effect. *Open Chemistry*, *16*(1), 79–86. <https://doi.org/10.1515/chem-2018-0009>
- Dozier, J. K., & Distefano, M. D. (2015). Site-specific pegylation of therapeutic proteins. *International Journal of Molecular Sciences*, *16*(10), 25831–25864. <https://doi.org/10.3390/ijms161025831>
- Ebbers, E. J., Ariaans, G. J. A., Houbiers, J. P. M., Bruggink, A., & Zwanenburg, B. (1997). Controlled racemization of optically active organic compounds: Prospects for asymmetric transformation. *Tetrahedron*, *53*(28), 9417–9476. [https://doi.org/10.1016/S0040-4020\(97\)00324-4](https://doi.org/10.1016/S0040-4020(97)00324-4)
- Eidsness, M. K., Richie, K. A., Burden, A. E., Kurtz, D. M., & Scott, R. A. (1997). Dissecting contributions to the thermostability of *Pyrococcus furiosus* rubredoxin: β -sheet chimeras. *Biochemistry*, *36*(34), 10406–10413. <https://doi.org/10.1021/bi970110r>
- Ensing, B., Tiwari, A., Tros, M., Hunger, J., Domingos, S. R., Pérez, C., Smits, G., Bonn, M.,

- Bonn, D., & Woutersen, S. (2019). On the origin of the extremely different solubilities of polyethers in water. *Nature Communications*, *10*(1), 1–8. <https://doi.org/10.1038/s41467-019-10783-z>
- Fontana, A., Gross, E. (1986). Fragmentation of Polypeptides by Chemical Methods. In: *Practical Protein Chemistry - A Handbook*, Darbre, A. ed., Wiley, pp. 67-120.
- Garanger, E., Weissleder, R., & Josephson, L. (2009). A multifunctional single-attachment-point reagent for controlled protein biotinylation. *Bioconjugate Chemistry*, *20*(1), 170–173. <https://doi.org/10.1021/bc800392t>
- Gasteiger, E., Gattiker, A., Hoogland, C., Ivanyi, I., Appel, R. D., & Bairoch, A. (2003). ExPASy: the proteomics server for in-depth protein knowledge and analysis. *Nucleic Acids Research*, *31*(13), 3784-3788. <https://doi.org/10.1093/nar/gkg563>
- Gerbino, E., Carasi, P., Mobili, P., Serradell, M. A., & Gómez-Zavaglia, A. (2015). Role of S-layer proteins in bacteria. *World Journal of Microbiology and Biotechnology*, *13*(12), 1877–1887). <https://doi.org/10.1007/s11274-015-1952-9>
- Goddard, T. D., Huang, C. C., & Ferrin, T. E. (2005). Software extensions to UCSF chimera for interactive visualization of large molecular assemblies. *Structure*, *13*(3), 473–482. <https://doi.org/10.1016/j.str.2005.01.006>
- Gomes, A. F., & Gozzo, F. C. (2010). Chemical cross-linking with a diazirine photoactivatable cross-linker investigated by MALDI- and ESI-MS/MS. *Journal of Mass Spectrometry*, *45*(8), 892–899. <https://doi.org/10.1002/jms.1776>
- González, M., Argaraña, C. E., & Fidelio, G. D. (1999). Extremely high thermal stability of streptavidin and avidin upon biotin binding. *Biomolecular Engineering*, *16*(1–4), 67–72. [https://doi.org/10.1016/S1050-3862\(99\)00041-8](https://doi.org/10.1016/S1050-3862(99)00041-8)
- Ha, Y. M., Kim, J. A., Park, Y. J., Park, D., Choi, Y. J., Kim, J. M., Chung, K. W., Han, Y. K., Park, J. Y., Lee, J. Y., Moon, H. R., & Chung, H. Y. (2011). Synthesis and biological activity of hydroxybenzylidene pyrrolidine-2,5-dione derivatives as new potent inhibitors of tyrosinase. *MedChemComm*, *2*(6), 542–549. <https://doi.org/10.1039/c0md00234h>
- Han, M. J., Xiong, D. C., & Ye, X. S. (2012). Enabling wittig reaction on site-specific protein modification. *Chemical Communications*, *48*(90), 11079–11081. <https://doi.org/10.1039/c2cc35738k>
- Harrison, P. M. (1986). The structure and function of ferritin. *Biochemical Education*, *14*(4), 154–162. [https://doi.org/10.1016/0307-4412\(86\)90203-7](https://doi.org/10.1016/0307-4412(86)90203-7)
- Härtner, S., Kim, H.-C., & Hampp, N. (2007). Phototriggered release of photolabile drugs via two-photon absorption-induced cleavage of polymer-bound dicoumarin. *Journal of Polymer Science Part A: Polymer Chemistry*, *45*(12), 2443–2452. <https://doi.org/10.1002/pola.22007>
- He, C., Honda, R., Kamitake, H., Uenuma, M., Ishikawa, Y., Yamashita, I., & Uraoka, Y. (2013). Distance controlled nanoparticles using PEG-ferritin for new functional devices. *IMFEDK 2013 - 2013 International Meeting for Future of Electron Devices, Kansai*, 26–27. <https://doi.org/10.1109/IMFEDK.2013.6602224>

- Heitzmann, H., & Richards, F. M. (1974). Use of the avidin biotin complex for specific staining of biological membranes in electron microscopy. *Proceedings of the National Academy of Sciences of the United States of America*, 71(9), 3537–3541. <https://doi.org/10.1073/pnas.71.9.3537>
- Hermanson, G. T. (1996). The chemistry of reactive groups. In: *Bioconjugate Techniques*. San Diego, California: Elsevier Science, pp: 137-165.
- Hiller, Y., Gershoni, J. M., Bayer, E. A., & Wilchek, M. (2015). Biotin binding to avidin. Oligosaccharide side chain not required for ligand association. *Biochemical Journal*, 248(1), 167–171. <https://doi.org/10.1042/bj2480167>
- Honarmand Ebrahimi, K., Hagedoorn, P.-L., & Hagen, W. R. (2013). Phosphate accelerates displacement of Fe(III) by Fe(II) in the ferroxidase center of *Pyrococcus furiosus* ferritin. *FEBS Letters*, 587(2), 220–225. <https://doi.org/10.1016/j.febslet.2012.11.029>
- Howorka, S. (2011). Rationally engineering natural protein assemblies in nanobiotechnology. *Current Opinion in Biotechnology*, 22(4), 485–491. <https://doi.org/10.1016/j.copbio.2011.05.003>
- Huberman, T., Eisenberg-Domovich, Y., Gitlin, G., Kulik, T., Bayer, E. A., Wilchek, M., & Livnah, O. (2001). Chicken avidin exhibits pseudo-catalytic properties. Biochemical, structural, and electrostatic consequences. *Journal of Biological Chemistry*, 276(34), 32031–32039. <https://doi.org/10.1074/jbc.M102018200>
- Huberman, T., Eisenberg-Domovich, Y., Gitlin, G., Kulik, T., Bayer, E. A., Wilchek, M., & Livnah, O. (2002). Chicken Avidin Exhibits Pseudo-catalytic Properties. *Journal of Biological Chemistry*, 276(34), 32031–32039. <https://doi.org/10.1074/jbc.m102018200>
- Jain, A., & Cheng, K. (2017). The principles and applications of avidin-based nanoparticles in drug delivery and diagnosis. *Journal of Controlled Release*, 245, 27–40. <https://doi.org/10.1016/j.jconrel.2016.11.016>
- Ji, H., Xi, K., Zhang, Q., & Jia, X. (2017). Photodegradable hydrogels for external manipulation of cellular microenvironments with real-time monitoring. *RSC Advances*, 7(39), 24331–24337. <https://doi.org/10.1039/c7ra02629c>
- Jiang, B., Fang, L., Wu, K., Yan, X., & Fan, K. (2020). Ferritins as natural and artificial nanozymes for theranostics. *Theranostics*, 10(2), 687–706. <https://doi.org/10.7150/thno.39827>
- Jung, K. Y., Samadani, R., Chauhan, J., Nevels, K., Yap, J. L., Zhang, J., Worlikar, S., Lanning, M. E., Chen, L., Ensey, M., Shukla, S., Salmo, R., Heinzl, G., Gordon, C., Dukes, T., MacKerell, A. D., Shapiro, P., & Fletcher, S. (2013). Structural modifications of (Z)-3-(2-aminoethyl)-5-(4-ethoxybenzylidene) thiazolidine-2,4-dione that improve selectivity for inhibiting the proliferation of melanoma cells containing active ERK signaling. *Organic and Biomolecular Chemistry*, 11(22), 3706–3732. <https://doi.org/10.1039/c3ob40199e>
- Jutz, G., van Rijn, P., Santos Miranda, B., & Böker, A. (2015). Ferritin: A Versatile Building Block for Bionanotechnology. *Chemical Reviews*, 115(4), 1653–1701. <https://doi.org/10.1021/cr400011b>

- Kajarabille, N., & Latunde-Dada, G. O. (2019). Programmed cell-death by ferroptosis: Antioxidants as mitigators. *International Journal of Molecular Sciences*, *20*(19). <https://doi.org/10.3390/ijms20194968>
- Kanbak-Aksu, S., Hasan, M. N., Hagen, W. R., Hollmann, F., Sordi, D., Sheldon, R. A., & Arends, I. W. C. E. (2012). Ferritin-supported palladium nanoclusters: Selective catalysts for aerobic oxidations in water. *Chemical Communications*, *48*(46), 5745–5747. <https://doi.org/10.1039/c2cc31401k>
- Kannan, N., & Vishveshwara, S. (2000). Aromatic clusters: a determinant of thermal stability of thermophilic proteins. *Protein Engineering*, *13*(11), 753–761. <https://doi.org/10.1093/protein/13.11.753>
- Kantner, T., Alkhawaja, B., & Watts, A. G. (2017). In Situ Quenching of Trialkylphosphine Reducing Agents Using Water-Soluble PEG-Azides Improves Maleimide Conjugation to Proteins. *ACS Omega*, *2*(9), 5785–5791. <https://doi.org/10.1021/acsomega.7b01094>
- Kantner, T., & Watts, A. G. (2016). Characterization of Reactions between Water-Soluble Trialkylphosphines and Thiol Alkylating Reagents: Implications for Protein-Conjugation Reactions. *Bioconjugate Chemistry*, *27*(10), 2400–2406. <https://doi.org/10.1021/acs.bioconjchem.6b00375>
- Kasyutich, O., Ilari, A., Fiorillo, A., Tatchev, D., Hoell, A., & Ceci, P. (2010). Silver Ion Incorporation and Nanoparticle Formation inside the Cavity of *Pyrococcus furiosus* Ferritin: Structural and Size-Distribution Analyses. *Journal of the American Chemical Society*, *132*(10), 3621–3627. <https://doi.org/10.1021/ja910918b>
- Kim, H., Cho, S. J., Yoo, M., Kang, S. K., Kim, K. R., Lee, H. H., Song, J. S., Rhee, S. D., Jung, W. H., Ahn, J. H., Jung, J. K., & Jung, K. Y. (2017). Synthesis and biological evaluation of thiazole derivatives as GPR119 agonists. *Bioorganic and Medicinal Chemistry Letters*, *27*(23), 5213–5220. <https://doi.org/10.1016/j.bmcl.2017.10.046>
- Kim, Y., Ho, S. O., Gassman, N. R., Korlann, Y., Landorf, E. V., Collart, F. R., & Weiss, S. (2008). Efficient site-specific labeling of proteins via cysteines. *Bioconjugate Chemistry*, *19*(3), 786–791. <https://doi.org/10.1021/bc7002499>
- Klingl, A. (2014). S-layer and cytoplasmic membrane - exceptions from the typical archaeal cell wall with a focus on double membranes. *Frontiers in Microbiology*, *5*(624). <https://doi.org/10.3389/fmicb.2014.00624>
- Koniev, O., & Wagner, A. (2015a). Developments and recent advancements in the field of endogenous amino acid selective bond forming reactions for bioconjugation. *Chemical Society Reviews*, *44*(15), 5495–5551. <https://doi.org/10.1039/c5cs00048c>
- Koniev, O., & Wagner, A. (2015b). Developments and recent advancements in the field of endogenous amino acid selective bond forming reactions for bioconjugation. *Chemical Society Reviews*, *44*(15), 5495–5551. <https://doi.org/10.1039/c5cs00048c>
- Lan, J., & Zenobi, R. (2019). Characterizing the iron loading pattern of ferritin using high-mass matrix-assisted laser desorption ionization mass spectrometry. *Rapid Communications in Mass Spectrometry*, *33*(24), 1855–1860. <https://doi.org/10.1002/rcm.8546>

- Lawson, D. M., Artymiuk, P. J., Yewdall, S. J., Smith, J. M. A., Livingstone, J. C., Treffry, A., Luzzago, A., Levi, S., Arosio, P., Cesareni, G., Thomas, C. D., Shaw, W. V., & Harrison, P. M. (1991). Solving the structure of human H ferritin by genetically engineering intermolecular crystal contacts. *Nature*, *349*(6309), 541–544. <https://doi.org/10.1038/349541a0>
- Levalley, P. J., Neelarapu, R., Sutherland, B. P., Dasgupta, S., Kloxin, C. J., & Kloxin, A. M. (2020). Photolabile Linkers: Exploiting Labile Bond Chemistry to Control Mode and Rate of Hydrogel Degradation and Protein Release. *Journal of the American Chemical Society*, *142*(10), 4671–4679. <https://doi.org/10.1021/jacs.9b11564>
- Li, A., Sowder, R. C., Henderson, L. E., Moore, S. P., Garfinkel, D. J., & Fisher, R. J. (2001). Chemical Cleavage at Aspartyl Residues for Protein Identification. *Analytical Chemistry*, *73*(22), 5395–5402. <https://doi.org/10.1021/ac010619z>
- Li, H., Doruker, P., Hu, G., & Bahar, I. (2020). Modulation of Toroidal Proteins Dynamics in Favor of Functional Mechanisms upon Ligand Binding. *Biophysical Journal*, *118*(7), 1782–1794. <https://doi.org/10.1016/j.bpj.2020.01.046>
- Li, M., Wong, K. K. W., & Mann, S. (1999). Organization of Inorganic Nanoparticles Using Biotin–Streptavidin Connectors. *Chemistry of Materials*, *11*(1), 23–26. <https://doi.org/10.1021/cm980610m>
- Listowsky, I., Englard, S., Bethel, J. J., & Blauer, G. (1972). Denaturation of Horse Spleen Ferritin in Aqueous Guanidinium Chloride Solutions. *Biochemistry*, *11*(11), 2176–2182. <https://doi.org/10.1021/bi00761a026>
- Liu, P., O'Mara, B. W., Warrack, B. M., Wu, W., Huang, Y., Zhang, Y., Zhao, R., Lin, M., Ackerman, M. S., Hocknell, P. K., Chen, G., Tao, L., Rieble, S., Wang, J., Wang-Iverson, D. B., Tymiak, A. A., Grace, M. J., & Russell, R. J. (2010). A Tris (2-Carboxyethyl) Phosphine (TCEP) Related Cleavage on Cysteine-Containing Proteins. *Journal of the American Society for Mass Spectrometry*, *21*(5), 837–844. <https://doi.org/10.1016/j.jasms.2010.01.016>
- Livnah, O., Bayer, E. A., Wilchek, M., & Sussman, J. L. (1993). Three-dimensional structures of avidin and the avidin-biotin complex. *Proceedings of the National Academy of Sciences of the United States of America*, *90*(11), 5076–5080. <https://doi.org/10.1073/pnas.90.11.5076>
- Lockett, M. R., Phillips, M. F., Jarecki, J. L., Peelen, D., & Smith, L. M. (2008). A tetrafluorophenyl activated ester self-assembled monolayer for the immobilization of amine-modified oligonucleotides. *Langmuir*, *24*(1), 69–75. <https://doi.org/10.1021/la702493u>
- Long, B. M., Hee, W. Y., Sharwood, R. E., Rae, B. D., Kaines, S., Lim, Y. L., Nguyen, N. D., Massey, B., Bala, S., von Caemmerer, S., Badger, M. R., & Price, G. D. (2018). Carboxysome encapsulation of the CO₂-fixing enzyme Rubisco in tobacco chloroplasts. *Nature Communications*, *9*(1), 1–14. <https://doi.org/10.1038/s41467-018-06044-0>
- Lu, T. S., Yiao, S. Y., Lim, K., Jensen, R. V., & Hsiao, L. L. (2010). Interpretation of biological and mechanical variations between the Lowry versus Bradford method for protein quantification. *North American Journal of Medical Sciences*, *2*(7), 325–328.

- Lum, K. M., Xavier, V. J., Ong, M. J. H., Johannes, C. W., & Chan, K. P. (2013). Stabilized Wittig olefination for bioconjugation. *Chemical Communications*, 49(95), 11188–11190. <https://doi.org/10.1039/c3cc45961f>
- Mardirossian, N., & Head-Gordon, M. (2016). How Accurate Are the Minnesota Density Functionals for Noncovalent Interactions, Isomerization Energies, Thermochemistry, and Barrier Heights Involving Molecules Composed of Main-Group Elements? *Journal of Chemical Theory and Computation*, 12(9), 4303–4325. <https://doi.org/10.1021/acs.jctc.6b00637>
- Matos, M. J., Oliveira, B. L., Martínez-Sáez, N., Guerreiro, A., Cal, P. M. S. D., Bertoldo, J., Maneiro, M., Perkins, E., Howard, J., Deery, M. J., Chalker, J. M., Corzana, F., Jiménez-Osés, G., & Bernardes, G. J. L. (2018). Chemo- and Regioselective Lysine Modification on Native Proteins. *Journal of the American Chemical Society*, 140(11), 4004–4017. <https://doi.org/10.1021/jacs.7b12874>
- Men, D., Zhang, T. T., Hou, L. W., Zhou, J., Zhang, Z. P., Shi, Y. Y., Zhang, J. L., Cui, Z. Q., Deng, J. Y., Wang, D. B., & Zhang, X. E. (2015). Self-Assembly of Ferritin Nanoparticles into an Enzyme Nanocomposite with Tunable Size for Ultrasensitive Immunoassay. *ACS Nano*, 9(11), 10852–10860. <https://doi.org/10.1021/acsnano.5b03607>
- Messina, M. S., Stauber, J. M., Waddington, M. A., Rheingold, A. L., Maynard, H. D., & Spokoiny, A. M. (2018). Organometallic Gold(III) Reagents for Cysteine Arylation. *Journal of the American Chemical Society*, 140(23), 7065–7069. <https://doi.org/10.1021/jacs.8b04115>
- Michalski, A., Damoc, E., Hauschild, J. P., Lange, O., Wieghaus, A., Makarov, A., Nagaraj, N., Cox, J., Mann, M., & Horning, S. (2011). Mass spectrometry-based proteomics using Q exactive, a high-performance benchtop quadrupole orbitrap mass spectrometer. *Molecular and Cellular Proteomics*, 10(9). <https://doi.org/10.1074/mcp.M111.011015>
- Moghaddam-Taaheri, P., & Karlsson, A. J. (2018). Protein Labeling in Live Cells for Immunological Applications. *Bioconjugate Chemistry*, 29(3), 680–685. <https://doi.org/10.1021/acs.bioconjchem.7b00722>
- Mohamad, N. R., Marzuki, N. H. C., Buang, N. A., Huyop, F., & Wahab, R. A. (2015). An overview of technologies for immobilization of enzymes and surface analysis techniques for immobilized enzymes. *Biotechnology and Biotechnological Equipment*, 29(2), 205–220. <https://doi.org/10.1080/13102818.2015.1008192>
- Moussa, Z., Judeh, Z. M. A., & Ahmed, S. A. (2019). Polymer-supported triphenylphosphine: Application in organic synthesis and organometallic reactions. *RSC Advances*, 9(60), 35217–35272. <https://doi.org/10.1039/c9ra07094j>
- Mthembu, S. N., Sharma, A., Albericio, F., & Torre, B. G. (2020). Breaking a Couple: Disulfide Reducing Agents. *ChemBioChem*, 21(14), 1947–1954. <https://doi.org/10.1002/cbic.202000092>
- Munro, H. N., & Linder, M. C. (1978). Ferritin: Structure, biosynthesis, and role in iron metabolism. *Physiological Reviews*, 58(2), 317–396. <https://doi.org/10.1152/physrev.1978.58.2.317>

- Nanna, A. R., Li, X., Walseng, E., Pedzisa, L., Goydel, R. S., Hymel, D., Burke, T. R., Roush, W. R., & Rader, C. (2017). Harnessing a catalytic lysine residue for the one-step preparation of homogeneous antibody-drug conjugates. *Nature Communications*, 8(1). <https://doi.org/10.1038/s41467-017-01257-1>
- Ohlinger, W. S., Klunzinger, P. E., Deppmeier, B. J., & Hehre, W. J. (2009). Efficient calculation of heats of formation. *Journal of Physical Chemistry A*, 113(10), 2165–2175. <https://doi.org/10.1021/jp810144q>
- Orino, K., Lehman, L., Tsuji, Y., Ayaki, H., Torti, S. V., & Torti, F. M. (2001). Ferritin and the response to oxidative stress. *Biochemical Journal*, 357(1), 241–247. <https://doi.org/10.1042/bj3570241>
- Parker, M. J., Allen, M. A., Ramsay, B., Klem, M. T., Young, M., & Douglas, T. (2008). Expanding the temperature range of biomimetic synthesis using a ferritin from the hyperthermophile *Pyrococcus furiosus*. *Chemistry of Materials*, 20(4), 1541–1547. <https://doi.org/10.1021/cm702732x>
- Pasparakis, G., Manouras, T., Argitis, P., & Vamvakaki, M. (2012). Photodegradable polymers for biotechnological applications. *Macromolecular Rapid Communications*, 33(3), 183–198. <https://doi.org/10.1002/marc.201100637>
- Pieters, B. J. G. E., Van Eldijk, M. B., Nolte, R. J. M., & Mecinović, J. (2016). Natural supramolecular protein assemblies. *Chemical Society Reviews*, 45(1), 24–39. <https://doi.org/10.1039/c5cs00157a>
- Plath, L. D., Ozdemir, A., Aksenov, A. A., & Bier, M. E. (2015). Determination of Iron Content and Dispersity of Intact Ferritin by Superconducting Tunnel Junction Cryodetection Mass Spectrometry. *Analytical Chemistry*, 87(17), 8985–8993. <https://doi.org/10.1021/acs.analchem.5b02180>
- Pocker, Y., Meany, J. E., & Davist, B. C. (1974). α -keto esters as substrates of erythrocyte carbonic anhydrase. Kinetic studies of enzyme catalyzed hydration of methyl and ethyl pyruvate. *Biochemistry*, 13(7), 1411–1416. <https://doi.org/10.1021/bi00704a015>
- Putri, R. M., Cornelissen, J. J. L. M., & Koay, M. S. T. (2015). Self-Assembled Cage-Like Protein Structures. *ChemPhysChem*, 16(5), 911–918. <https://doi.org/10.1002/cphc.201402722>
- Saito, R., Sato, T., Ikai, A., & Tanaka, N. (2004). Structure of bovine carbonic anhydrase II at 1.95 Å resolution. *Acta Crystallographica Section D: Biological Crystallography*, 60(4), 792–795. <https://doi.org/10.1107/S0907444904003166>
- Sára, M., & Sleytr, U. B. (2000). S-layer proteins. *Journal of Bacteriology* (Vol. 182, Issue 4, pp. 859–868). <https://doi.org/10.1128/JB.182.4.859-868.2000>
- Schindelin, J., Arganda-Carreras, I., Frise, E., Kaynig, V., Longair, M., Pietzsch, T., Preibisch, S., Rueden, C., Saalfeld, S., Schmid, B., Tinevez, J. Y., White, D. J., Hartenstein, V., Eliceiri, K., Tomancak, P., & Cardona, A. (2012). Fiji: An open-source platform for biological-image analysis. *Nature Methods*, 9(7), 676–682. <https://doi.org/10.1038/nmeth.2019>

- Schoonen, L., & Van Hest, J. C. M. (2014). Functionalization of protein-based nanocages for drug delivery applications. *Nanoscale*, *6*(13), 7124–7141. <https://doi.org/10.1039/c4nr00915k>
- Sevcenco, A. M., Paravidino, M., Vrouwenvelder, J. S., Wolterbeek, H. T., van Loosdrecht, M. C. M., & Hagen, W. R. (2015). Phosphate and arsenate removal efficiency by thermostable ferritin enzyme from *Pyrococcus furiosus* using radioisotopes. *Water Research*, *76*, 181–186. <https://doi.org/10.1016/j.watres.2015.02.054>
- Shinjyo, S., Abe, H., & Masuda, M. (1975). Carbohydrate composition of horse spleen ferritin. *BBA - General Subjects*, *411*(1), 165–167. [https://doi.org/10.1016/0304-4165\(75\)90295-0](https://doi.org/10.1016/0304-4165(75)90295-0)
- Shukla, S., Ablack, A. L., Wen, A. M., Lee, K. L., Lewis, J. D., & Steinmetz, N. F. (2013). Increased tumor homing and tissue penetration of the filamentous plant viral nanoparticle potato virus X. *Molecular Pharmaceutics*, *10*(1), 33–42. <https://doi.org/10.1021/mp300240m>
- Sleytr, U. B., & Sára, M. (1986). Ultrafiltration membranes with uniform pores from crystalline bacterial cell envelope layers. *Applied Microbiology and Biotechnology*, *25*(2), 83–90. <https://doi.org/10.1007/BF00938929>
- Sleytr, U. B., Schuster, B., Egelseer, E. M., & Pum, D. (2014). S-layers: Principles and applications. *FEMS Microbiology Reviews*, *38*(5), 823–864. <https://doi.org/10.1111/1574-6976.12063>
- Spears, R. J., & Fascione, M. A. (2016). Site-selective incorporation and ligation of protein aldehydes. *Organic and Biomolecular Chemistry*, *14*(32), 7622–7638. <https://doi.org/10.1039/c6ob00778c>
- Spicer, C. D., & Davis, B. G. (2014). Selective chemical protein modification. *Nature Communications*, *5*(1), 1–14. <https://doi.org/10.1038/ncomms5740>
- Stephanopoulos, N. (2019). Peptide-oligonucleotide hybrid molecules for bioactive nanomaterials. *Bioconjugate Chemistry*, *30*(7), 1915–1922. <https://doi.org/10.1021/acs.bioconjchem.9b00259>
- Strzelczyk, P., Bujacz, A., Plazuk, D., Zakrzewski, J., & Bujacz, G. (2013). Structural investigation of the interactions of biotinylruthenocene with avidin. *Chemico-Biological Interactions*, *204*(1), 6–12. <https://doi.org/10.1016/j.cbi.2013.04.005>
- Tamura, T., & Hamachi, I. (2019). Chemistry for Covalent Modification of Endogenous/Native Proteins: From Test Tubes to Complex Biological Systems. *Journal of the American Chemical Society*, *141*(7), 2782–2799. <https://doi.org/10.1021/jacs.8b11747>
- Tatur, J., Hagedoorn, P. L., Overeijnder, M. L., & Hagen, W. R. (2006). A highly thermostable ferritin from the hyperthermophilic archaeal anaerobe *Pyrococcus furiosus*. *Extremophiles*, *10*(2), 139–148. <https://doi.org/10.1007/s00792-005-0484-x>
- Tatur, J., Hagen, W. R., & Matias, P. M. (2007). Crystal structure of the ferritin from the hyperthermophilic archaeal anaerobe *Pyrococcus furiosus*. *Journal of Biological Inorganic Chemistry*, *12*(5), 615–630. <https://doi.org/10.1007/s00775-007-0212-3>

- Theil, E. C. (2013). Ferritin: The protein nanocage and iron biomineral in health and in disease. *Inorganic Chemistry*, 52(21), 12223–12233. <https://doi.org/10.1021/ic400484n>
- Thiemann, T. (2007). Solventless Wittig olefination with fluorinated benzaldehydes. *Journal of Chemical Research*, 2007(6), 336–341. <https://doi.org/10.3184/030823407X225464>
- Urushizaki, I., Niitsu, Y., Ishitani, K., Matsuda, M., & Fukuda, M. (1971). Microheterogeneity of horse spleen ferritin and apoferritin. *BBA - Protein Structure*, 243(2), 187–192. [https://doi.org/10.1016/0005-2795\(71\)90075-4](https://doi.org/10.1016/0005-2795(71)90075-4)
- van Roy, N., Mangelschots, K., & Speleman, F. (1993). Improved immunocytochemical detection of biotinylated probes with neutralite avidin. *Trends in Genetics*, 9(3), 71–72. [https://doi.org/10.1016/0168-9525\(93\)90217-6](https://doi.org/10.1016/0168-9525(93)90217-6)
- Vinogradova, E. V., Zhang, C., Spokoyny, A. M., Pentelute, B. L., & Buchwald, S. L. (2015). Organometallic palladium reagents for cysteine bioconjugation. *Nature*, 526(7575), 687–691. <https://doi.org/10.1038/nature15739>
- Watt, G. D., Kim, J.-W., Zhang, B., Miller, T., Harb, J. N., Davis, R. C., & Choi, S. H. (2012). A Protein-Based Ferritin Bio-Nanobattery. *Journal of Nanotechnology*, 2012. <https://doi.org/10.1155/2012/516309>
- Xiao, Q., Draper, S. R. E., Smith, M. S., Brown, N., Pugmire, N. A. B., Ashton, D. S., Carter, A. J., Lawrence, E. E. K., & Price, J. L. (2019). Influence of PEGylation on the Strength of Protein Surface Salt Bridges. *ACS Chemical Biology*, 14(7), 1652–1659. <https://doi.org/10.1021/acscchembio.9b00432>
- Yeates, T. O., Jorda, J., & Bobik, T. A. (2013). The shells of BMC-Type microcompartment organelles in bacteria. *Journal of Molecular Microbiology and Biotechnology*, 23(4–5), 290–299. <https://doi.org/10.1159/000351347>
- Yévenes, A. (2017). The ferritin superfamily. *Sub-Cellular Biochemistry*, 83, 75–102. https://doi.org/10.1007/978-3-319-46503-6_3
- Yewdall, N. A., Allison, T. M., Pearce, F. G., Robinson, C. V., & Gerrard, J. A. (2018). Self-assembly of toroidal proteins explored using native mass spectrometry. *Chemical Science*, 9(28), 6099–6106. <https://doi.org/10.1039/c8sc01379a>
- Yokoi, N., Miura, Y., Huang, C. Y., Takatani, N., Inaba, H., Koshiyama, T., Kanamaru, S., Arisaka, F., Watanabe, Y., Kitagawa, S., & Ueno, T. (2011). Dual modification of a triple-stranded β -helix nanotube with Ru and Re metal complexes to promote photocatalytic reduction of CO₂. *Chemical Communications*, 47(7), 2074–2076. <https://doi.org/10.1039/c0cc03015e>
- Zaia, J. (2010). Mass spectrometry and glycomics. In *OMICS A Journal of Integrative Biology*, 14(4), 401–418. Mary Ann Liebert, Inc. <https://doi.org/10.1089/omi.2009.0146>
- Zang, J., Chen, H., Zhao, G., Wang, F., & Ren, F. (2017). Ferritin cage for encapsulation and delivery of bioactive nutrients: From structure, property to applications. *Critical Reviews in Food Science and Nutrition*, 57(17), 3673–3683. <https://doi.org/10.1080/10408398.2016.1149690>

- Zeng, Q., Reuther, R., Oxsher, J., & Wang, Q. (2008). Characterization of horse spleen apoferritin reactive lysines by MALDI-TOF mass spectrometry combined with enzymatic digestion. *Bioorganic Chemistry*, 36(5), 255–260. <https://doi.org/10.1016/j.bioorg.2008.06.001>
- Zhang, Y., & Orner, B. P. (2011). Self-assembly in the ferritin nano-cage protein superfamily. *International Journal of Molecular Sciences*, 12(8), 5406–5421. <https://doi.org/10.3390/ijms12085406>
- Zhao, G. (2010). Phytoferritin and its implications for human health and nutrition. *Biochimica et Biophysica Acta*, 1800(8), 815–823. *Biochim Biophys Acta*. <https://doi.org/10.1016/j.bbagen.2010.01.009>
- Zhong, X., & Wright, J. F. (2013). Biological Insights into Therapeutic Protein Modifications throughout Trafficking and Their Biopharmaceutical Applications. *International Journal of Cell Biology*, 2013. <https://doi.org/10.1155/2013/273086>
- Zhu, S., Yang, Q., Antaris, A. L., Yue, J., Ma, Z., Wang, H., Huang, W., Wan, H., Wang, J., Diao, S., Zhang, B., Li, X., Zhong, Y., Yu, K., Hong, G., Luo, J., Liang, Y., & Dai, H. (2017). Molecular imaging of biological systems with a clickable dye in the broad 800- to 1,700-nm near-infrared window. *Proceedings of the National Academy of Sciences of the United States of America*, 114(5), 962–967. <https://doi.org/10.1073/pnas.1617990114>

Appendix: Letters of Copyright Permission

Copyright use for Figure 1.6



Dear Fatima Omar Merza,

Your permission requested is granted and there is no fee for this reuse. In your planned reuse, you must cite the ACS article as the source, add this direct link <https://pubs.acs.org/doi/10.1021/acs.bioconjchem.9b00259>, and include a notice to readers that further permissions related to the material excerpted should be directed to the ACS.



If you need further assistance, please let me know.


Sincerely,

Raquel Picar-Simpson
ACS Publications Support
Customer Services & Information
Website: <https://help.acs.org/>

Incident #:	3706659	
Date Created:	2020-07-28T11:40:51	
Priority:	3	
Customer:	Fatima Omar Merza	
Title:	Permission request -- DOI: 10.1021/acs.bioconjchem.9b00259	

Copyright use for Figure 1.7

HomeHelpEmail SupportFatima Merza ▾



Fabrication of Patterned Hydrogel Interfaces: Exploiting the Maleimide Group as a Dual Purpose Handle for Cross-Linking and Bioconjugation

Author: Nergiz Cengiz, Tugce Nihal Gevrek, Rana Sanyal, et al
Publication: Bioconjugate Chemistry
Publisher: American Chemical Society
Date: May 1, 2020

Copyright © 2020, American Chemical Society

PERMISSION/LICENSE IS GRANTED FOR YOUR ORDER AT NO CHARGE

This type of permission/license, instead of the standard Terms & Conditions, is sent to you because no fee is being charged for your order. Please note the following:

- Permission is granted for your request in both print and electronic formats, and translations.
- If figures and/or tables were requested, they may be adapted or used in part.
- Please print this page for your records and send a copy of it to your publisher/graduate school.
- Appropriate credit for the requested material should be given as follows: "Reprinted (adapted) with permission from (COMPLETE REFERENCE CITATION). Copyright (YEAR) American Chemical Society." Insert appropriate information in place of the capitalized words.
- One-time permission is granted only for the use specified in your request. No additional uses are granted (such as derivative works or other editions). For any other uses, please submit a new request.

If credit is given to another source for the material you requested, permission must be obtained from that source.

[BACK](#) [CLOSE WINDOW](#)

Copyright use for Figure 1.10

Dear Fatima Merza,

Thank you for your email. As to your request, I am pleased to inform you that permission is granted hereby to reprint Figure 1 from the article

Yeates T, O, Jorda J, Bobik T, A: The Shells of BMC-Type Microcompartment Organelles in Bacteria. J Mol Microbiol Biotechnol 2013;23:290-299. doi: 10.1159/000351347

in the printed and electronic version of your **thesis/doctoral dissertation**, provided that proper credit will be given to the original source and that S. Karger AG, Basel will be mentioned.

Please note that this is a non-exclusive permission, hence any further use, edition, translation or distribution, either in print or electronically, requires written permission again as this permission is valid for the above mentioned purpose only.

This permission applies only to copyrighted content that S. Karger AG owns, and not to copyrighted content from other sources. If any material in our work appears with credit to another source, you must also obtain permission from the original source cited in our work. All content reproduced from copyrighted material owned by S. Karger AG remains the sole and exclusive property of S. Karger AG. The right to grant permission to a third party is reserved solely by S. Karger AG.

Thank you for your understanding and cooperation.

Hopefully, I have been of assistance to you with the above.

Kind regards,

Erika Brunner

ePartner Manager
Rights & Permissions Manager

+41 61 306 12 48
e.brunner@karger.com



Copyright use for Figure 1.11

ELSEVIER LICENSE
TERMS AND CONDITIONS
Aug 01, 2020

This Agreement between Ms. Fatima Merza ("You") and Elsevier ("Elsevier") consists of your license details and the terms and conditions provided by Elsevier and Copyright Clearance Center.

License Number	4877690823054
License date	Jul 28, 2020
Licensed Content Publisher	Elsevier
Licensed Content Publication	Current Opinion in Biotechnology
Licensed Content Title	Self-assembled two-dimensional protein arrays in bionanotechnology: from S-layers to designed lattices
Licensed Content Author	François Baneyx, James F Mattheai
Licensed Content Date	Aug 1, 2014
Licensed Content Volume	28
Licensed Content Issue	n/a
Licensed Content Pages	7
Start Page	39
End Page	45
Type of Use	reuse in a thesis/dissertation
Portion	figures/tables/illustrations
Number of figures/tables/illustrations	1
Format	electronic
Are you the author of this Elsevier article?	No
Will you be translating?	No
Title	Supramolecular Assembly of Three-Dimensional Protein Networks
Institution name	University of Waterloo
Expected presentation date	Aug 2020
Order reference number	None
Portions	Figure 2 (b) Ms. Fatima Merza 196 Westmount Rd N
Requestor Location	Waterloo, ON N2L 3G5 Canada Attn: University of Waterloo
Publisher Tax ID	GB 494 6272 12

Copyright use for Figure 1.13



Marketplace™

Royal Society of Chemistry - License Terms and Conditions

This is a License Agreement between Fatima Merza ("You") and Royal Society of Chemistry ("Publisher") provided by Copyright Clearance Center ("CCC"). The license consists of your order details, the terms and conditions provided by Royal Society of Chemistry, and the CCC terms and conditions.

All payments must be made in full to CCC.

Order Date	28-Jul-2020	Type of Use	Republish in a thesis/dissertation
Order license ID	1051558-1	Publisher	ROYAL SOCIETY OF CHEMISTRY
ISSN	1364-548X	Portion	Image/photo/illustration

LICENSED CONTENT

Publication Title	Chemical communications	Country	United Kingdom of Great Britain and Northern Ireland
Author/Editor	Royal Society of Chemistry (Great Britain)	Rightsholder	Royal Society of Chemistry
Date	01/01/1996	Publication Type	e-Journal
Language	English		

REQUEST DETAILS

Portion Type	Image/photo/illustration	Distribution	Worldwide
Number of images / photos / illustrations	1	Translation	Original language of publication
Format (select all that apply)	Electronic	Copies for the disabled?	No
Who will republish the content?	Academic institution	Minor editing privileges?	No
Duration of Use	Current edition and up to 5 years	Incidental promotional use?	No
Lifetime Unit Quantity	Up to 499	Currency	CAD
Rights Requested	Main product		

NEW WORK DETAILS

Title	Supramolecular Assembly of Three-Dimensional Protein Networks	Institution name	University of Waterloo
Instructor name	John Honek	Expected presentation date	2020-08-18

ADDITIONAL DETAILS

Order reference number	None	The requesting person / organization to appear on the license	Fatima Merza
------------------------	------	---	--------------

REUSE CONTENT DETAILS

Title, description or numeric reference of the portion(s)	Dual modification of a triple-stranded β -helix nanotube with Ru and Re metal complexes to promote photocatalytic reduction of CO ₂	Title of the article/chapter the portion is from	Dual modification of a triple-stranded β -helix nanotube with Ru and Re metal complexes to promote photocatalytic reduction of CO ₂
Editor of portion(s)	N/A	Author of portion(s)	Royal Society of Chemistry (Great Britain)
Volume of serial or monograph	N/A	Issue, if republishing an article from a serial	N/A
Page or page range of portion	Figure 1	Publication date of portion	1996-01-01

Copyright use for Figure 1.14



RightsLink®



Home



Help



Email Support



Fatima Merza ▾

Self-Assembly of Ferritin Nanoparticles into an Enzyme Nanocomposite with Tunable Size for Ultrasensitive Immunoassay



Author: Dong Men, Ting-Ting Zhang, Li-Wei Hou, et al

Publication: ACS Nano

Publisher: American Chemical Society

Date: Nov 1, 2015

Copyright © 2015, American Chemical Society

PERMISSION/LICENSE IS GRANTED FOR YOUR ORDER AT NO CHARGE

This type of permission/license, instead of the standard Terms & Conditions, is sent to you because no fee is being charged for your order. Please note the following:

- Permission is granted for your request in both print and electronic formats, and translations.
 - If figures and/or tables were requested, they may be adapted or used in part.
 - Please print this page for your records and send a copy of it to your publisher/graduate school.
 - Appropriate credit for the requested material should be given as follows: "Reprinted (adapted) with permission from (COMPLETE REFERENCE CITATION). Copyright (YEAR) American Chemical Society." Insert appropriate information in place of the capitalized words.
 - One-time permission is granted only for the use specified in your request. No additional uses are granted (such as derivative works or other editions). For any other uses, please submit a new request.
- If credit is given to another source for the material you requested, permission must be obtained from that source.

BACK

CLOSE WINDOW